Deep fluid characteristics in the subduction zone:

A window from metamorphic quartz veins

by

KENTA YOSHIDA

December 12, 2014

Thesis submitted for the Degree of Doctor of Science

Graduate School of Science

Kyoto University

Abstract

Aqueous fluids in subduction zones play important roles in geochemical and geophysical processes, such as slab seismicity, arc magmatism, metamorphism, mantle metasomatism, and the transport of several components to the surface from deep parts of the Earth. In order to determine the chemical compositions of deep fluids, this study examines in detail fluid inclusions trapped in high-pressure type metamorphic rocks.

Part 1 of this study determines the density of a fluid inclusion in metamorphic quartz, the entrapment timing of which is estimated as prograde stage. Detailed morphological study was performed by microsampling using a focused ion beam (FIB) system and high-resolution X-ray computed tomography (XCT). The volumetric data obtained from CT data, combined with microthermometric data and Raman microscopy, enable precise estimation of the bulk composition and density. The isochore calculation from the estimated bulk property yielded significantly lower pressure conditions compared with the peak pressure-temperature (*P*-*T*) conditions of the host rock even though the studied inclusion was expected to have undergone reequilibration during the pressure increase. According to Küster and Stöckhert (1997), fluid inclusions trapped in metamorphic quartz can record the *P*-*T* conditions present at approximately 300 ºC, which is highly consistent with the data obtained here. This fact attests that the densities of fluid inclusions in metamorphic quartz veins rarely retain the condition of their entrapment or peak *P*-*T* conditions they suffered, even at the *P*-*T* conditions (<700 ºC, <2.5 GPa) of the Sanbagawa metamorphic belt.

Part 2 of this study deals with the chemical composition of fluid inclusions extracted by the crush-leach method. On the basis of detailed textural observation of the

fluid inclusions and host quartz veins, we can distinguish the entrapment stage of the fluid inclusions relative to the stage of metamorphism. The investigated samples were collected from the Sanbagawa metamorphic belt, SW Japan, covering the metamorphic grade from the pumpellyite-actinolite facies (300 ºC/ 0.5 GPa) to the quartz-eclogite facies (550-650 ºC/ 1.5-2.5 GPa). The results show that quartz veins can be classified into the following three groups on the basis of their fabrics: polygonal type (P-type), deformed-interlobate-grain type (DI-type) and pervasively-deformed-domain type (DD-type). P-type fabrics in the studied samples indicate textural development under the conditions of very low differential stress with relatively high temperature and the absence of subsequent brittle deformation, thus, corresponding fluid inclusions should have been trapped during the peak metamorphic stage or in the early stage of exhumation. On the contrary, fabrics of DI- and DD-type, such as those with deformation lamellae and undulatory extinction, are believed to be formed under high differential stress and low temperatures (<400 ºC) during the later stage of exhumation; thus, fluid inclusions in DI- and DD-type veins are thought to be trapped in association with the later-stage deformation event and corresponding fluid infiltration. P-type veins tend to contain relatively high saline aqueous fluids (5-10 mass%$_{NaCleq}$) and their compositions are mainly Na-Cl dominated. DI- and DD-type veins contain dilute aqueous fluids (<5 mass%$_{NaCleq}$) and some are characterized by the dominance of HCO_3^- in the anions. The relative B-Li-Cl compositions of the studied fluids are characterized by high (B+Li)/Cl ratio, which is characteristics of Arima-type hydrothermal fluids, believed to be derived directly from the subducting-slab at the present fore-arc region of the Japanese island chain. The Li/B ratios of the studied fluids show a large variation from a low value of 0.02 obtained from the sample of the pumpellyite-actinolite facies

with DD-type fabric, to a high value of 1.99 obtained from the sample of the eclogite facies with P-type sample. These results suggest that high-saline and B-Li-enriched fluids are supplied from subducting slabs to the hanging wall mantle wedge in the subduction zone. Furthermore, the geochemical cycle of boron and lithium on the basis of the aforementioned deep fluid composition were considered. Previous studies have reported that the boron and lithium concentrations subducted together with sedimentary and mafic rocks are mostly at the order of 100-1000 μg/g. Deep-origin fluids would contain approximately 300 μg/g of boron and lithium. Given the dehydration amount from the subducting metamorphic rocks as a few mass percentages, the released fluids with each 300 μg/g of boron and lithium would remove approximately 10 μg/g of the solute from the rock. This finding indicates that boron- and lithium-enriched aqueous fluid can be generated without large impact on the compositions of the subducting materials. Furthermore, ascent of deep-origin boron- and lithium-enriched fluids from the surface of subducting materials to the shallow part of the crust, a disequilibrium fluid transport is the essential process involved for retaining high concentrations of boron and lithium. This process may suggest that the fluid ascended in the style of the channelized flow.

和文要旨

変成石英脈を用いた沈み込み帯深部流体組成の研究

沈み込み帯に存在している“水”は，地球化学・地球物理学的な諸過程において重要な物質の一つと見なされている．その役割は，地震発生や島弧マグマ形成の要因となったり，マントル交代作用をはじめとする種々の物質移動の担い手となるなど，多岐にわたる．この“水”（地下深部流体）の地下深部での実態を明らかにするため，本研究では沈み込み帯由来の高圧型変成岩とそこに捕獲された流体包有物を用いて，地下深部流体の化学組成を詳細に検討した．

本研究の第一章では，変成石英中に捕獲された昇圧時の流体包有物の密度推定を行った．流体包有物の密度推定のために，集束イオンビーム装置（FIB）によるマイクロサンプリングと，高分解能 X 線コンピュータ断層撮影（XCT）を用いて，詳細な形態記載を実施した．CT 像から求まった流体包有物の体積データと，マイクロサーモメトリ・ラマン分光で得られた流体の特性を元に，流体包有物全体の組成と密度を正確に決定した．得られた組成・密度データから流体包有物の等密度線を温度圧力空間内で計算したところ，この流体包有物は昇圧期の再平衡組織を伴うにも拘わらずピーク時の温度圧力よりも遙かに低い圧力条件を呈した．このことは，変成石英中の流体包有物は概ね 300 ºC 程度での密度を保存するという考え (Küster and Stöckhert, 1997) で説明することが出来る．以上から，変成石英中の流体包有物は，その密度から捕獲時期を推定するのが非常に困難であることがわかった．

第一章の結果を踏まえて，第二章では流体包有物の密度によらず，その組織から捕獲時期の推定を行った．また，石英の粉砕により包有物中の流体を溶媒中に集積し，主要・微量成分について化学分析を行った．流体包有物の捕獲時期（沈み込み帯での深度）と化学組成との関係を調べるため，分析に用いた試料は西南

日本四国・和歌山地域の三波川変成帯において緑泥石帯（パンペリー石－アクチノ閃石相相当：300 ºC・0.5 GPa 程度）からエクロジャイト岩体（角閃石エクロジャイト相相当：550－650 ºC・1.5－2.5 GPa 程度）に渡る変成度範囲で採取した．採取した石英脈はその組織から，完晶質な類型（polygonal: P-type），変形の卓越する類型のうち房状組織を呈するもの（deformed-interlobate-grain: DI-type），非常に大きな変形領域が卓越するもの（deformed-domain: DD-type）の三種類に分類することが出来た．P-type の石英脈は高温・低差応力下での組織形成によるものと考えられ，組織形成後の大規模な変形を免れている．その為，P-type の脈に捕獲されている流体包有物は変成ピーク時以前或いはピーク時から岩体上昇の比較的早期（高温期）に捕獲されたものであると考えられる．一方で，DI-type・DD-type の組織は低温（＜400 ºC）・高差応力下で形成されたものと考えられ，これらに伴われる流体包有物は岩体上昇の後期にあった大規模な変形とそれに伴う流体の浸潤により捕獲されたものと考えられる．P-type の脈は比較的塩濃度の高い水溶液包有物（5－10 mass%NaCleq）を伴い，主要な溶質は Na-Cl が卓越している．一方 DI-・DD-type の脈中の包有物は希薄な水溶液（＜5 mass%NaCleq）であり，陰イオンとして HCO_3 が卓越する傾向がある．これらの流体包有物の B-Li-Cl 組成に注目したところ，全ての試料に関して，海水と比較して(B+Li)/Cl の比が高いことがわかった．その組成範囲は，日本列島下に沈み込んでいるスラブから直接上昇してきていると考えられている「有馬型熱水」のものと非常に似通っている．また，Li/B 比に着目すると，試料ごとに大きく異なる値が得られた．最小値は低変成度・DD-type の試料で Li/B=0.02 の値が，最高値はエクロジャイト相・P-type の試料で Li/B=1.99 という値となり，DD-・DI-type のもので小さく P-type のもので大きくなる傾向が見られた．これらの結果から，沈み込み帯深部での流体の特徴として Na-Cl が卓越し Li と B 両方に富むもの，沈み込み帯浅部での流体の特徴として HCO_3 が卓越し B に富むものが，それぞれ挙げられることがわかった．更に，得ら

れた流体組成に基づいて，沈み込み帯でのホウ素・リチウムの循環について検討を行った．先行研究から，変質 MORB や堆積物により沈み込み帯に持ち込まれるホウ素・リチウムは，岩石中で概ね 100－1000 μg/g の濃度であると考えられる．この濃度のホウ素とリチウムを保持する岩石から，流体包有物から組成を見積もった深部流体が放出されたと考えて物質移動の考察を行ったところ，ホウ素・リチウムに富む流体の放出は全岩濃度に対してはあまり大きな影響を与えないという結果が得られた．更に，このホウ素やリチウムに富む流体が地殻の浅部までそのホウ素・リチウム量を保持したまま上昇するためには，流体は岩石と非平衡に上昇する必要があるということもわかった．これらのことは，地下深部からの流体上昇はチャネリングにより「水みち」のようなものを作って行われていることを示唆するであろう．

Acknowledgements

This thesis marks the conclusion of my work that began in 2009 and that is built on the previous achievements of my fore-colleagues. I could never have done anything, including the research and writing that turned into this dissertation, without the support and encouragement of a lot of people.

First and foremost, I must thank Prof. Takao Hirajima, my supervisor, who provided direction and gave valuable discussions. I appreciate all his contributions of time, advices, and funding to make my Ph.D. experience productive and stimulating. The members of the petrology group have contributed greatly to my personal and academic time at Kyoto. I am especially grateful for Dr. Tetsuo Kawakami and Dr. Tomoyuki Kobayashi, who has moved to Nagoya Gakuin University, for constructive recommendations and guidance for analytical techniques. I also would like to thank to Ms. Fumiko Higashino and Mr. Yoshiteru Sengen for valuable discussions.

Prof. Shinji Ohsawa, Mr. Taketoshi Mishima, Prof. Akira Tsuchiyama, Dr. Akira Miyake, and Dr. Tetsu Kogiso provided me a precious opportunity to carry out lateral approaches to the geofluid study. Prof. Eiichi Takahashi of Tokyo Institute of Technology and his research project “Geofluids” (Grant-in-Aid for Scientific Research on Innovative Areas No. 2018), that was so much of stimulus and improved my study works, was acknowledged. This study is partly supported by the JSPS (Grant-in-Aid for JSPS Fellows for KY, No. 25-57) and Nozomi Farm, Ltd.

Finally, I wish to express my greatest thanks to my parents for their hospitable supports and encouragement throughout my college life.

Contents

Preface

Of many the special features of the planet Earth, the existence of water is one of the most fantastic. Despite its small abundance compared with other components in the solid Earth, water can make significant impacts on many of the earth processes, such as slab seismicity (e.g., Hacker et al., 2003), melting of rocks (e.g., Kushiro et al., 1968), weathering of the surface (e.g., Miller and Drever, 1977), and rheological properties of deeply-seated rocks (e.g., Karato et al., 1986). These effects of water are scarcely observed in other terrestrial planets; thus, the distribution of water is of importance for understanding the past, present, and future of the planet Earth. With respect to aqueous fluid activity in the Earth processes, a number of studies, covering observation of natural samples, experiments at high-pressure and high-temperature conditions, and numerical model calculations, have been performed to document and predict the dynamics and evolution of the Earth.

I. Rocks as tools for the fluid study

Metamorphic rocks are accessible, deep-origin materials that provide records of geological processes occurring at root zones of convergent margins, such as plate subduction and continental collision zones, the depth of which exceeds 100 km (e.g., Chopin, 1984; Smith, 1984). Thus these rocks are powerful tools for investigating the physicochemical properties of deep-parts of the Earth. Conventional studies using petrographical descriptions, chemical analyses, and thermodynamic calculations have revealed complicated *P*-*T* histories of metamorphic rocks which are now exposed on the land surface.

After the development of quantitative chemical analyses using an electron microprobe (e.g., Bence and Albee, 1968), we can say that the progress in petrology depends on the advancements in the analytical technique such as improvements in spatial resolution and sensitivity of concentration. Recent progress in more sensitive analytical techniques such as mass spectrometry has increasingly enriched our knowledge of the geochemical processes occurring in the solid part of the Earth. We can now obtain images of the structures of minerals in the resolution of individual atoms by using transmission electron microscopy (Bell et al., 2012). Moreover, we can determine the abundance of trace elements in the order of less than parts per million by using several mass spectrometers (Jochum et al., 1988). Therefore, we can examine objects in an extremely fine scale. Trace element analysis of solid phases combined with the reaction textures of minerals revealed vestiges of fluid-rock interactions, such as B-enriched rims of white mica in metamorphic rocks (Konrad-Schmolke and Halama, 2014). On the basis of such composite petrographical studies, petrologists are now interested in deciphering paleo-fluid activity to predict future Earth processes.

II. Subduction zone emissions

Volcanic rocks are typical materials of emissions from subduction zone processes and are expected to record the fluid-rock interaction occurring beneath the volcanoes. Several specific elements have generated a substantial amount of attention as trace element of deep fluids. For example, Nakamura and Iwamori (2009) performed geochemical studies with respect to the isotopic systematics (Nd and Sr) of arc lavas obtained from Japan island arc and revealed the amount of the contribution of slab-derived fluid for the generation of these arc lavas. The imprint of slab-derived fluid in

arc lavas is also observed in the compositions of volcanic rocks that show depletions of high field strength elements (HFSE: Ti, Zr, Nb) relative to large ion lithophile elements (LILE: Sr, K, Ba) and light rare earth elements (LREE), indicating the penetration of some metasomatic agents enriched with fluid mobile components (Hawkesworth et al., 1993; Kelemen et al., 1993; Brenan et al., 1994).

Several recent studies on hot- and mineral-springs invoked that specific springs, which are known as "Arima-type hydrothermal fluids" (Matsubaya et al., 1973) occurring mainly in southwest Japan, have the deep-origin component that directly comes from the subducting slab (e.g., Kusuda et al., 2014; Amita et al., 2014; Kazahaya et al., 2014). Ohsawa (2004) and Kazahaya et al. (2014) found hot-springs that have high Li/Cl ratio and attributed them to the signature of deep-origin. Their detailed geochemical studies show their characteristics of high salinity, high $^{3}He/^{4}He$ ratio, heavy oxygen isotope value, and light hydrogen isotope value compared to the modern seawater. Ohsawa et al. (2010) also reported B-enriched hot-springs from the Miyazaki plain, in the fore-arc region of southwest Japan, which are attributed to the preferential release of boron by a smectite/illite transition reaction occurring at approximately 130ºC during diagenetic processes.

III. Metamorphic rocks as markers of fluid–rock interaction

Records of fluid activities can be detected in metamorphic and metasomatic rocks in the whole rock chemistry and also in the compositional variations of independent minerals. Fluid–mobile elements such as boron and lithium provide good clues for deciphering the fluid-rock interaction in subduction zone processes (e.g., Bebout et al., 1993; Marschall et al., 2009). Such elements tend to have relatively high concentration in

altered oceanic crusts and pelagic sediments (Shaw et al., 1977; Donnelly et al., 1980; Leeman and Sisson, 1996) through the high-temperature hydrothermal processes (Seyfried et al., 1984). During the subduction processes, these elements are believed to be released from the subducting slab due to fluid-rock interactions (Bebout et al., 1993; Marschall et al., 2006; 2007). However, some recent studies indicated that the process of releasing these elements is not significant because the released fluid-mobile elements are stored *in situ* by other favored minerals and therefore undergo redistribution (Nakano and Nakamura, 2001; Bebout et al., 2013).

On the contrary, Marschall et al. (2009) investigated metamafic rocks collected from Greece by comparing B/Be and Li/Be ratios of these rocks with those obtained from metasomatic rocks. They concluded that lithium concentration is a good indicator of retrograde metasomatic processes and that boron abundance can be used to trace prograde dehydration.

Whole rock abundances of boron and lithium are affected by several factors such as infiltration of external fluids and fluid release due to the dehydration. In order to document the details of these phenomena, information of deeply-seated fluid is required.

IV. Fluid inclusions as deep fluid samples

The emissions from volcanic activities indicate that a specific amount of aqueous fluid with fluid mobile components undergoes a geochemical cycle. Therefore, information on the nature of deeply-seated fluid itself is crucial. Despite the progress made in analytical techniques, direct observation of deeply-seated fluid remains a challenge. Because the deepest drilling core is far less than twenty kilometers, it is impossible to obtain samples tens of kilometers deep. Fortunately, however, high-pressure type

metamorphic rocks or some kind of mantle xenolith exposed on the Earth's surface make a clue. Constituent minerals of metamorphic rocks commonly contain fluid inclusions that can serve as a direct evidence of the deep fluid coexisting with the metamorphic rocks. The syn-metamorphic fluid inclusion can be defined as inclusions originating from fluids in equilibrium with a given mineral assemblage (Touret, 2001). Although such fluid inclusions are generally believed to preserve the fluid composition at the given *P*-*T* conditions, several degrees of reequilibration of the constituent fluid generally occur during the decompression and cooling of the rock (e.g., Vityk et al., 1994; Küster and Stöckhert, 1997; Boullier, 1999; Baumgartner et al., 2014).

Many researchers have reported the chemical analysis of fluid inclusions with respect to (1) chemical species, (2) major solute content of aqueous fluid, and (3) trace element composition of aqueous fluid. For (1) and (2), conventional techniques such as microthermometry and laser Raman microspectroscopy are available. For trace element analysis, however, extraction of inclusion-content from the host phase can be a powerful tool for analyzing the trace element composition of aqueous fluid. Roedder (1970) published a useful design for a crushing stage used for extraction of the inclusion content. A laser ablation technique is another method for determining the chemical compositions of fluid inclusions (Heinrich et al., 2003). As a non-destructive approach, quantitative analysis using proton-induced X-ray emission (PIXE) has also been established for this purpose (Kurosawa et al., 2003). However, such analytical strategies require a considerable amount of inclusion content for quantitative analysis. The aforementioned techniques require an inclusion size larger than several tens of microns, which is rare in metamorphic rocks.

The small sizes of the fluid inclusions in metamorphic rocks, which are commonly < 10 μm in high pressure type metamorphic rocks, create difficulties in quantitative determination of the chemical compositions of fluid inclusions. In order to perform a chemical analysis of very small object such as inclusions, it is advisable to accumulate an amount of similar materials sufficient for quantitative analysis. For example, laser-ablation in liquid (Okabayashi et al., 2011) is a powerful method for trace element analysis of a very thin layer (< 10 μm) of solid material. For fluid inclusion analysis, the crush-leach method (Bottrell et al., 1988; Banks and Yardley, 1992), is appropriate because in this technique, numerous fluid inclusions are accumulated by crushing the host material into a liquid medium.

V. Objective of the thesis

The objective of this thesis is to demonstrate the subduction-related cycle of boron and lithium, with special focus on the composition of aqueous fluid existing in the deep part of the subduction zone. In order to document the composition of the deep-origin fluid directly, we used metamorphic quartz veins developed parallel to the main schistosity of the host rock, because such veins can work as the container of the deep-origin fluid trapped as fluid inclusions (Nishimura et al., 2008; Yoshida and Hirajima, 2012). Because the stable *P*-*T* range of quartz is very wide, once a quartz vein develops in metamorphic rocks, the vein is retained through the *P*-*T* trajectory. Therefore, such types of veins are suitable for investigating the composition of deep-origin fluid.

However, the wide stability of quartz can be somewhat problematic because it rarely indicates the formation timing or fluid entrapment timing. In part 1 of this study, we evaluate the recorded *P*-*T* conditions of the fluid inclusion trapped during the

subduction stage of the rock. By using conventional microthermometry, Raman microcopy, and high-resolution three-dimensional morphological study using focused ion beam microsampling (FIB) and X-ray computed tomography (XCT), we estimate the bulk composition and density of the fluid inclusion. We obtained the result that the density of the fluid inclusion was frozen at the specific temperature of the decompression and cooling stage; therefore, the density of the fluid inclusion was no longer available for estimating the entrapment timing. FIB-microsampling was operated at the Department of Geology and Mineralogy, Kyoto University, by A. Miyake. The XCT imaging experiment was performed at BL47XU in SPring-8, with the approval of the Japan Synchrotron Radiation Research Institute (Proposal No. 2013B1459, A. Tsuchiyama), operated by the members of the mineralogy group of Kyoto University. EBSD analysis was performed by S. Ohi at the Department of Geology and Mineralogy, Kyoto University. Other analyses were performed by the author.

Part 2 of this study classifies the fabrics of the quartz veins and microtextures of the trapped fluid inclusions, on the basis of careful petrographical observation. In accordance with the results presented in part 1, we focus on the textures of the inclusions. Moreover, we extract the fluid inclusion by using the crush-leach method and determine the chemical composition of fluid trapped in the quartz vein. We combine petrographical observation and chemical composition analysis of the extracted fluids, to reveal the typical characteristics of the deep-origin fluids. The obtained characteristics had high salinity and B- and Li-enrichment, which is very similar to those obtained from specific hot spring water, known as Arima-type hydrothermal fluids. Furthermore, a simple model calculation is performed for fluid-related material transport in the subduction zone. The model calculation indicates that aqueous fluid

with a considerable amount of lithium and boron can be generated at the deep part of the subduction zone without a significant impact on the concentration in solid phases due to the small amount of dehydrated fluid. The considered model requires disequilibrium fluid transport in order to maintain the B- and Li-enrichment of the fluid until the shallow depth of the crust is reached. These results strongly indicate the existence of channelized fluid flow from the deep part of the subduction zone. The crush-leach experiment was performed at the Institute for Geothermal Sciences (IGS), Kyoto University, by the author with the assistance of members of the petrology group of Kyoto University. Chemical analyses of the extracted fluids were conducted at IGS by T. Mishima and T. Kobayashi.

References

Amita, K., Ohsawa, S., Nishimura, K., Yamada, M., Mishima, T., Kazahaya, K., Morikawa, N. and Hirajima, T. (2014) Origin of saline waters distributed along the Median Tectonic Line in southwest Japan: Hydrogeochemical investigation on possibility of derivation of metamorphic dehydrated fluid from subducting oceanic plate. *Journal of Japanese Association of Hydrological Sciences*, **44**, 17–38.

Banks, D. A. and Yardley, B. W. D. (1992) Crush-leach analysis of fluid inclusions in small natural and synthetic samples. *Geochimica et Cosmochimica Acta*, **56**, 245–248.

Baumgartner, M., Bakker, R. J. and Doppler, G. (2014) Re-equilibration of natural H_2O–CO_2–salt-rich fluid inclusions in quartz—Part 1: experiments in pure water at constant pressures and differential pressures at 600 ^{o}C. *Contributions to Mineralogy and Petrology*, **168**, 1017.

Bebout, G. E., Agard, P., Kobayashi, K., Moriguti, T. and Nakamura, E. (2013) Devolatilization history and trace element mobility in deeply subducted sedimentary rocks: Evidence from Western Alps HP/UHP suites. *Chemical Geology*, **342**, 1–20.

Bebout, G. E., Ryan, J. G. and Leeman, W. P. (1993) B-Be systematics in subduction-related metamorphic rocks: Characterization of the subducted component. *Geochimica et Cosmochimica Acta*, **57**, 2227–2237.

Bell, D. C., Russo, C. J. and Kolmykov, D. V (2012) 40 keV atomic resolution TEM. *Ultramicroscopy*, **114**, 31–37.

Bence, A. E. and Albee, A. L. (1968) Empirical correction factors for the electron microanalysis of silicates and oxides. *The Journal of Geology* ,**76**, 382–403.

Bottrell, S. H., Yardley, B. W. D. and Buckley, F. (1988) A modified crush-leach method for the analysis of fluid inclusion electrolytes. *Bulletin de minéralogie*, **111**, 279–290.

Boullier, A.-M. (1999) Fluid inclusions: tectonic indicators. *Journal of Structural Geology*, **21**, 1229–1235.

Brenan, J. M., Shaw, H. F., Phinney, D. and Ryerson, F. (1994) Rutile-aqueous fluid partitioning of Nb, Ta, Hf, Zr, U and Th: implications for high field strength element depletions in island-arc basalts. *Earth and Planetary Science Letters*, **128**, 327–339.

Chopin, C. (1984) Coesite and pure pyrope in high-grade blueschists of the Western Alps: a first record and some consequences. *Contributions to Mineralogy and Petrology*, **86**, 107–118.

Donnelly, T. W., Thompson, G. and Salisbury, M. H. (1980) The chemistry of altered basalts at site 417, Deep Sea Drilling Project Leg 75. *Institute Report of DSPS*, **51-53**, 1319–1330.

Hacker, B. R., Peacock, S. M., Abers, G. A. and Holloway, S. D. (2003) Subduction factory 2. Are intermediate-depth earthquakes in subducting slabs linked to metamorphic dehydration reactions? *Journal of Geophysical Research*, **108**.

Hawkesworth, C. J., Gallagher, K., Hergt, J. M. and McDermott, F. (1993) Mantle and slab contribution in arc magmas. *Annual Review of Earth and Planetary Sciences*, **21**, 175–204.

Heinrich, C. A., Pettke, T. T., Halter, W. E., Aigner-Torres, M., Audétat, A., Günther, D., Hattendorf, B., Bleiner, D., Guillong, M. and Horn, I. (2003) Quantitative multi-element analysis of minerals, fluid and melt inclusions by laser-ablation inductively-coupled-plasma mass-spectrometry. *Geochimica et Cosmochimica Acta*, **67**, 3473–3497.

Jochum, K. P., Matus, L. and Seufert, H. M. (1988) Trace element analysis by laser plasma mass spectrometry. *Fresenius Zeitschrift für Analytische Chemie*, **331**, 136–139.

Karato, S., Paterson, M. S. and FitzGerald, J. D. (1986) Rheology of synthetic olivine aggregates: Influence of grain size and water. *Journal of Geophysical Research*, **91**, 8151–8176.

Kazahaya, K., Takahashi, M., Yasuhara, M., Nishio, Y., Inamura, A., Morikawa, N., Sato, T., Takahashi, H. a., Kitaoka, K., Ohsawa, S., Oyama, Y., Ohwada, M., Tsukamoto, H., Horiguchi, K., Tosaki, Y. and Kirita, T. (2014) Spatial distribution and feature of slab-related deep-seated fluid in SW Japan. *Journal of Japanese Association of Hydrological Sciences*, **44**, 3–16.

Kelemen, P. B., Shimizu, N. and Dunn, T. (1993) Relative depletion of niobium in some arc magmas and the continental crust: partitioning of K, Nb, La and Ce during melt/rock reaction in the upper mantle. *Earth and Planetary Science Letters*, **120**, 111–134.

Konrad-Schmolke, M. and Halama, R. (2014) Combined thermodynamic–geochemical modeling in metamorphic geology: Boron as tracer of fluid–rock interaction. *Lithos*, **208-209**, 393–414.

Kurosawa, M., Shimano, S., Ishii, S., Shima, K., Nakajima, T. and Kato, T. (2003) Quantitative PIXE analysis of single fluid inclusions in quartz vein: Chemical

composition of hydrothermal fluids related to granite. *Nuclear Instruments and Methods in Physics Research Section B: Beam Interactions with Materials and Atoms*, **210**, 464–467.

Kushiro, I., Yoder, H. and Nishikawa, M. (1968) Effect of water on the melting of enstatite. *Geological Society of America Bulletin*, **79**, 1685.

Küster, M. and Stöckhert, B. (1997) Density changes of fluid inclusions in high-pressure low-temperature metamorphic rocks from Crete: A thermobarometric approach based on the creep strength of the host minerals. *Lithos*, **41**, 151–167.

Leeman, W. P. and Sisson, V. B. (1996) Geochemistry of boron and its implications for crustal and mantle processes. *Reviews in Mineralogy and Geochemistry*, **33**, 645–707.

Marschall, H. R., Altherr, R., Gméling, K. and Kasztovszky, Z. (2009) Lithium, boron and chlorine as tracers for metasomatism in high-pressure metamorphic rocks: a case study from Syros (Greece). *Mineralogy and Petrology*, **95**, 291–302.

Marschall, H. R., Altherr, R., Ludwig, T., Kalt, A., Gméling, K. and Kasztovszky, Z. (2006) Partitioning and budget of Li, Be and B in high-pressure metamorphic rocks. *Geochimica et Cosmochimica Acta*, **70**, 4750–4769.

Marschall, H. R., Altherr, R. and Rüpke, L. (2007) Squeezing out the slab–modelling the release of Li, Be and B during progressive high-pressure metamorphism. *Chemical Geology*, **239**, 323–335.

Matsubaya, O., Sakai, H., Kusachi, I. and Satake, H. (1973) Hydrogen and oxygen isotopic ratios and major element chemistry of Japanese thermal water systems. *Geochemical Journal*, **7**, 123–151.

Miller, W. R. and Drever, J. I. (1977) Chemical weathering and related controls on surface water chemistry in the Absaroka Mountains, Wyoming. *Geochimica et Cosmochimica Acta*, **41**, 1693–1702.

Nakamura, H. and Iwamori, H. (2009) Contribution of slab-fluid in arc magmas beneath the Japan arcs. *Gondwana Research*, **16**, 431–445.

Nakano, T. and Nakamura, E. (2001) Boron isotope geochemistry of metasedimentary rocks and tourmalines in a subduction zone metamorphic suite. *Physics of The Earth and Planetary Interiors*, **127**, 233–252.

Nishimura, K., Amita, K., Ohsawa, S., Kobayashi, T. and Hirajima, T. (2008) Chemical characteristics and trapping P-T conditions of fluid inclusions in quartz veins from the Sanbagawa metamorphic belt, SW Japan. *Journal of Mineralogical and Petrological Sciences*, **103**, 94–99.

Ohsawa, S., Amita, K., Yamada, M., Mishima, T. and Kazahaya, K. (2010) Geochemical features and genetic process of hot-spring waters discharged from deep hot-spring wells in the Miyazaki Plain, Kyushu Island, Japan: Diagenetic dehydrated fluid as a source fluid of hot-spring water. *Journal of Hot Spring Science*, **59**, 295–319.

Okabayashi, S., Yokoyama, T. D., Kon, Y., Yamamoto, S., Yokoyama, T. and Hirata, T. (2011) Evaluation of Laser Ablation in Liquid (LAL) technique as a new sampling technique for elemental and isotopic analysis using ICP-mass spectrometry. *Journal of Analytical Atomic Spectrometry*, **26**, 1393.

Roedder, E. (1970) Application of an improved crushing stage to studies of gases in fluid inclusions. *Schweizersche Mineralogische und Petrographische Mitteilungen*, **50**, 41–58.

Seyfried, Jr. W. E., Janecky, D. and Mottl, M. (1984) Alteration of the oceanic crust: Implications for geochemical cycles of lithium and boron. *Geochimica et Cosmochimica Acta*, **48**, 557–569.

Shaw, D. M., Vatin-Perignon, N. and Muysson, J. R. (1977) Lithium in spilites. *Geochimica et Cosmochimica Acta*, **41**, 1601–1607.

Smith, D. C. (1984) Coesite in clinopyroxene in the Caledonides and its implications for geodynamics. *Nature*, **310**, 641–644.

Touret, J. L. . (2001) Fluids in metamorphic rocks. *Lithos*, **55**, 1–25.

Vityk, M. O., Bodnar, R. J. and Schmidt C. S. (1994) Fluid inclusions as tectonothermobarometers: Relation between pressure-temperature history and reequilibration morphology during crustal thickening. *Geology*, **22**, 731–734.

Yoshida, K. and Hirajima, T. (2012) Annular fluid inclusions from a quartz vein intercalated with metapelites from the Besshi area of the Sanbagawa belt, SW Japan. *Journal of Mineralogical and Petrological Sciences*, **107**, 50–55.

Part 1: Recorded density of fluid inclusions trapped in metamorphosed quartz veins: aspects from the morphological study by the FIB-XCT technique

1.1. Introduction

Fluid inclusions, which are characterized by a cavity filled with fluid phases within a solid phase, are a common feature in natural minerals of various occurrences. The trapped fluids are often considered to represent the environment of fluid entrapment, either chemically or physically, and are thus good candidates for investigating the nature of fluid activity under various fluid-rock interaction processes such as ore formation, metasomatism, and metamorphism (e.g., Kurosawa et al., 2010; Scambelluri et al., 2004; Touret, 2001; Van den Kerkhof et al., 1991; Yoshida et al., 2011). In the case of high-grade metamorphic rocks, fluid inclusions are thought to be originally trapped as a homogeneous single-phase (supercritical) fluid, but they commonly show phase-separation into more than two phases under laboratory conditions. In the laboratory, the bulk density of inclusions can be estimated using the experimental database on pressure, temperature, molar volume, and compositional (*P*-*T*-*V*-*x*) properties. However, when analyzing aqueous inclusions with a considerable amount of volatile components, such as CO_2, CH_4, and N_2, it can be difficult to estimate the bulk properties of the inclusions (e.g., Bakker and Diamond, 2006; Raimbourg et al., 2014). The greatest uncertainty for bulk property estimation of fluid inclusions is generally derived from the phase volume fraction and bulk volume estimations (Diamond, 2003).

Morphological study of small inclusions is sometimes useful for deducing the thermal history of igneous/metamorphic rocks (e.g., Asada et al., 2002). A few studies have used the approaches of exposing inclusion cavities on the surface of a thin section and observing the wall of the inclusions after fluid-escape. Hochella et al. (1990) performed detailed surface micro-texture analysis of an albite crystal using an atomic-force microscope (AFM) and found a faceted pocket on a cleavage surface, which was interpreted as the remnant of a primary fluid inclusion. Some researchers have carried out transmission electron microscopy (TEM) on fluid minerals containing fluid inclusions, and have described microstructures such as dislocations around inclusions (e.g., Bakker and Jansen 1994; Boullier et al., 1989; Vityk et al., 2000). These techniques provide an advantage for studying very tiny inclusions, as TEM observations make it possible to describe the outline of submicron-scale fluid inclusions (Vityk et al., 2000). However, most of these techniques are destructive to the fluid inclusions and therefore make it impossible to estimate the volume fraction of fluid phases.

For fluid inclusions containing fluorescent hydrocarbon molecule, such as petroleum-bearing inclusions, volume fractions can be determined with acceptable accuracy by using scanning confocal fluorescent microscopy (Pironon et al., 1998; Aplin et al., 1999). However, such inclusions are not very common, especially in metamorphic rocks. For precise estimation of volumetric data, fluid inclusionists have developed techniques to determine volume fractions under an optical microscope with special equipment such as the spindle stage (Anderson & Bodnar, 1993; Bakker and Diamond., 2006). Bakker and Diamond (2006) observed synthetic fluid inclusions showing a variety of shapes and investigated the relationship between their two-dimensional area-fractions and the calculated volume-fractions for synthetic conditions.

They suggested that the two-dimensional area-fraction can be approximated as the volume fraction of phases, when it is observed at the angle at which the projection area is the maximum. This method is acceptable for fairly large inclusions (probably better to apply for inclusions with diameters >10 μm). On the other hand, a mass balance calculation can be performed to estimate phase volume fractions for fluid inclusions with known densities (Bodnar, 1983). Recently, an improved approach for such mass balance calculations was proposed for simple systems such as H_2O-NaCl-CH_4 based on a combination of Raman spectroscopic data and *P-T-V-x* properties, resulting in good precision for the estimation of bulk density and composition (Becker et al., 2010). Despite these developments, it remains difficult to estimate the volumetric property of inclusions with tiny size and complex compositions, which are common in natural metamorphic rocks.

X-ray computed tomography (XCT) is a method for non-destructive three-dimensional observation of materials. Synchrotron radiation-based high-resolution XCT imaging provides sub-micron scale spatial resolution and can be applied for microstructural analysis of extraterrestrial materials, such as cometary particles (Tsuchiyama et al., 2014a; Zolensky et al., 2006), micrometeorites (Tsuchiyama et al., 2009), particles on an asteroid surface (Tsuchiyama et al., 2011; Tsuchiyama et al., 2014a), and nanoglobules in meteorites (Matsumoto et al., 2013). Furthermore, recent progress on the focused ion beam (FIB) system has achieved a microsampling from an area of interest with very good precision (Reyntjens & Puers, 2001; Wirth, 2004). Combination of these techniques can provide seamless three-dimensional (3D) observation of sample from thin section scale to micrometer or further fine resolution (Miyake et al., 2014).

The goal of this study was a detailed morphological examination of a fluid inclusion using FIB microsampling and high-resolution XCT imaging. The high-resolution XCT image provides precise phase volume fractions of the fluid inclusion, which is indispensable information for determining the nature of trapped fluid. By using the volume fractions, we also estimated the bulk properties of the inclusion, which indicate reequilibration of the density during exhumation of the metamorphic rock. Mineral abbreviations are after Whitney and Evans (2010) and symbols for fluid inclusion properties are after Bakker (2011).

1.2. Experimental Methods

FIB microsampling and XCT imaging were performed for one typical fluid inclusion after conventional petrographical observation on fluid inclusions and their host minerals. Qualitative/semi-quantitative analyses of the fluid inclusions were performed by a laser Raman spectrophotometer (JASCO, NRS-3100) at the Department of Geology and Mineralogy, Kyoto University, using the 514.5 nm line of Ar ion at 5-40 mW with a spot size of 1.0 μm on the sample surface. Calibration was performed using the 520 cm^{-1} Si-wafer band and neon (Ne) spectrum.

After the petrographical observation, one typical inclusion was chosen for XCT three-dimensional observation. In order to perform XCT on a specific fluid inclusion, a microsample of quartz containing a fluid inclusion was picked up from the thin section, using the focused ion beam (FIB) system (FEI, Quanta 200 3DS) at the Department of Geology and Mineralogy, Kyoto University (Miyake et al., 2012; Tsuchiyama et al., 2014b; Miyake et al., 2014). The FIB system used a Ga^{+} ion gun at the conditions of 30

kV and 3-65 nA. A specific area (ca. 20 × 20 μm^2) of the quartz was cut out to a depth of ca. 20 μm like an upside-down “house” shape by FIB. Then obtained “house” was held at the tip of a tungsten needle with platinum (Fig. 1.1) and observed by an imaging tomography system using a Fresnel zone plate at BL47XU in SPring-8, a synchrotron facility in Japan (Uesugi et al., 2006). The imaging experiment was performed at the X-ray energy of 7 keV, with the voxel size of 71.6 × 71.6 × 71.6 nm, which provided an effective spatial resolution of 200-300 nm. CT images were reconstructed from 1800 projection images (0.1 deg/projection) by using a convolution back-projection algorithm (Nakano et al., 2000). It took about 20 minutes to image the sample. The three-dimensional (3D) structure was obtained by stacking successive CT images taken of different slices through the particle. The obtained 3D-CT images were processed (e.g., binarization) and analyzed using the software package ‘Slice’ (Nakano et al., 2006).

To investigate the relationship between facets of the fluid inclusion and the crystal orientation of its host quartz, we measured the crystal orientation of the host quartz in the original thin section using a field emission scanning microscope (FE-SEM) equipped with an electron-backscatter diffraction (EBSD) system (JEOL, JSM7001F) at the Department of Geology and Mineralogy, Kyoto University. A thin section polished with colloidal silica was analyzed, where the specimen tilted at 70º.

1.3. Studied Sample

1.3.1. Sample locality

The fluid inclusion sample used in this study was collected from the Sanbagawa metamorphic belt of the Besshi District, central Shikoku, Japan. The Sanbagawa metamorphic belt is a high-pressure intermediate type metamorphic belt, exposed mainly in southwest Japan (Fig. 1.2a), whose peak *P-T* conditions vary from pumpellyite-actinolite facies (300 ºC/ 0.5 GPa) to epidote-amphibolite facies (610 ºC/ 1.0 GPa) (Higashino, 1990; Enami et al., 1994). In the higher metamorphic grade part, eclogite facies rocks are locally present (Takasu, 1984; Wallis & Aoya, 2000; Endo et al., 2012; Aoya et al., 2013).

The Iratsu body is the largest coarse-grained amphibolite body with an areal extent of ca. 7 × 2 km in the Besshi District, central Shikoku (Kugimiya & Takasu, 2002; Endo, 2010; Endo et al., 2009). The metamorphic history of the western part of the Iratsu body (WI body) is thought to have two distinct metamorphic stages: early metamorphism at the high-pressure amphibolite facies conditions (660 ºC and 1.2 GPa, Endo et al., 2012) and subsequent eclogite-facies metamorphism (525-565 ºC and 1.9-2.1 GPa, Endo, 2010).

The studied sample IR04 was collected from the western margin area of the WI body, where the WI body contacts the Higashi-Akaishi peridotite body (Fig. 1.2b). Fluid inclusions were found in a foliation-parallel quartz vein intercalated with a Grt-Hbl-Ph schist (Yoshida & Hirajima, 2012).

1.3.2. Occurrence of the fluid inclusions

Detailed petrographic studies on the fluid inclusions in the quartz vein indicated that three groups of fluid inclusions (groups 1, 2, and 3, in chronological order of entrapment) are observed in the studied quartz vein (Yoshida and Hirajima, 2012). Group 1 inclusions are arranged at intragranular fluid inclusion planes, and are composed of CH_4 gas and aqueous liquid with a salinity range of 7.0-8.7 mass%$_{NaCleq}$ (Na-Cl equivalent salinity). Rare annular-shaped fluid inclusions or large inclusion with implosion halos are observed in group 1 inclusions, the textures of which are thought to have originated from an increase of confining pressure and corresponding internal underpressure of the fluid inclusions. Group 2 inclusions are also arranged at intragranular fluid inclusion planes, but these inclusions are composed of the mixed volatile components of CH_4, N_2, CO_2, and H_2. Group 3 inclusions are arranged at transgranular fluid inclusion planes and are composed of aqueous liquid (8.8-9.5 mass%$_{NaCleq}$) and mixed gas of CH_4 and N_2. Based on textural observations and the finding of annular-shaped inclusions in group 1 inclusions, Yoshida and Hirajima (2012) concluded that (1) group 1 inclusions were trapped before the peak pressure stage, (2) group 2 inclusions were trapped near or during the peak pressure or temperature stage, and (3) group 3 inclusions were trapped during the early stage of exhumation.

In this study, we selected the fluid inclusion of group 1 for the morphological study. Since group 1 inclusions are trapped at prograde stage, they are expected to have suffered almost entire *P-T* evolution. Furthermore, the studied fluid inclusion is composed of the simple system of H_2O-NaCl-CH_4 and the estimated volumetric

properties and bulk compositions can be compared with those estimated by other methods in order to verify the quality of our analysis.

1.4. Results

1.4.1. Observation of CT images

Within the group 1 inclusions, we observed three kinds of inclusions: 1) annular-shaped inclusions; 2) inclusions with an implosion halo; 3) ordinary-shaped inclusions that do not show the above two textures. For the XCT study, we selected an ordinary-shaped, small-sized (~7 μm) inclusion (Fig. 1.3) because the annular-shaped and implosion halo type inclusions could have changed from their original composition due to the separation of fluid during annularization/implosion.

A set of CT images of the quartz microsample containing the fluid inclusion is shown in Figure 1.4a. Figure 1.4b shows a specific slice of the CT images. The observed contrast quantitatively indicates the difference in the X-ray linear absorption coefficient (LAC) of a material (or void), which is a function of the chemical composition and density (e.g., Tsuchiyama et al., 2013). Figure 1.4b clearly indicates that the bubble consists of a single phase and that there is no other liquid phase that is immiscible with the aqueous liquid. The interfaces among the host quartz, the aqueous liquid, and the bubble have bright and dark contrasts in the CT image, which are due to X-ray refraction at the interfaces (a material with a higher density has a brighter edge, and *vice versa*). The liquid and bubble were extracted from the 3D-CT images by binarization (Fig. 1.4c). Since the bubble and liquid phases have a moderate difference

of LAC, the binarization was done based on the discontinuous change of the contrasts at interphase boundaries and the inside of the interphase boundaries was treated as a single continuous phase. The wall of the fluid inclusion seems to have smooth surfaces.

Figures 1.5a and 1.5b show bird's eye views of the fluid inclusion. Figure 1.5a shows the wall of the inclusion together with a spherical bubble, which exists at the upper part of the fluid inclusion due to the gravity effect. Figure 1.5b shows only the inclusion wall. These figures clearly show that the outline of the fluid inclusion has a faceted shape (Figs. 1.5a, b). The individual facets seem to correspond to the crystallographic faces of α-quartz shown in Figure 1.5b. Hereafter, we refer to the facets m', r' and z', adding primes to the corresponding crystallographic faces, m, r and z, respectively (Figure 1.5b). We identify c'-axis, which correspond to the c-axis of α-quartz, as the direction of the edge between two m' surfaces.

Based on the three-dimensional CT image, the bubble occupies a volume of 11.8 μm^3 whereas the volume of liquid is 86.4 μm^3. The uncertainty of the volume cannot be evaluated theoretically, but it is expected to be fairly small (maximum of 1-3 μm^3). The calculated volume fraction of the vapor phase (φ_{vap} = volume of vapor / total volume) from the volumetric data is 0.12.

1.4.2. Morphology of the fluid inclusion

In order to investigate the relationships between facets of the fluid inclusion, we measured the interfacial angles between the facets using the binary images of the inclusion.

We made two slices along the directions shown in Figure 1.6a for measurement of the interfacial angles (Fig. 1.6b). Slice A in Figure 1.6b is almost perpendicular to the c'-axis, thus the sides of the hexagonal shape show the relationship among m' surfaces. As shown in this figure, m' surfaces join together at angles ranging 116-123º, which are mostly identical to the crystallographic interfacial angle of m surfaces of α-quartz (120º). Slice B shown in Figure 1.6b is almost parallel to the c'-axis, and show the relationship between r'/z' and m' surfaces. The interfacial angles range 138-146º, similar to the interfacial angle between r/z and m surfaces of α-quartz (142º).

The crystallographic orientation of the host quartz (a- and c-axes) determined by the EBSD analysis is plotted in a stereo projection in Figure 1.6c. The c'-axis and the poles of m' surfaces of the fluid inclusion, which were measured by the slice perpendicular to the c'-axis (Fig. 1.6b-A), are also plotted in the same diagram. Figure 1.6c shows clear accordance between the c-axis of the host quartz and c'-axis of the inclusion. The plane indices of m surfaces of α-quartz are {1 0 -1 0} and {1 -1 0 0}, and thus, the poles of the m' surface have a direction of ~30º to the a-axes of the quartz. The consistent relationship between facets of the inclusion and the crystal orientation was verified by the combination of CT images and EBSD analysis.

1.4.3. Density of the fluid inclusion

Since group 1 inclusions contain a considerable amount of methane as vapor phase at room temperature, we estimated the bulk density and composition of the inclusion based on the volume fraction and density of each phase, after Nishimura et al. (2008). As shown in Figure 1.4b, the studied fluid inclusion has one liquid phase and one bubble.

Based on the CT image, the bubble has no immiscible phases, thus we can treat it as pure methane gas (whether this is gas or liquid is also checked by the internal pressure estimation below). The amount of H_2O in vapor phase and methane in liquid phase is also discussed below.

In order to consider the equation of state (EoS) of the bubble, its internal pressure was determined by Raman spectroscopy. The bubble part of the inclusion is composed of CH_4 and no other gas species was detected by Raman analysis. The internal pressure of the methane gas can be estimated from the downshift of the Raman peak position of the C-H symmetric stretching band (v_1) (e.g., Fabre and Couty, 1986; Lin et al., 2007). The relationship between downshift and internal pressure (P, in mega-pascals) can be expressed as follows (Lu et al., 2007):

$$P(\text{MPa}) = -0.0148D^5 - 0.1791D^4 - 0.8479D^3 - 1.765D^2 - 5.876D, \qquad (1)$$

where, D is defined as $D=v_{\text{sample}}- v_0$, the difference between the peak position of the sample (v_{sample}) and near zero pressure (v_0, measured under atmospheric pressure). The peak position of the methane v_1 band was further corrected using the Ne lines of 2851.38 and 2972.44 cm^{-1} (Fig. 1.7) and the following expression (Lin et al., 2007):

$$\nu_{\text{calibrated}}^{CH_4} = \nu_{\text{measured}}^{CH_4} + \frac{1}{2}(\nu_{\text{real}}^{\text{Ne, 2851.38}} - \nu_{\text{measured}}^{\text{Ne, 2851.38}} + \nu_{\text{real}}^{\text{Ne, 2972.44}} - \nu_{\text{measured}}^{\text{Ne, 2972.44}}) \qquad (2)$$

The studied inclusion shows the peak position of 2916.58 cm^{-1}, corresponding to an internal pressure of 5.5 MPa. Since the vapor phase coexists with the aqueous liquid, the vapor phase inevitably contains a small amount of vapor H_2O. The amount of vapor H_2O coexisting with aqueous liquid was calculated by the thermodynamic model (Duan & Mao, 2006) under the conditions of the room temperature (24 ºC), average salinity of the group 1 inclusions (7.7 mass%), and coexisting methane partial pressure (5.5 MPa).

The result shows that vapor H_2O takes up only 0.59 mol% in the vapor phase. This fraction is small and negligible compared with methane, thus methane can be treated as pure gas, as we assumed. The internal pressure of the methane gas was then calculated into the molar volume of 407.7 cm^3/mol (0.932 g/cm^3) (at 24 ºC) based on the thermodynamic property of Angus et al. (1978).

The density of the liquid phase was estimated using the software package BULK (Bakker, 2003) based on the thermodynamic model of Duan and Mao (2006) and Spivey et al. (2004) at the same conditions mentioned above. Methane solubility in the aqueous liquid at such conditions is as low as 0.047 mol/kgH_2O and considered to be negligible. The molar volume of the liquid phase was calculated as 17.6 cm^3/mol (at the salinity of 7.7 mass%).

Using the above-calculated properties, we estimated the bulk composition and bulk molar volume of the fluid inclusion. As mentioned above, the molar volume of the liquid and the vapor was 17.6 cm^3/mol and 407.7 cm^3/mol, respectively. Using these molar volumes and volume fractions, the bulk composition of the studied fluid inclusion was calculated as 91.8% H_2O, 0.5% CH_4, and 7.7% NaCl (in mass fraction). The bulk molar volume was then calculated using the following relationship:

$$\frac{1}{V_{\mathrm{m}}^{\mathrm{bulk}}} = \frac{\varphi_{\mathrm{liq}}}{V_{\mathrm{m}}^{\mathrm{liq}}} + \frac{\varphi_{\mathrm{vap}}}{V_{\mathrm{m}}^{\mathrm{vap}}}$$

resulting in the molar volume of 19.9 cm^3/mol.

The isochore of the fluid inclusion was calculated for the estimated bulk composition and bulk molar volume, by using LonerAP of the software package

FLUIDS 2 (Bakker, 2003; 2009) and applying the EoS of Anderko and Pitzer (1993) and Duan et al. (2003). The calculated isochore is shown in Figure 1.8.

1.5. Discussion and Implications

1.5.1. Comparison with other methods

Becker et al. (2010) proposed a calculation method to determine the bulk density of H_2O-NaCl-CH_4 fluid inclusions. Their method uses the input data including homogenization temperature, salinity of the aqueous phase, and pressure of the vapor phase. They performed the iterative calculation of the combination of the EoS for H_2O-NaCl-CH_4 (Duan et al., 2006) and the mass balance calculation (Bodnar, 1983) to finally obtain reliable bulk properties. We performed this calculation with our data obtained from the studied inclusion (homogenization temperature = 228 ºC, salinity = 7.7 mass%: Yoshida and Hirajima, 2012). The calculated results are the following: φ_{vap}=0.12; 91.75% H_2O, 0.59% CH_4, and 7.65% NaCl (in mass fraction). The calculated phase volume fraction is well consistent with those estimated from the CT data.

On the other hand, phase fractions can be approximated from the two-dimensional area fraction of each phase in the inclusion (Bakker and Diamond, 2006). Since the studied inclusion is small (<10 μm) and the phase boundaries have obscureness due to the refraction, the exact two-dimensional area fraction could not be determined easily. The measured area fraction for the studied inclusion yields φ_{vap}=0.17-0.19, a considerably higher value than the CT data.

According to the above comparisons, the quality of the XCT volume analysis is well comparable to that of the combination of microthermometry and *P-T-V-x* properties, whereas optical observation seems to have some difficulty due to the small size of the inclusion. In the case of suitable composition, microthermometric study can also be a powerful tool for tiny fluid inclusions. However, the important point is that XCT observation is applicable for volume analysis of multi-phase inclusions irrespective of their compositions. Morphological and volumetric studies on tiny fluid inclusions by means of the FIB-XCT technique should be considered to become a new investigative tool offering an improved understanding of fluid-rock interaction processes, especially those of high-pressure metamorphic rocks.

1.5.2. Reequilibration of the fluid inclusion density

Although fluid inclusions are thought to be a natural strongbox as a first approximation, it is known that fluid inclusions are generally modified in their volume to several degrees after entrapment, i.e., they are commonly reequilibrated (Pêcher, 1981; Sterner & Bodnar, 1984; Vityk & Bodnar, 1995). This means that the reequilibration of fluid inclusions can be used as a good tool for deciphering the history of environmental change (e.g., Bodnar, 2003; Boullier, 1999; Küster & Stöckhert, 1997; Vityk et al., 1994). Our petrographical observation showed that group 1 inclusions contain annular-shaped inclusions (Yoshida and Hirajima, 2012), flattened inclusions with an implosion halo, and negative-crystal-shaped inclusions. Since smaller inclusions require higher differential pressure for non-elastic reequilibration (Bodnar et al., 1989), specific

reequilibration textures (annular shape and implosion halos) are thought to be observed only in large inclusions.

On the other hand, the densities of small fluid inclusions showing negative crystal shapes are also expected to have adapted to the *P-T* change, despite lacking significant reequilibration textures. When fluid inclusions suffer a slightly different condition from the original isochores, a dissolution-crystallization process would occur to adapt the density to new *P-T* conditions with or without significant texture (Gratier and Jenatton, 1984, Boullier, 1999). Experimental studies have shown that such non-textural reequilibration can be taken place within a few days to several weeks at around 500-600ºC, and are thus geologically rapid (Sterner and Bodnar, 1989; Vityk and Bodnar, 1995). Therefore, densities of all group 1 fluid inclusions are expected to have adapted to the *P-T* conditions near or around the peak pressure stage (ca. 600 ºC, 2.0GPa: Fig. 1.8). However, the estimated isochore of the studied inclusion is located at much lower pressure than the peak pressure stage of the host rock (Fig. 1.8). This result suggests that fluid inclusions are further reequilibrated during the decompression and cooling stage of the metamorphic rocks. Küster and Stöckhert (1997) indicated that the density of a fluid inclusion in quartz easily adapts to its surrounding *P-T* conditions above 300 ºC, i.e. the density closure temperature of the quartz is 300 ºC, based on the quartz flow law data set (Paterson & Luan, 1990). However, their indication considered only physical processes and ignored chemical processes such as the dissolution-crystallization process. Therefore, the mechanism and nature of the closure temperature of fluid inclusion density remain unclear to present. Figure 1.8 shows the peak *P-T* conditions and proposed exhumation *P-T* paths of the Sanbagawa metamorphic belt from the literature (Okamoto & Toriumi, 2004; Endo, 2010; Endo et al., 2012). The estimated isochore of

the studied fluid inclusion seems to crosscut the inferred exhumation *P-T* paths at ca. 560 ºC, 0.8 GPa, where fluid inclusions in quartz would easily adapt to the *P-T* changes (Küster and Stöckhert, 1997; Vityk and Bodnar, 1995). Therefore, the recorded density of the studied fluid inclusion would indicate much lower-*T* conditions. Exhumation *P-T* conditions of previous studies are based on the chemical equilibrium of silicate minerals and are thus mostly at temperatures higher than 350 ºC. If we extrapolate these *P-T* conditions to the lower temperature side (gray dashed arrow in Fig. 1.8), the hypothetical *P-T* path and estimated isochore would cross at around 300 ºC and 0.2-0.3 GPa (Fig. 1.8), although there could be a large error due to the low angle difference between isochore and exhumation *P-T* path. This result possibly suggests that the density closure temperature of fluid inclusions in quartz could be near 300 ºC as indicated by Küster and Stöckhert (1997), even though their assumption seems to have the above-mentioned problems.

References

Anderko, A. & Pitzer, K. S. (1993) Equation-of-state representation of phase equilibria and volumetric properties of the system NaCl-H_2O above 573 K. *Geochimica et Cosmochimica Acta*, **57**, 1657–1680.

Anderson, A. J. & Bodnar, R. J. (1993) An adaptation of the spindle stage for geometric analysis of fluid inclusions. *American Mineralogist*, **78**, 657–664.

Angus, S., Armstrong, B., de Reuck, K. M. (1978) International thermodynamic tables of the fluid state. 5. Methane., Pergamon Press, Oxford.

Aoya, M., Noda, A., Mizuno, K., Mizukami, T., Miyachi, Y., Matsuura, H., Endo, S., Toshimitsu, S., Aoki, M. (2013) Geology of the Niihama District. Quadrangle Series, 1 :50,000., Geological Survery of Japan, AIST.

Aplin, A. C., Macleod, G., Larter, S. R., Pedersen, K. S., Sorensen, H., Booth, T. (1999) Combined use of Confocal Laser Scanning Microscopyand PVT simulation for estimating the composition andphysical properties of petroleum in fluid inclusions. *Marine and Petroleum Geology*, **16**, 97–110.

Asada, R., Shimobayashi, N., Kitamura, M. (2002) Equilibrium form of negative crystals in igneous quartz. *Journal of Mineralogical and Petrological Sciences*, **97**, 59–69.

Bakker, R. J. (2003) Package FLUIDS 1. Computer programs for analysis of fluid inclusion data and for modelling bulk fluid properties. *Chemical Geology*, **194**, 3–23.

Bakker, R. J. (2009) Package FLUIDS. Part 3: correlations between equations of state, thermodynamics and fluid inclusions. *Geofluids*, **9**, 63–74.

Bakker, R. J. (2011) The use of quantities, units and symbols in fluid inclusion research. *Berichte der Geologischen Bundesanstalt*, **87**, 5–11.

Bakker, R. J. & Diamond, L. W. (2006) Estimation of volume fractions of liquid and vapor phases in fluid inclusions, and definition of inclusion shapes. *American Mineralogist*, **91**, 635–657.

Bakker, R. & Jansen, J. (1994) A mechanism for preferential H2O leakage from fluid inclusions in quartz, based on TEM observations. *Contributions to Mineralogy and Petrology*, **4**, 7–20.

Becker, S. P., Eichhubl, P., Laubach, S. E., Reed, R. M., Lander, R. H., Bodnar R. J. (2010) A 48 m.y. history of fracture opening, temperature, and fluid pressure:

Cretaceous Travis Peak Formation, East Texas basin. *Geological Society of America Bulletin*, **122**, 1081–1093.

Bodnar, R. J. (1983) A method of calculating fluid inclusion volumes based on vapor bubble diameters and P-V-T-X properties of inclusion fluids. *Economic Geology*, **78**, 535–542.

Bodnar, R. J. (2003) Reequilibration of Fluid Inclusions. In *Fluid Inclusions: Analysis and Interpretation* (eds. I. Samson, A. Anderson, and D. Marshall). Mineralogical Association of Canada,. pp. 213–230.

Bodnar, R. J., Binns, P. R., Hall, D. L. (1989) Synthetic fluid inclusion - VI. Quantitative evaluation of the decrepitation behaviour of fluid inclusions in quartz at one atmosphere confining pressure. *Journal of Metamorphic Geology*, **7**, 229–242.

Boullier A.-M. (1999) Fluid inclusions: tectonic indicators. *Journal of Structural Geology*, **21**, 1229–1235.

Boullier, A.-M., Michot, G., Pêcher, A., Barres, O. (1989) Diffusion and/or plastic deformation around fluid inclusions in synthetic quartz: new investigations. In *Fluid Movements — Element Transport and the Composition of the Deep Crust* (ed. D. Bridgwater). Springer Netherlands. pp. 345–360.

Diamond, L. W. (2003) Introduction to gas-bearing aqueous fluid inclusions. In *Fluid Inclusions: Analysis and Interpretation* (eds. I. Samson, A. Anderson, and D. Marshall). Mineralogical Association of Canada, pp. 101–158.

Duan, Z., Møller, N., Weare, J. H. (2003) Equations of state for the NaCl-H_2O-CH_4 system and the NaCl-H_2O-CO_2-CH_4 system. *Geochimica et Cosmochimica Acta*, **67**, 671–680.

Duan, Z. & Mao, S. (2006) A thermodynamic model for calculating methane solubility, density and gas phase composition of methane-bearing aqueous fluids from 273 to 523K and from 1 to 2000bar. *Geochimica et Cosmochimica Acta*, **70**, 3369–3386.

Enami, M., Wallis, S. R., Banno, Y. (1994) Paragenesis of sodic pyroxene-bearing quartz schists: implications for the P-T history of the Sanbagawa belt. *Contributions to Mineralogy and Petrology*, **116**, 182–198.

Endo, S., Wallis, S. R., Hirata, T., Anczkiewicz, R., Platt, J., Thirlwall, M., Asahara, Y. (2009) Age and early metamorphic history of the Sanbagawa belt: Lu-Hf and P - T constraints from the Western Iratsu eclogite. *Journal of Metamorphic Geology*, **27**, 371–384.

Endo, S. (2010) Pressure-temperature history of titanite-bearing eclogite from the Western Iratsu body, Sanbagawa Metamorphic Belt, Japan. *Island Arc*, **19**, 313–335.

Endo, S., Wallis, S. R., Tsuboi, M., Aoya, M., Uehara S. (2012) Slow subduction and buoyant exhumation of the Sanbagawa eclogite. *Lithos*, **146-147**, 183–201.

Fabre, D. & Couty, R. (1986) Investigation on the density effects in the Raman-spectrum of methane up to 3,000 bar - application to the determination of pressure in fluid inclusions trapped in minerals. *Comptes Rendus l Acad. des Sci. Ser. II*, **303**, 1305–1308.

Gratter, J. P. & Jenatton, L. (1984) Deformation by solution-deposition, and re-equilibration of fluid inclusions in crystals depending on temperature, internal pressure and stress. *Journal of Structural Geology*, **6**, 189–200.

Higashino, T. (1990) The higher grade metamorphic zonation of the Sambagawa metamorphic belt in central Shikoku, Japan. *Journal of Metamorphic Geology*, **8**, 413–423.

Hochella, M. F. J., Eggleston, C. M., Elings, V. B., Thompson M. S. (1990) Atomic structure and morphology of the albite (010) surface: An atomic-force microscope and electron diffraction study. *American Mineralogist*, **75**, 723–730.

Kugimiya Y. & Takasu A. (2002) Geology of the Western Iratsu mass within the tectonic merange zone in the Sambagawa metamorphic belt, Besshi district, central Shikoku, Japan. *Journal of Geological Society of Japan*, **108**, 644–662 (In Japanese).

Kurosawa, M., Ishii, S., Sasa K. (2010) Trace-element compositions of single fluid inclusions in the Kofu granite, Japan: Implications for compositions of granite-derived fluids. *Island Arc*, **19**, 40–59.

Küster, M. & Stöckhert, B. (1997) Density changes of fluid inclusions in high-pressure low-temperature metamorphic rocks from Crete: A thermobarometric approach based on the creep strength of the host minerals. *Lithos*, **41**, 151–167.

Lin, F., Bodnar, R. J., Becker, S. P. (2007) Experimental determination of the Raman CH4 symmetric stretching (v1) band position from 1–650bar and 0.3–22°C: Application to fluid inclusion studies. *Geochimica et Cosmochimica Acta*, **71**, 3746–3756.

Lu, W., Chou, I.-M., Burruss, R. C., Song, Y. (2007) A unified equation for calculating methane vapor pressures in the CH_4–H_2O system with measured Raman shifts. *Geochimica et Cosmochimica Acta*, **71**, 3969–3978.

Matsumoto, T., Tsuchiyama, A., Nakamura-Messenger, K., Nakano, T., Uesug,i K., Takeuchi, A., Zolensky, M. E. (2013) Three-dimensional observation and morphological analysis of organic nanoglobules in a carbonaceous chondrite using X-ray micro-tomography. *Geochimica et Cosmochimica Acta*, **116**, 84–95.

Miyake, A., Ikeda, M., Yoshida, K., Tsuchiyama, A., Seto, Y., Toh, S. (2012) Phase analysis of inclusions in mineral. In *The Abstracts with Program 2012 Annual Meeting of Japan Association of Mineralogical Sciences* p. 69.

Miyake, A., Matsuno, J., Toh, S. (2014) Sample preparation toward seamless 3D imaging technique from micrometer to nanometer scale. *Microscopy*, **63**, i24–i25. doi:10.1093/jmicro/dfu055

Nakano, T., Nakashima, Y., Nakamura, K., Ikeda, S. (2000) Observation and analysis of internal structure of rock using X-ray CT. *Journal of Geological Society of Japan*, **106**, 363–378.

Nakano, T., Tsuchiyama, A., Uesugi, K., Uesugi, M., Shinohara K. (2006) "Slice" - Softwares for basic 3-D analysis-, Slice Home Page (http://www-bl20.spring8.or.jp/slice/). *Japan Synchrotron Radiation Research Institute (JASRI).*

Nishimura, K., Amita, K., Ohsawa, S., Kobayashi, T., Hirajima, T. (2008) Chemical characteristics and trapping P-T conditions of fluid inclusions in quartz veins from the Sanbagawa metamorphic belt, SW Japan. *Journal of Mineralogical and Petrological Sciences*, **103**, 94–99.

Okamoto, A. & Toriumi, M. (2004) Optimal mixing properties of calcic and subcalcic amphiboles: application of Gibbs' method to the Sanbagawa schists, SW Japan. *Contributions to Mineralogy and Petrology*, **146**, 529–545.

Paterson, M. S. & Luan, F. C. (1990) Quartzite rheology under geological conditions. In *Deformation Mechanisms, Rheology and Tectonics.* (eds. R. J. Knipe and E. H. Rutter). Geological Society, London. pp. 299–307.

Pêcher, A. (1981) Experimental decrepitation and re-equilibration of fluid inclusions in synthetic quartz. *Tectonophysics*, **78**, 567–583.

Pironon, J., Canals, M., Dubessy, J., Walgenwitz, F., Laplace-Builhe, C. (1998) Volumetric reconstruction of individual oil inclusions by confocal scanning laser microscopy. *European Journal of Mineralogy*, **10**, 1143–1150.

Raimbourg, H., Thiéry, R., Vacelet, M., Ramboz, C., Cluzel, N., Le Trong, E., Yamaguchi, A., Kimura, G. (2014) A new method of reconstituting the P–T conditions of fluid circulation in an accretionary prism (Shimanto, Japan) from microthermometry of methane-bearing aqueous inclusions. *Geochimica et Cosmochimica Acta*, **125**, 96–109.

Reyntjens, S. & Puers, R. (2001) A review of focused ion beam applications in microsystem technology. *Journal of Micromechanics and Microengineering*, **11**, 287–300.

Scambelluri, M., Müntener, O., Ottolini, L., Pettke, T. T., Vannucci, R. (2004) The fate of B, Cl and Li in the subducted oceanic mantle and in the antigorite breakdown fluids. *Earth and Planetary Science Letters*, **222**, 217–234.

Spivey, J. P., Mccainm, W. D., North, R. (2004) Estimating density, formation volume factor, compressibility, methane solubility, and viscosity for oilfield brines at temperatures from 0 to 275 C, pressures to 200 MPa, and salinities to 5.7 mole/kg. *Journal of Canadian Petroleum Technology*, **43**, 52–61.

Sterner, S. M. & Bodnar, R. J. (1984) Synthetic fluid inclusions in natural quartz I. Compositional types synthesized and applications to experimental geochemistry. *Geochimica et Cosmochimica Acta*, **48**, 2659–2668.

Sterner, S. M. & Bodnar, R. J. (1989) Synthetic fluid inclusions - VII. Re-equilibration of fluid inclusions in quartz during laboratory-simulated metamorphic burial and uplift. *Journal of Metamorphic Geology*, **7**, 243–260.

Takasu, A. (1984) Prograde and retrograde eclogites in the Sambagawa metamorphic belt, Besshi district, Japan. *Journal of Petrology*, **25**, 619–643.

Touret, J. L. (2001) Fluids in metamorphic rocks. *Lithos*, **55**, 1–25.

Tsuchiyama, A., Nakamura, T., Okazaki, T., Uesugi, K., Nakano, T., Sakamoto, K., Akaki, T., Iida, Y., Kadono, T., Jogo, K., Suzuki, Y. (2009) Three-dimensional structures and elemental distributions of Stardust impact tracks using synchrotron microtomography and X-ray fluorescence analysis. *Meteoritics & Planetary Science*, **44**, 1203–1224.

Tsuchiyama, A., Uesugi, M., Matsushima, T., Michikami, T., Kadono, T., Nakamura, T., Uesugi, K., Nakano, T., Sandford, S. A, Noguchi, R., Matsumoto, T., Matsuno, J., Nagano, T., Imai, Y., Takeuchi, A., Suzuki, Y., Ogami, T., Katagiri, J., Ebihara, M., Ireland, T. R., Kitajima, F., Nagao, K., Naraoka, H., Noguchi, T., Okazaki, R., Yurimoto, H., Zolensky, M. E., Mukai, T., Abe, M., Yada, T., Fujimura, A., Yoshikawa M., Kawaguchi J. (2011) Three-dimensional structure of Hayabusa samples: Origin and evolution of Itokawa regolith. *Science*, **333**, 1125–1128.

Tsuchiyama, A., Nakano, T., Uesugi, K., Uesugi, M., Takeuchi, A., Suzuki, Y., Noguchi, R., Matsumoto, T., Matsuno, J., Nagano, T., Imai, Y., Nakamura, T., Ogami, T., Noguchi, T., Abe, M., Yada, T., Fujimura, A. (2013) Analytical dual-energy microtomography: A new method for obtaining three-dimensional mineral phase images and its application to Hayabusa samples. *Geochimica et Cosmochimica Acta*, **116**, 5–16.

Tsuchiyama, A., Uesugi, M., Uesugi, K., Nakano, T., Noguchi, R., Matsumoto, T., Matsuno, J., Nagano, T., Imai, Y., Shimada, A., Takeuchi, A., Suzuki, Y., Nakamura, T., Noguchi, T., Abe, M., Yada, T., Fujimura, A. (2014a) Three-dimensional microstructure of samples recovered from asteroid 25143 Itokawa: Comparison with LL5 and LL6 chondrite particles. *Meteoritics & Planetary Science*, **49**, 172–187.

Tsuchiyama, A., Miyake, A., Zolensky, M. E., Uesugi, K., Takeuchi, A., Suzuki, Y., Nakano, T., Yoshida, K. (2014b) Search for solar system primitive water from meteorites using FIB and tomography. In *The 70th Annual Meeting of the Japanese Society of Microscopy* pp. 13amD_SP3–04.

Uesugi, K., Takeuchi, A., Suzuki, Y. (2006) Development of micro-tomography system with Fresnel zone plate optics at SPring-8. *Proceedings of SPIE*, **6318**, 63181F.

Van den Kerkhof, A., Touret, J.L.R., Maijer, C., Jansen, J. (1991) Retrograde methane-dominated fluid inclusions from high-temperature granulites of Rogaland, southwestern Norway. *Geochimica et Cosmochimica Acta*, **55**, 2533–2544.

Vityk, M. O. & Bodnar, R. J. (1995) Textural evolution of synthetic fluid inclusions in quartz during reequilibration, with applications to tectonic reconstruction. *Contributions to Mineralogy and Petrology*, **121**, 309–323.

Vityk, M. O., Bodnar, R. J., Schmidt, C. S. (1994) Fluid inclusions as tectonothermobarometers: Relation between pressure-temperature history and reequilibration morphology during crustal thickening. *Geology*, **22**, 731–734.

Vityk, M. O., Bodnar, R. J., Doukhan, J. (2000) Synthetic fluid inclusions. XV. TEM investigation of plastic flow associated with reequilibration of fluid inclusions in natural quartz. *Contributions to Mineralogy and Petrology*, 285–297.

Wallis, S. R. & Aoya, M. (2000) A re-evaluation of eclogite facies metamorphism in SW Japan: proposal for an eclogite nappe. *Journal of Metamorphic Geology*, **18**, 653–664.

Whitney, D. L. & Evans, B. W. (2010) Abbreviations for names of rock-forming minerals. *American Mineralogist*, **95**, 185–187.

Wirth, R. (2004) Focused Ion Beam (FIB) A novel technology for advanced application of micro-and nanoanalysis in geosciences and applied mineralogy. *European Journal of Mineralogy*, **16**, 863–876.

Yoshida, K. & Hirajima, T. (2012) Annular fluid inclusions from a quartz vein intercalated with metapelites from the Besshi area of the Sanbagawa belt, SW Japan. *Journal of Mineralogical and Petrological Sciences*, **107**, 50–55.

Yoshida, K., Sengen, Y., Tsuchiya, S., Minagawa, K., Kobayashi, T., Mishima, T., Ohsawa, S., Hirajima, T. (2011) Fluid inclusions with high Li/B ratio in a quartz vein from the Besshi area of the Sambagawa metamorphic belt: implications for deep geofluid evolution. *Journal of Mineralogical and Petrological Sciences*, **106**, 164–168.

Zolensky, M.E., Zega, T.J., Yano, H., Wirick, S., Westphal, A.J., Weisberg, M.K., Weber, I., Warren, J.L., Velbel, M. a, Tsuchiyama, A., Tsou, P., Toppani, A., Tomioka, N., Tomeoka, K., Teslich, N., Taheri, M., Susini, J., Stroud, R., Stephan, T., Stadermann, F.J., Snead, C.J., Simon, S.B., Simionovici, A., See, T.H., Robert, F., Rietmeijer, F.J.M., Rao, W., Perronnet, M.C., Papanastassiou, D. A, Okudaira, K., Ohsumi, K., Ohnishi, I., Nakamura-Messenger, K., Nakamura, T., Mostefaoui, S., Mikouchi, T., Meibom, A., Matrajt, G., Marcus, M. a, Leroux, H., Lemelle, L., Le, L., Lanzirotti, A., Langenhorst, F., Krot, A.N., Keller, L.P., Kearsley, A.T., Joswiak, D., Jacob, D., Ishii, H., Harvey, R., Hagiya, K., Grossman, L., Grossman, J.N., Graham, G. a, Gounelle, M., Gillet, P., Genge, M.J., Flynn, G., Ferroir, T., Fallon, S., Fakra, S., Ebel, D.S., Dai, Z.R., Cordier, P., Clark, B., Chi, M., Butterworth, A.L., Brownlee, D.E., Bridges, J.C., Brennan, S., Brearley, A., Bradley, J.P., Bleuet, P., Bland, P. A, Bastien, R. (2006) Mineralogy and petrology of comet 81P/Wild 2 nucleus samples. *Science.*, **314**, 1735–1739.

Schematic image of microsampling "house"

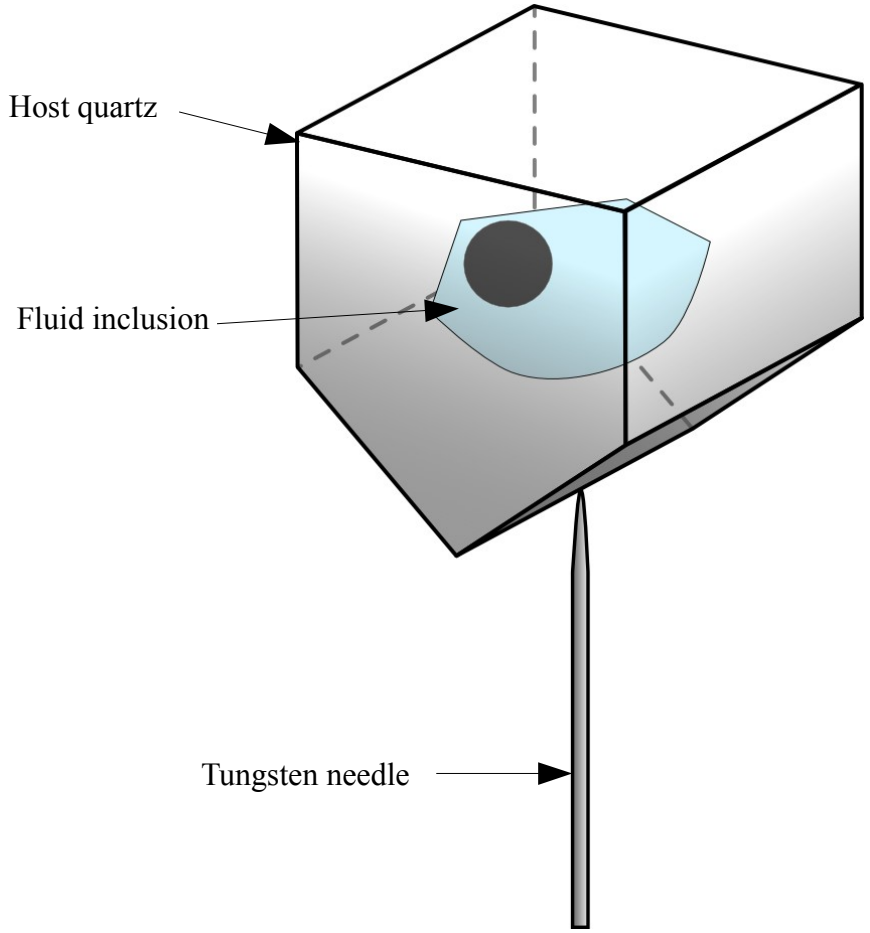

Fig. 1.1

A specific area (ca. 20 × 20 μm²) of the quartz was cut out to a depth of ca. 20 μm showing an upside-down "house" shape. Then "house" was held at the tip of a tungsten needle with platinum

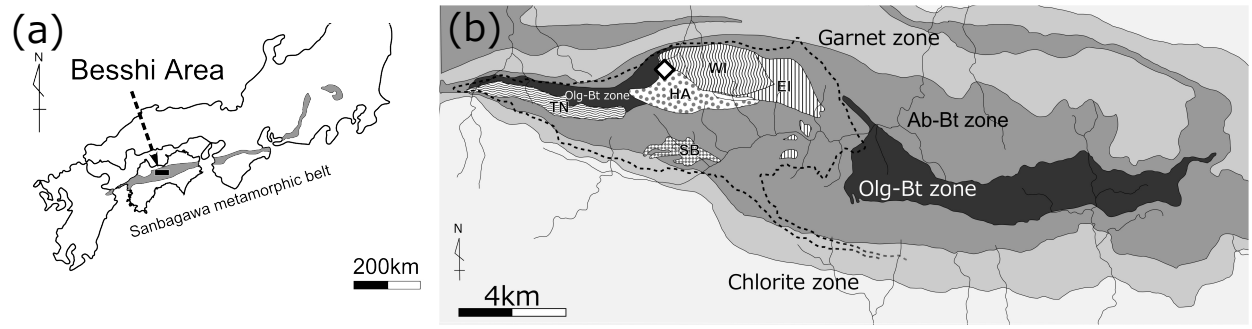

Fig. 1.2

(a) Distribution of the Sanbagawa metamorphic belt in Japan and in the study area, Besshi District, Shikoku. (b) Metamorphic zone map of the study area. Grayscale shows the metamorphic zonation of the chlorite, garnet, albite-biotite, and oligoclase-biotite zone defined by the mineral assemblage of pelitic schists (Higashino, 1990). Representative eclogite masses are abbreviated as: WI, Western Iratsu body; EI, Eastern Iratsu body; HA, Higashi-Akaishi peridotite body; TN, Tonaru body; and SB, Seba body. Inside area of the broken line is supposed to have suffered eclogite-facies metamorphism once (Aoya *et al*., 2013). The sampling locality is shown as the open diamond located at the western edge of the WI body near the contact with the HA body.

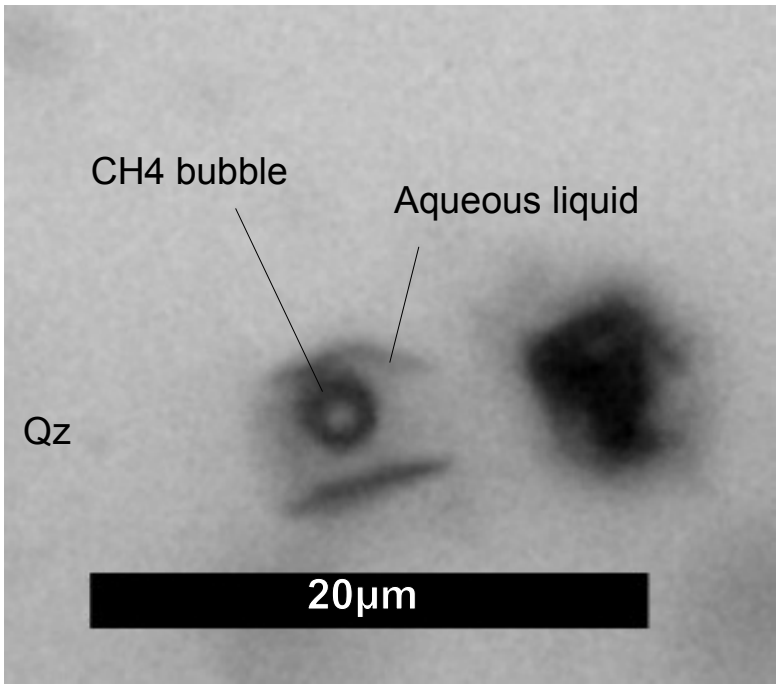

Fig. 1.3

Microphotograph of the group 1 fluid inclusion used for XCT study. The inclusion shows an angulated shape.

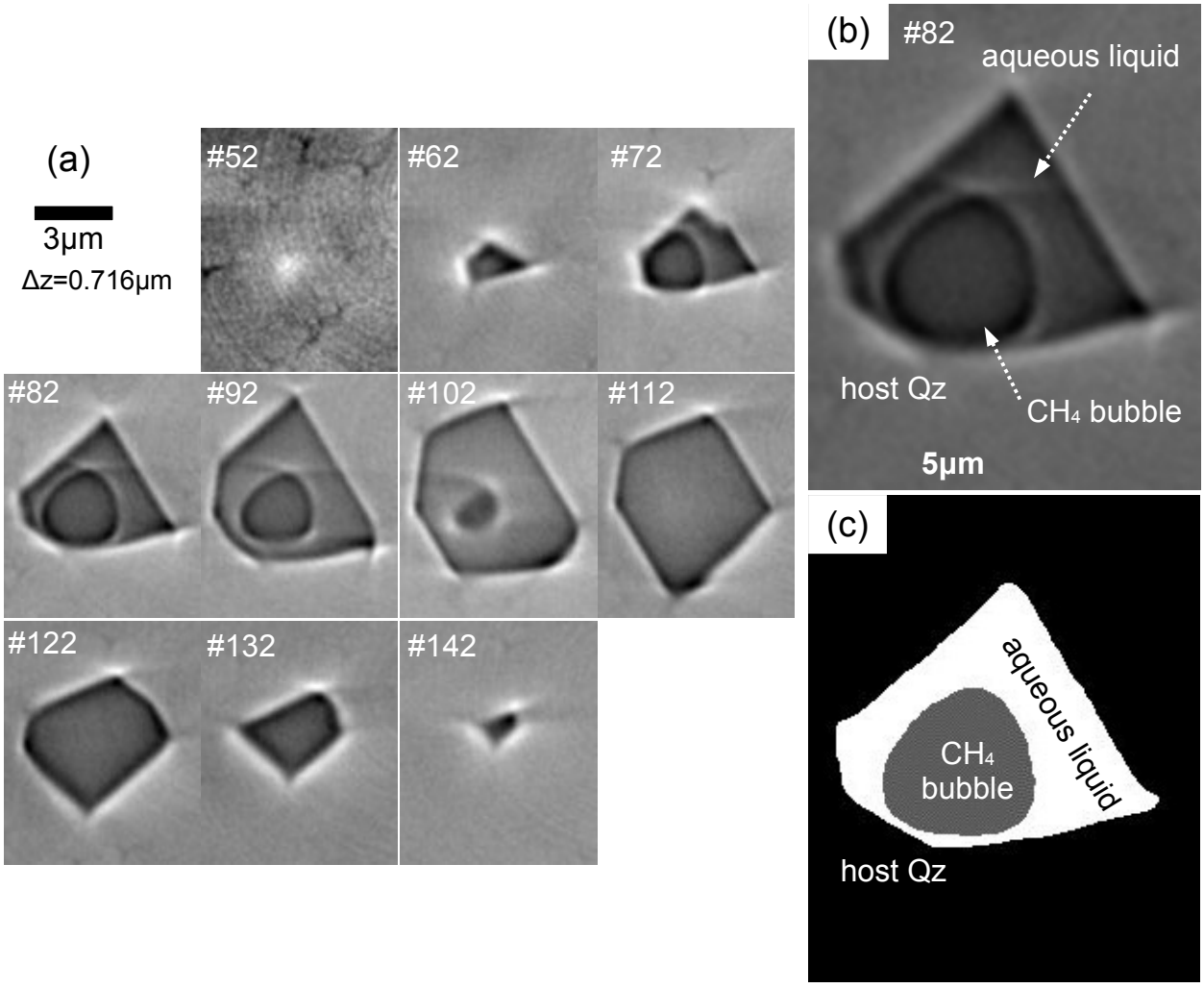

Fig. 1.4

(a) A set of successive three-dimensional CT images of the quartz particle containing a fluid inclusion, at every 10 slices (0.716 μm interval). Concentric rings are artifacts (ring artifact). (b) A specific slice of the X-ray CT data of the studied fluid inclusion. Grayscale corresponds to the density of the specimen and shows the darkest CH_4 bubble, slightly brighter aqueous liquid, and bright host quartz. (c) Binarized image of Figure 1.4b, showing the distribution of host quartz, CH_4 bubble, and aqueous fluid.

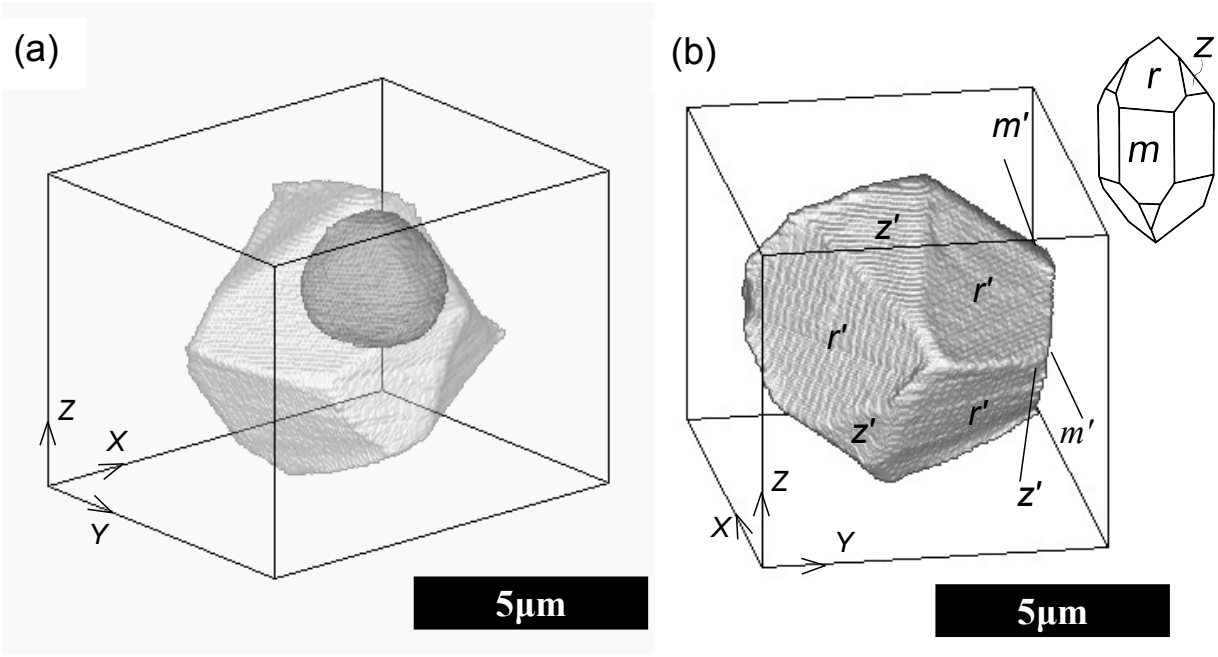

Fig. 1.5

(a) A bird's eye view of the fluid inclusion shown in Fig. 1.3. The bright-colored faceted object is the wall of the fluid inclusion and the dark-colored spherical object inby is the bubble. Three dimensional directions are shown by the capital X, Y, and Z. (b) A bird's eye view from a different direction, focused on the inclusion surface and not showing the bubble. "*r* ′", "*z* ′", and "*m* ′" are r', z', and m' surfaces, respectively (please see the text for details). Simplified crystallographic facial relationship of α-quartz is also shown for comparison. Whether this is right-handed or left-handed is not shown. "*r*", "*z*", and "*m*" are r, z, and m surfaces, respectively.

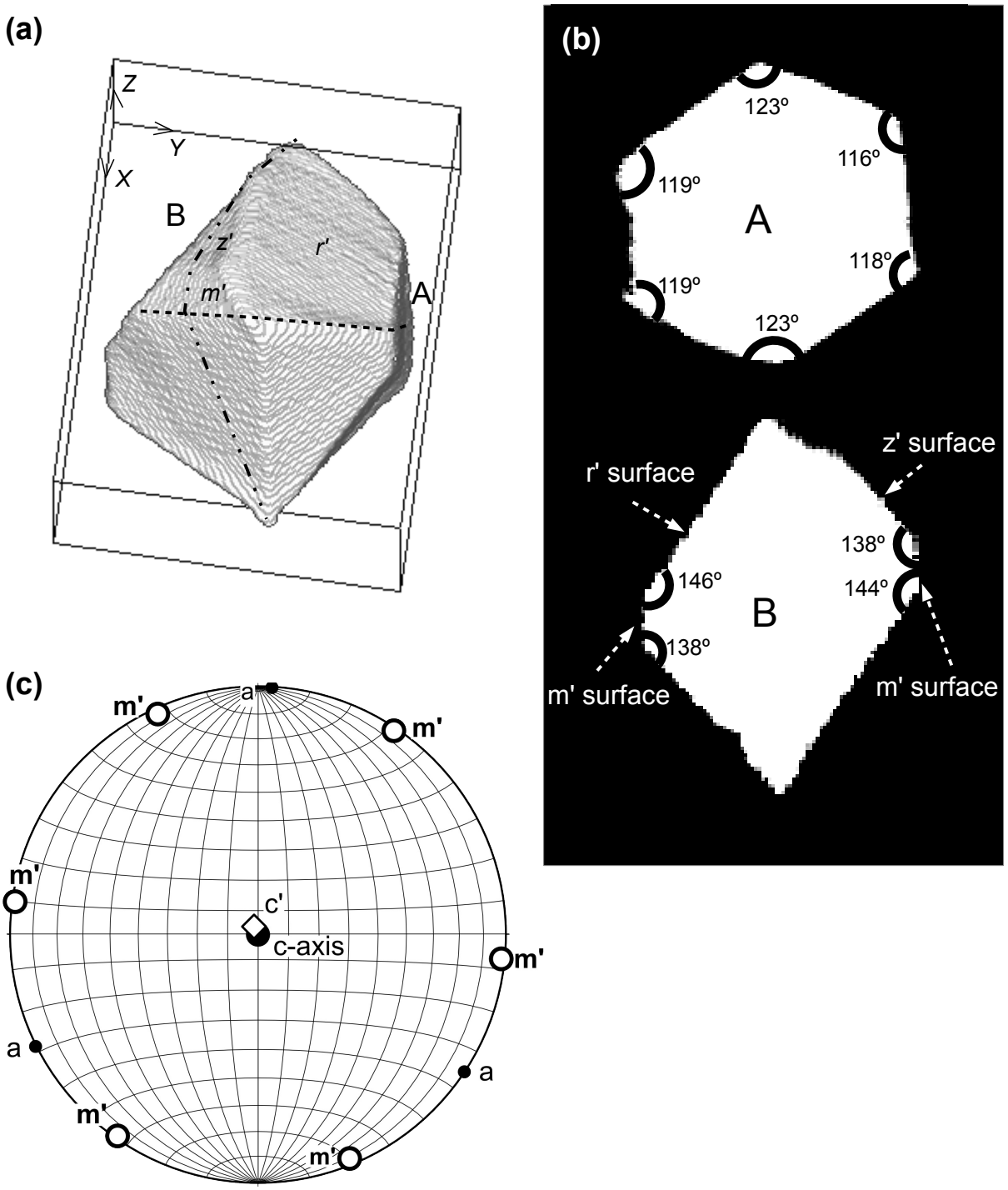

Fig. 1.6

(a) The slice direction of A and B in Figure 1.6b are shown. The A direction is shown by the broken line, which is perpendicular to the c' axis, and the B direction is shown as a double dotted line, which is parallel to the c' axis. X, Y, and Z are the same coordinate as shown in Fig. 1.5. (b) Slice images of the plane shown in Figure 1.6a. (c) The relationship between the facets of the fluid inclusion and the orientation of the host quartz. The stereo-plot is shown from the direction of c-axis of the host quartz. The c-axis of the host quartz and c'-axis of the fluid inclusion plot very near one another, and the poles of m' surfaces also have a specific relationship with the a-axis of the host quartz.

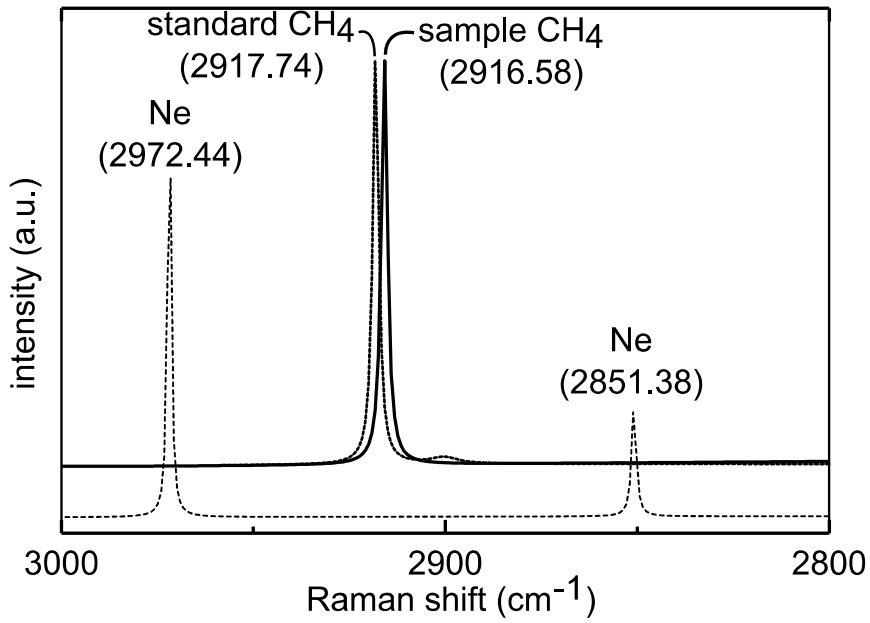

Fig. 1.7

Raman spectrum of the methane in the studied fluid inclusion, with neon peaks at 2972 and 2851 cm^{-1}. The methane peak measured at atmospheric pressure is also shown as the standard methane. Methane contained in the fluid inclusion shows a downshift of the peak position by ca. 1 cm^{-1}, corresponding to 5.5 MPa (please see text for details).

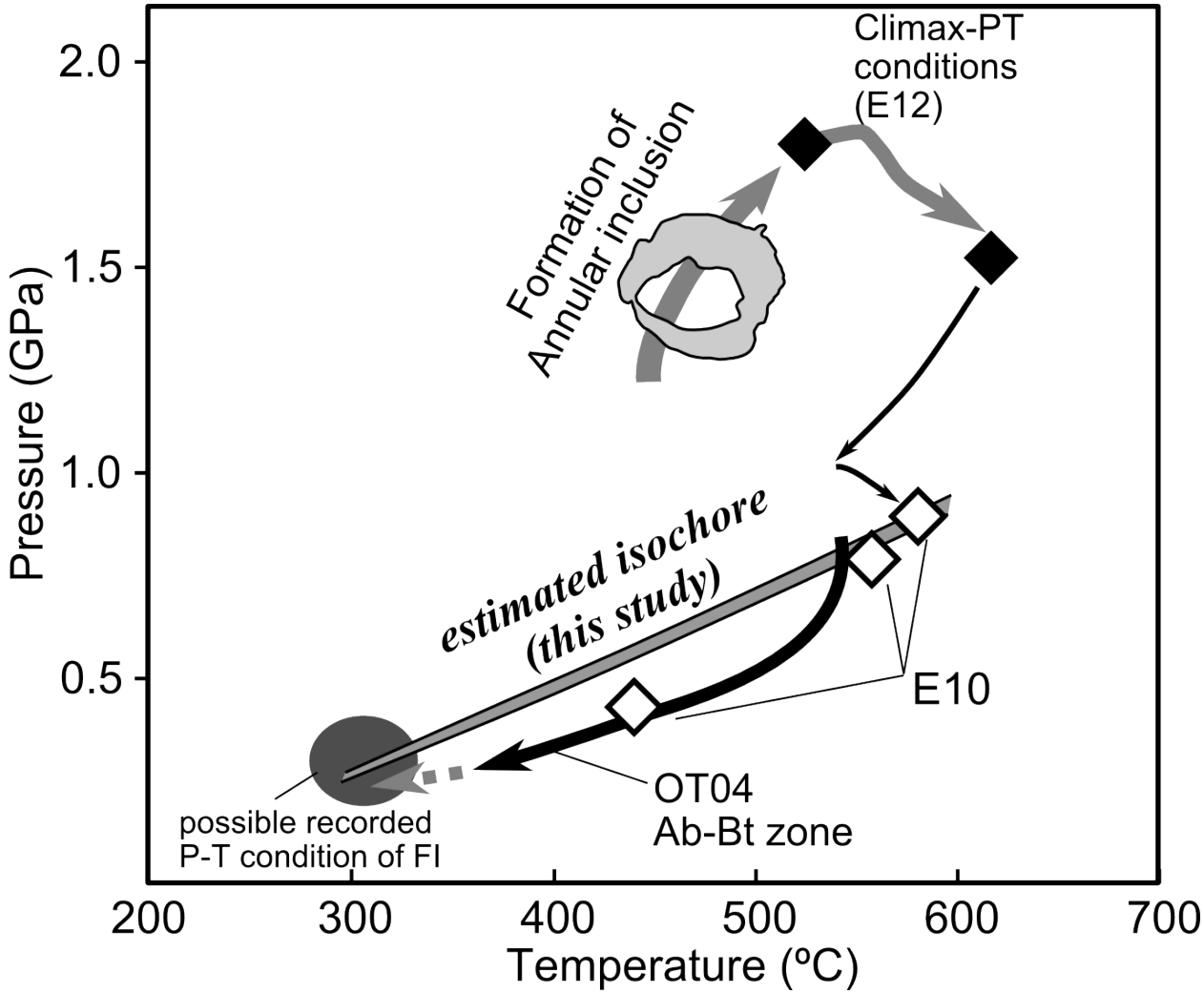

Fig. 1.8

The estimated isochore of the studied fluid inclusion is shown as a gray line with a black edge. The inferred exhumation *P-T* path of the studied rock from the climax *P-T* conditions (ca. 650 ºC) to the lower temperature condition (350 ºC) estimated mainly by chemical equilibrium. The dotted gray line is the extrapolation of the previous studies. Abbreviations are: OT04, Okamoto and Toriumi (2004); E10, Endo (2010); E12, Endo *et al*. (2012).

Part 2: Geochemical features of fluids trapped in high-pressure type metamorphic rocks

2.1. Introduction

Aqueous fluids in subduction zones play an important role in geochemical and geophysical processes, such as slab seismicity, arc magmatism, metamorphism, mantle metasomatism, and the transport of several components to the surface from the deep part of the earth (Tatsumi, 1989; Bebout, 2007; Hacker, 2008). Such fluids are generally believed to originate from mineral-bound water in hydrous minerals in the subducting materials, and pore-fluids carried by oceanic sediments. The latter are occasionally assumed to be expelled at very shallow depths (<~5 km) due to compaction (Peacock, 1990; Jarrard, 2003; Hacker, 2008), however, some amount of marine pore-fluids survive at depths of ~100 km (Sumino et al., 2010). Although dehydrated aqueous fluids have been treated as pure water as a first approximation in many previous studies, natural aqueous fluids found from metamorphic rocks occasionally contain a considerable amount of solute, sometimes showing higher salinity than halite saturation (Yardley & Graham, 2002). The chemical composition of the fluids, such as the chlorine content, affects the solubility/mobility of some specific elements (e.g., Newton and Manning, 2010; Higashino et al., 2013), thus the chemical compositions of major elements in natural deep fluids provide indispensable information for understanding the role of deep fluids in subduction zones.

Minor light elements such as lithium and boron are thought to be good tracers during fluid migration and fluid-rock interaction including hydrothermal alteration in

oceanic crusts and dehydration/hydration reactions in subduction zones (Bebout, 2007; Bebout et al., 1999; Konrad-Schmolke et al., 2011; Marschall et al., 2009; Seyfried et al., 1984). Those elements tend to be relatively highly concentrated in altered oceanic crusts and pelagic sediments (Donnelly et al., 1980; Shaw et al., 1977; Leeman & Sisson, 1996) because of the high temperature hydrothermal process (Seyfried et al., 1984). To quantify the mass transport during magma processes in subduction zones, behaviors of lithium and boron in hydrothermal systems have been investigated experimentally (You et al., 1996; Kogiso et al., 1997; Brenan et al., 1998; Tenthorey & Hermann, 2004; Kessel et al., 2005). Experimental and natural sample studies have determined preliminary estimates of partition coefficients of these elements (Brenan et al., 1998; Tenthorey & Hermann, 2004; Marschall et al., 2006). Based on simple mass balance calculations, some studies indicated that the concentration ratios of the above-mentioned elements in fluid, i.e. Be/B, B/Cl, and Li/B, increase with dehydration degree, that is to say, the progress of metamorphism (Bebout et al., 1993; Scambelluri et al., 2004; Marschall et al., 2007). It should be noted that such mass balance calculations are strongly dependent on the whole rock composition and related whole rock partition coefficient (Domanik et al., 1993; Marschall et al., 2007; Yoshida et al., 2011).

Recent geochemical studies of hot- and mineral-springs indicate that B- and/or Li-rich hot-spring waters are directly derived from the subducting-slab to the surface region upward to the crustal surface (Ohsawa, 2004; Ohsawa et al., 2010; Kazahaya et al., 2014; Kusuda et al., 2014). Ohsawa (2004) and Kazahaya et al. (2014) suggested that the high Li/Cl ratio of hot-spring water is an indicator of the deep-origin slab derived fluid, so called Arima-type hydrothermal fluids (Matsubaya et al., 1973). Such fluids are characterized by high salinity, high $^{3}He/^{4}He$ ratio, heavy oxygen isotope ratio,

and light hydrogen isotope ratio compared to the modern sea water. Ohsawa et al. (2010) also pointed out that the composition of hot-spring waters collected from the Miyazaki plain, in the fore-arc region of southwest Japan, are high in B concentrations, and that their high B/Cl ratio are originated from the diagenetic dehydration of smectite at around 130ºC. They showed that some Li- and B-rich spring waters originated from diagenetic/metamorphic processes and also experienced subsequent groundwater dilution.

Fluid inclusions preserved in H*P*/L*T* metamorphic rocks provide direct information on the subduction-related fluids which develop under the fore-arc to sub-arc region, and provide clues to interpret the results of the geochemical studies mentioned above. However, few studies deal with the trace element chemistry of the fluid phase, because of the difficulty of the analysis mainly derived from the small size of fluid inclusions, even though a number of fluid inclusion studies have been performed with respect to the metamorphic and/or tectonic processes (Boullier, 1999; Küster & Stöckhert, 1997; Bakker & Mamtani, 2000; Touret, 2001; Van den Kerkhof, 2001; Krenn et al., 2008; Nishimura et al., 2008; Krenn, 2010). One possible solution to this problem is the crush-leach method (Bottrell et al., 1988; Banks & Yardley, 1992) applied to quartz veins developed parallel to the main foliation of the metamorphic rocks, which are capable of retaining pre-peak-/peak-metamorphic stage fluids as fluid inclusions (Nishimura et al., 2008; Yoshida & Hirajima, 2012).

In order to directly determine the chemical compositions of deep fluids and evaluate their signature with respect to their entrapment depth, we carried out systematic sampling of foliation-parallel quartz veins in the Sanbagawa belt, Japan,

which covers the formation depths from ca. 15 km to 60 km, and performed petrographical and geochemical studies on fluid inclusions. Our results show that fluid inclusions in such quartz veins have highly Li- and B-enriched compositions similar to those of Arima-type hydrothermal fluids. Among the studied samples, quartz veins with less-deformed textures retain fluid inclusions with higher salinities and high Li/Cl and/or B/Cl compositions. In this part, we show the mode of occurrence and chemical characteristics of fluid inclusions trapped in quartz veins. We also discuss about the relative B-Li-Cl compositions of the fluids and their significance to geofluid evolution during prograde metamorphism in subduction zones. Mineral abbreviations are after Whitney and Evans (2010).

2.2. Analytical method

Chemical compositions of minerals are analyzed with an electron microprobe analyzer with five wavelength-dispersive spectrometers (JEOL, JXA-8105) at the Department of Geology and Mineralogy, Kyoto University. Some qualitative and semi-quantitative analyses were also performed on a scanning electron microprobe (HITACHI, S-3500H) equipped with an energy-dispersive spectrometer (EDAX, Phoenix) at Kyoto University.

Microthermometric measurements of fluid inclusions were performed using a heating and cooling stage (LINKAM, LK-600) at the Department of Geology and Mineralogy, Kyoto University. The stage was calibrated with a melting-point of synthetic fluid inclusion standards (10 mass% NaCl solution and pure water). The accuracy of the ice melting temperatures within the range -80 to 0 ºC was estimated to be ±0.1 ºC at a heating rate of 2 ºC/min, and for the homogenization temperatures

within the range from 0 to 400 ºC, was ± 1 ºC at a heating rate of 10 ºC/min. Melting temperatures of aqueous fluids were converted into Na-Cl equivalent salinity ($mass\%_{NaCleq}$) using the equation of Bodnar (1993).

The qualitative analysis of fluid inclusions was carried out by using a laser Raman spectrophotometer (JASCO, NRS-3100) at the Department of Geology and Mineralogy, Kyoto University using the 514.5 nm line of Ar-ion at 10-80 mW with a spot size of 1.0 μm on the surface. Calibration was performed using a 520 cm^{-1} Si-wafer band and neon spectrum.

To determine the chemical characteristics of the aqueous fluid of fluid inclusions, we extracted fluids using the crush-leach method after Bottrell et al. (1988) and Banks and Yardley (1992). To prepare pure quartz grains, the vein sample was roughly crushed and sieved into 425–2000 μm size. Quartz grains without extraneous matters were handpicked under a stereoscopic microscope. Separated quartz grains were boiled in concentrated nitric acid and rinsed with ultrapure water to eliminate impurities. Some 50 g of cleaned sample was milled into white powder in an agate mortar, in order to crush-out the fluid inclusions. The milled powder was, then, transferred to a Teflon bottle and a solute of fluid inclusions were leached with 50–60 mL of ultrapure water (Wako Pure Chemical Industries, Ltd.: solutes are less than 10 pg/g in each element) as a “fluid inclusion solution” for major/trace component analysis. The solution sample with quartz powder was filtered out with 0.22 μm mesh filter before chemical analysis. Na^+, K^+, Ca^{2+}, Mg^{2+}, NH_4^+, F^-, Cl^- and SO_4^{2-} were analyzed by an ion chromatography (DIONEX, DX-120) at the Institute for Geothermal Sciences, Kyoto University, Beppu, Japan. The bicarbonate ion content was calculated by the valance of charge. Li and B

were analyzed by ICP-MS at TOSOH Analysis and Research Center, Nan-yo City, Yamaguchi, Japan. Blank values for the crush-leach technique were obtained either by water soaked in a Teflon bottle for about 12 hours to evaluate the contamination from the Teflon bottles (blank1), by rubbing the agate mortar and pouring ultrapure water into the mortar to be treated in the same manner as the samples for the contamination from the air and mortar (blank2). The values obtained from the blank1 is near zero and negligible, while blank2 contained a low amount of Li (0.11 μg/L) and a considerable amount of B (9.5 μg/L), which were subtracted from the raw data of the sample concentrations.

2.3. Geological background

Studied samples were collected from the Sanbagawa metamorphic belt, which is exposed in southwest Japan (Fig. 2.1a). The Sanbagawa metamorphic belt is divided into four mineral zones based on the mineral assemblages of pelitic schists (Kurata & Banno, 1974; Enami, 1982; Higashino, 1990): chlorite, garnet, albite-biotite and oligoclase-biotite zones. Peak metamorphic *P*-*T* conditions of the four mineral zones were estimated as 300 ºC/ 0.5 GPa for the lowest grade chlorite zone which is pumpellyite-actinolite facies equivalent, through 440–480 ºC/ 0.7–0.85 GPa for the garnet zone and 520–540 ºC/ 0.8–0.95 GPa for the albite-biotite zone, to 610 ºC/ 1.0 GPa for the highest grade of oligoclase-biotite zone which is epidote-amphibolite facies equivalent (Enami, 1994). In central and eastern Shikoku, eclogite facies rocks are also locally present (Takasu, 1984; Wallis & Aoya, 2000; Ota et al., 2004). These eclogitic rocks show a pressure gap against surrounding non-eclogitic rocks, and some of them

show complex and different metamorphic histories before the juxtaposition with above-mentioned non-eclogitic rocks of the Sanbagawa belt (Takasu, 1984; Kunugiza et al., 1986).

Specifically, the investigated samples were collected from the Besshi area in central Shikoku (Fig. 2.1b) and the Wakayama area in Honshu Island (Fig. 2.1e). In the Besshi area, two eclogite units, the Western Iratsu (WI) body and the Seba (SB) body, and their neighboring non-eclogitic areas (Fig. 2.1c, d) were investigated. The WI body is thought to have suffered two distinct stages of subduction-related metamorphism, referred as M1 and M2, whose peak metamorphic conditions were estimated as ca. 660 ºC/ 1.2 GPa and 550–680 ºC/ 1.4–2.0 GPa, respectively (Fig. 2.1f: Endo, 2010; Endo et al., 2012). Peak metamorphic conditions of the Seba body are estimated as 520–640 ºC/ 1.3–2.4 GPa (Aoya, 2001; Zaw et al., 2005). Recent studies found remnants of eclogite facies metamorphism around these eclogite bodies and suggest that these eclogite bodies once consisted of continuous eclogite-nappe at eclogite facies conditions (Fig. 2.1c: Aoya et al., 2013; Kouketsu et al., 2010; 2014; Wallis and Aoya, 2000). The surrounding part of these eclogite units mainly belong to the albite- and oligoclase-biotite zone of the Sanbagawa metamorphic belt. Samples of lower metamorphic grades were collected from the Wakayama area where the chlorite, garnet and biotite zones are exposed (Fig. 2.1e: Makimoto et al., 2004). Since oligoclase is not observed in the biotite zone, the biotite zone of the Wakayama area is thought to be equivalent to the albite-biotite zone of central Shikoku. Thus, the samples investigated in this study cover the peak pressure range of 0.5–2.5 GPa and the temperature range of 300–610 ºC (Fig. 2.1f).

2.4. Investigated samples

In order to determine the deep fluid characteristics, we studied quartz veins developed parallel with the main foliation of the host rocks (hereafter foliation-parallel quartz vein) (Fig. 2.2, 2.3a-c). Some veins show the boudinaged shape concordant with the deformation structure of the host metamorphic rock, indicating pre-tectonic existence of veins, whereas others are only foliation-parallel occurrence concordant with the small deformation structure of the host rock. Such kind of veins has a potential to retain the fluid trapped during prograde or near-peak metamorphic conditions (Fig. 2.2: Nishimura et al., 2008; Yoshida and Hirajima, 2012). The studied veins are almost monomineralic, except for some samples contain very small amount of accessory minerals such as rutile and phengite. Nishimura et al. (2008) investigated a foliation-parallel quartz vein collected from chlorite zone of the Sanbagawa area, the Saganoseki area, SW Japan. They investigated the fluid inclusion in the quartz vein and found fluid inclusions possibly trapped at the peak metamorphic stage. Yoshida and Hirajima (2012) also investigated a foliation-parallel quartz vein (sample IR04 used in this study) intercalated with the eclogite facies rock and found annular shaped fluid inclusions which suggest the pressure increase after their entrapment. These findings indicate that foliation-parallel quartz veins can trap the fluid at the deep part of the subduction zone and can work as the container of the deep fluids.

Six samples from the non-eclogitic area and five samples from the eclogite unit were investigated in this study. A quartz vein sample crosscutting the main foliation of the host rock was also investigated to reveal the character of fluid activity during the very later stage of exhumation of the Sanbagawa belt (Fig. 2.3d). In this section, we describe the characteristics of the host rocks.

Volume fractions of the main constituent minerals of the host metamorphic rocks were determined using X-ray mapping of major elements for nine samples (Table 2.1). For other two samples, simple point counting based on either semi-quantitative multi-point analysis using EDX (Matsumoto & Hirajima, 2006) or optical microscopic observation was performed. Among the investigated samples, potential minerals to contain boron or lithium as main constituent (such as tourmaline, lepidolite…) were not observed. Representative chemical compositions of mica, amphibole, and apatite which are candidate for the container of the halogens at peak metamorphic conditions, are shown in Tables 2.2-4. However, all mica and amphibole contain no or scarce amount of halogens (mostly <0.01 mass%) and there is no obvious relationship between halogen content of minerals and fluid inclusion composition described in the following section. Apatites observed in some samples also contain small amount of Cl (up to 0.2 mass%) and are classified as fluorapatite (Table 2.4).

Chlorite zone (mafic: WS04)

One mafic rock sample (WS04) was chosen as a representative sample for the chlorite zone. WS04 is composed of the main metamorphic minerals of epidote, chlorite, actinolite, phengite, albite, titanite and quartz with a small amount of chalcopyrite. Later stage calcite veins cutting the main foliation are locally developed.

Garnet zone (mafic: WS02)

The investigated mafic schist (WS02) mainly consists of epidote, chlorite, amphibole, albite and phengite with small amounts of calcite, titanite and apatite. Later-stage calcite veins are also observed. Albite porphyroblasts contain epidote, chlorite, amphibole, quartz, calcite and titanite. Compositions of amphibole are from actinolite to magnesiohornblende.

Albite-biotite zone (mafic: 07113002)

This sample mainly consists of albite, phengite, epidote, amphibole, titanite and calcite with accessory apatite and chalcopyrite. Compositions of the amphiboles are barroisite and magnesiohornblende.

Albite-biotite zone (pelitic: SD09, IR28)

These samples are mainly composed of quartz, phengite, chlorite, albite and garnet with additional phases such as apatite (SD09) and amphibole (IR28). The garnet shows Mn bell shape type zoning with X_{Sps} up to 0.31 at their apparent core. SD09 was collected from near the boundary between the suggested eclogite-nappe and surrounding lower grade part, however, no remnant of eclogite-facies metamorphism was found in sample SD09, thus this sample is treated as a non-eclogitic sample.

Oligoclase-biotite zone (pelitic: IR27)

IR27 is a metapelite composed of quartz, phengite, plagioclase, garnet, amphibole and epidote with small amounts of iron oxide and rutile. Plagioclase contains anorthite component up to 10 mol%. The garnet shows Mn bell shape type zoning with X_{Sps} up to 0.26 at their apparent core.

Eclogite unit (mafic: SSB03, SSB04, SEBA, SSB19)

Four mafic rocks are collected from the Seba eclogite body. They consist mainly of quartz, phengite, garnet, chlorite, amphibole, epidote, rutile and hematite. Samples SEBA and SSB19 contain clinopyroxene (omphacite). In addition, sample SEBA contains biotite frequently associated with garnet, which was probably a product of the decompression stage. Samples SEBA and SSB19 also show relatively large grain size compared to other two samples. Main schistosity of the host rock is defined by the oriented occurrence of amphibole, epidote, and phengite if it is abundant. The occurrence of schistosity is relatively weak for the sample SSB03 and SSB04, while SSB19 and SEBA show the strong schistosity composed of coarse grained minerals. The former characteristic is comparable to that of R-type or I-type eclogite reported by Aoya and Wallis (1999) and the latter is comparable to L-type eclogite. Samples SSB03 and SSB04 are free of clinopyroxene even though they are collected from the eclogite unit, probably because of the bulk rock composition or some other reasons. Samples SEBA and SSB19 underwent rehydration reactions which decomposed clinopyroxene to symplectite of varying degrees.

Eclogite unit (metasediment: IR04)

The protolith of IR04 is thought to be a sedimentary rock with unique composition with very low SiO_2 content and contain very high amount of amphibole and phengite (>40 vol% respectively) (Yoshida & Hirajima, 2012). The main constituent minerals are amphibole, phengite and garnet with small amounts of retrograde chlorite and albite. Accessory minerals of rutile, apatite and quartz are also observed.

Later stage vein (10AS18)

Sample 10AS18 was collected from the chlorite zone of the Asemigawa area, central Shikoku (Fig. 2.1b). The vein of 10AS18 crosscuts the foliation of the host rock, indicating that it was formed at the later stage of exhumation after the peak *P-T* conditions of the chlorite zone. Therefore, sample 10AS18 is thought to contain fluids trapped at the lowest metamorphic conditions (<300 ºC and <0.5 GPa) during the retrograde evolution.

2.5. Macro and microscale structure of quartz veins

Macroscale observations show that foliation-parallel quartz veins collected from the WI body and its proximal area (IR04, IR27 and IR28) are almost free from obvious deformation structure (Fig. 2.3b). On the other hand, quartz veins collected from the Seba eclogite body and the Wakayama area experienced deformation resulting in a boudinaged shape of several degrees (Fig. 2.3a, c). However, some of the boudinaged samples have less-deformed microstructure, as described below.

The studied foliation-parallel quartz veins are classified into two groups based on the quartz grain fabrics: one is less-deformed polygonal fabric type (P-type, Fig. 2.4a, b) and the other is pervasively deformed and recrystallized type (Fig. 2.4c, d). The latter type veins are further subdivided into two groups on the basis of their grain size: interlobate fabric type (DI-type, Fig. 2.4c) with relatively smaller grains (<~1mm) and pervasively deformed domain type (DD-type, Fig. 2.4d). No quartz grains showed fibrous textures (e.g., Bons, 2000) among the studied samples.

Six samples collected from the eclogite bodies and their proximal area (SSB03, SSB04, SEBA, IR04, IR27 and IR28) are classified as P-type (Fig. 2.4a, b, Table 2.5). These veins are characterized by polygonal fabric with coarse grains up to 5 mm in diameter, which is identical to the “foam microstructure” (Krenn, 2010). This type of texture is thought to be formed under relatively high temperatures (>300–400 ºC) and low differential stress in the deep crust (Stöckhert et al., 1997; Krenn, 2010; Passchier & Trouw, 2005). Fluid inclusions in P-type veins are arranged along specific planes developed in intragranular and/or transgranular settings.

Samples SSB19 and SD09 are DI-type, which is characterized by interlobate fabrics with grains of various sizes. Most samples of this type show seriate grain size distribution with the largest grain size of ca. 2 mm. Coarse grains in DI-type veins sometimes show deformation lamellae and/or undulatory extinction (Fig. 2.4c), suggesting that they suffered tectonic stress and deformation at low-grade metamorphic conditions (300–400 ºC). DI-type veins contain fluid inclusions comprising specific planes or dusty clusters.

Samples collected from the non-eclogitic area in the Wakayama area (07113002, WS02, and WS04) and the foliation-cutting vein sample 10AS18 collected from the chlorite zone of the Asemigawa area are classified as DD-type. Most parts of DD-type veins show no obvious grain boundaries (Fig. 2.4d) and there appear the pervasive deformed domains, the sizes of which are sometimes larger than several centimeters. Most fluid inclusions in DD-type veins occur in randomly-oriented transgranular plane developed at subgrain boundaries.

2.6. Characteristics of fluid inclusions

2.6.1. Microtexture, microthermometry and chemical species

Within the studied quartz veins, single or multiple fluid inclusion groups are observed in each sample. Microthermometric data and textural characteristics are shown in Table 2.5. All the observed fluid inclusions were arranged along intragranular (Fig. 2.5a) or transgranular planes (Fig. 2.5b) except for one sample (SSB03c) containing isolated type. Among the observed groups, four fluid inclusion types are identified based on their chemical species and salinity of aqueous fluids: type 1) dilute aqueous fluids near to or lower than sea-water salinity (<3–5 mass% $_{NaCleq}$); type 2) relatively high saline aqueous fluids (>5 mass%$_{NaCleq}$); type 3) high saline fluids exceeding halite saturation; type 4) anhydrous fluids. Aqueous fluids were measured their ice melting temperature (T_m) and total homogenization temperature (T_h). All measured fluid inclusions homogenized into one phase below 350 ºC. Average values and ranges of T_m and T_h are

shown in Table 2.5 and histograms of the microthermometric data are shown in Figure 2.6.

Type 1 fluid inclusions accompany with or without some volatile gaseous component such as N_2 or CH_4. Type 1 is further divided into the following classes: type 1A arranged along intragranular planes, type 1B arranged along transgranular planes and type 1C scattered along subgrain boundaries (a kind of transgranular plane, distinct from ordinary ones). However, microthermometric results of these subtypes are very similar. Average T_m of type 1 inclusions are concentrated between -0.2 to -2.0 ºC and average T_h are between 170 to 241 ºC, except for later-stage fluid (10AS18: T_h = 137).

Type 2 fluid inclusions are arranged along intragranular (type 2A) or transgranular planes (type 2B). Average T_m of type 2 fluid inclusions in four fluid inclusion groups vary from -4.9 to -8.6 ºC, obviously lower (i.e., higher in salinity) than the modern sea water. Average T_h for each sample also show a range from 202 to 250 ºC (Table 2.5). Type 2 fluid in SSB03 (SSB03a) has a relatively wide range of T_m (-3.0 to -18 ºC), although the systematic relationship between salinity, volatile compositions, and occurrences are hardly recognized.

Type 3 fluid inclusions are very rare, recognized only in SSB03 (SSB03c) and shows isolated occurrence with very high salinity, exceeding halite saturation (Fig. 2.5g).

Fluid inclusions of type 4 are characterized by dark color with one or two phases without H_2O (Fig. 2.5d). They are also subdivided into intragranular type 4A and transgranular type 4B. All fluid inclusions of type 4 contain N_2 and CH_4 except for

SSB03b, which contains only N_2. Samples SD09a and SSB04c contain CO_2 in addition to N_2 and CH_4, and IR04c additionally has H_2.

Estimation of the total volume of fluid inclusions contained in a specific volume of bulk sample is difficult, since they occur as discrete assemblages along healed cracks. Therefore it is difficult to denote quantitatively which fluid inclusion group is most dominant in the sample containing multiple fluid inclusion groups, and thus, the abundances of each fluid inclusion group are roughly presented in Table 2.5.

2.6.2. Hydrochemical facies of crush-leached fluids

The chemical compositions of the crush-leached fluids are shown in Table 2.6. Note that these data do not represent absolute concentration of each element of the fluid inclusions, but the result of diluted "fluid inclusion solutions" obtained by the crush-leach method. The ratio of the major components, i.e. Na^+, K^+, Ca^{2+}, Mg^{2+}, Cl^-, HCO_3^- and SO_4^{2-} (valence number of ions are omitted hereafter) of the crush-leached fluid are shown in a "Piper's diagram" (Fig. 2.7, constructed after Piper, 1944). Hydrochemical characteristics are considered based on the most concentrated components among anions and cations. The studied crush-leached fluids are divided into three types: Na-Cl type, X-HCO_3 type (X refers to Na or K) and intermediate type. Most fluid samples have either Cl or HCO_3 as the major anion and are mostly free of F or SO_4. All Cl-dominated samples contain Na as the primary cation. On the other hand, HCO_3 dominated samples contain Na or K as primary cations. Two samples, 07113002 and WS02, contain considerable amounts of both Cl and HCO_3, and are classified as

intermediate type. The threshold to be included in the intermediate type is defined as $0.67 < Cl/HCO_3 < 1.5$ (in mass ratio).

As shown in Fig. 2.7, samples SSB04, SSB03, SEBA, IR04 and IR27 are classified as Na-Cl type, and samples IR28, SSB19, SD09, WS04 and the later stage vein of 10AS18 are classified as X-HCO_3 type. Two mafic-hosted samples, 07113002 and WS02, are intermediate type.

2.6.3. Relative B-Li-Cl composition of crush-leached fluids

Lithium, boron and chlorine characteristics of the crush-leached fluids are shown in B×500-Li×2000-Cl ternary diagram after Ohsawa et al. (2010), concerning with the hydrochemical characteristics and lithotype of the vein-hosting–rock (host rock) (Fig. 2.8a, b). Quartz vein samples hosted by sedimentary and mafic rocks are shown in Fig. 2.8a and 2.8b, respectively. Symbols of circle, square and triangle represent Na-Cl, X-HCO_3 and intermediate type hydrochemical characteristics, respectively. The filled grey-scale represents the metamorphic grade of the host rocks, i.e. the darker the color, the higher the metamorphic grade.

Na-Cl type fluid extracted from metasediment-hosted veins (IR27 and IR04) have high (B+Li)/Cl ratios and are plotted near the B-Li side of the ternary diagram (Fig. 2.8a), although some of them show higher salinity than modern seawater and have high Cl contents (cf. Table 2.5). Their Li/B ratios are very high (1.70 and 1.99, respectively) compared to other samples, meaning those samples are rich in both Li and B. Na-Cl type samples extracted from mafic-rock-hosted veins were all collected from the Seba eclogite body. The Li/B ratios of these samples show a range of 0.10–0.44 (Fig. 2.8b),

which are lower values than those of the metasediment-hosted samples (IR27 and IR28) (Fig. 2.8a).

X-HCO_3 type samples obtained from metasediment-hosted veins show distinct Li/B values of 0.09 and 0.36 in spite of the same metamorphic grade of their host rocks, although they are plotted on the B-Li side. X-HCO_3 type of mafic rocks also shows a wide Li/B range (0.02–0.19), slightly lower than those of the metasediments.

Intermediate type samples (WS02 and 07113002) are found only in mafic-rock-hosted veins, as mentioned above, and have relatively higher-Cl ratios compared to Na-Cl and X-HCO_3 type samples (Fig. 2.8b).

As an overall trend, all crush-leached fluids from quartz veins show very high (B+Li)/Cl compositions, though some fluid inclusions were certainly entrapped during the later stage of the exhumation of the rock. Li/B ratios of the fluid seem to vary depending on several factors such as host rock lithology, quartz grain fabric (deformation history), and metamorphic grade. However, P-type samples collected from high-metamorphic-grade parts, i.e. samples expected to retain the fluid in the deep part of the subduction zone, have a tendency to show a high content of both Li and B. One typical example of high saline, Li- and B-enriched fluid is IR27 collected from the oligoclase-biotite zone, which contains predominant type 2B inclusions (IR27a) and a very small amount of IR27b (type undetermined: Table 2.5), and thus, the composition of the crush-leached fluid are expected to represent the composition of fluids of IR27a. The Li and B content of crush-leached fluid from IR27 (63.89 and 39.5 μg/L, respectively) are recalculated into the original concentration of fluid inclusions, 348 and 256 μg/g based on the Cl-content and microthermometry results of IR27a. Notably, in

metasediment-hosted and mafic rock-hosted samples, respectively, Na-Cl type fluids tend to be high in both Li and B and such Li- and B-enriched fluids are found from higher metamorphic grade part, i.e. the eclogite nappe and its proximal area in central Shikoku.

2.7. Discussion

2.7.1. Entrapment timing of fluid inclusions

As fluid inclusions in the common natural sample were generally trapped through the multistage fluid activities suffered by the host metamorphic rock, the extracted fluids obtained by the crush-leach method usually give the integrated result of the whole history of fluid activity. Therefore careful observation of the fluid inclusion textures associated with the deformation texture of the host minerals is necessary to interpret the compositions of crush-leached fluids. Anhydrous type 4 fluid inclusions are thought to have little or no contributions to the chemical composition of crush-leached fluids, although they do provide indispensable information for reconstructing the deep fluid activity that took place in the subduction zone.

To be noted at first, “primary fluid inclusion” in a strict sense, which is trapped during the nucleation and crystal growth process of the host minerals (quartz in this study), should be almost absent due to the metamorphic recrystallization in the studied samples. Thus we have to consider the timing of fluid entrapment to be linked to the specific stage of the metamorphism, i.e. prograde, peak and retrograde stages.

Fluid inclusions arranged along intragranular planes in P-type veins (Fig. 2.5a; IR04a, b, and SSB04c) are possibly trapped during the recrystallization of the host quartz. Thus, they are interpreted as fluid inclusions trapped during the prograde or peak metamorphic stage. P-type textures in the studied samples are equivalent to "foam microstructure" (Stöckhert et al., 1997; Krenn, 2010), and such veins are expected to have escaped from the deformation and corresponding fluid infiltration during the later stage of exhumation. Therefore fluid inclusions arranged along transgranular planes in P-type veins also would have been trapped during the peak metamorphic stage or early stage of exhumation with relatively high temperatures. Furthermore, Yoshida and Hirajima (2012) also found annular shaped fluid inclusions in IR04 (IR04a) suggesting the increase of confining pressure of the inclusion, and therefore concluded that fluid inclusions observed in IR04a were trapped at the prograde stage of the metamorphism.

On the other hand, fabrics of DI- and DD-type, represented by deformation lamellae and undulatory extinction (Figs. 2.4c, d), are thought to be formed under high differential stress and relatively low temperature (<400 ºC) (Passchier & Trouw, 2005). Given the metamorphic history of the Sanbagawa metamorphic belt, such conditions are expected for the large scale deformation event during the later stage of exhumation (e.g., Mori and Wallis, 2010 and references therein). Fluid inclusions arranged along transgranular planes of DI-/DD-type veins are thought to be trapped in association with the later-stage deformation event and corresponding fluid infiltration. However, the exact timings of fluid infiltration have not been determined.

Fluid inclusions in the chlorite zone sample (WS04) and later-stage vein (10AS18) are arranged at subgrain boundaries (Fig. 2.5e). Such fluid inclusion arrays

may have been trapped in conjunction with the recrystallization of host quartz veins under high differential stress. Such conditions are expected to be both peak metamorphic stage of the chlorite zone (300 ºC/ 0.5 GPa) and the later exhumation stage.

In conclusion, P-type veins are capable of retaining fluids trapped at pre-peak metamorphic stages, and further of containing fluid inclusions trapped at the peak metamorphic stage or early stage of exhumation. DI-/DD-type veins have trapped post-peak metamorphic fluid during the exhumation stage, except for WS04, which we cannot distinguish the conditions of the peak metamorphic stage of the chlorite zone and the exhumation stage.

2.7.2. Hydrochemical characteristics

The results of ion chromatography and ICP-MS analysis presented here (Table 2.6) can provide fruitful information to constrain the nature of deep fluids trapped at ca. 15 km and 60 km depths. Samples containing type 2 or 3 fluid inclusions (relatively higher salinity fluids) tend to be characterized by Na-Cl type hydrochemical characteristics, i.e. three out of five (IR27, IR04 and SSB03) are Na-Cl type and one sample (WS04) is intermediate type (Fig. 2.7). On the other hand, samples free from type 2 and type3 inclusions, i.e. samples containing only the dilute fluid, show both Na-Cl type (two out of seven) and X-HCO_3 type (four out of seven) fluid.

These features are closely correlated with the fabrics of quartz grains in the vein: five P-type veins (out of six) are Na-Cl type and all DI- and DD-type veins are intermediate or X-HCO_3 type (Fig. 2.7). The later stage vein (10AS18) shows the most

HCO_3-rich composition. Dominance of HCO_3 is known to be characteristic of pore fluids in near surface fracture of continental crust (Bucher & Stober, 2010) thus, HCO_3-dominated composition probably indicates one of the typical characteristics of shallow-depth fluid that have infiltrated during the later stage of exhumation of the Sanbagawa belt.

Based on reviewing more than thirty published papers, Yardley and Graham (2002) pointed out that there is scarce correlation between metamorphic grade and salinity of corresponding fluid inclusions. They also suggested that fluid inclusions hosted in metamorphic rocks originated from oceanic crust or accretionary prisms would be relatively dilute fluid compared to those in metamorphic rocks derived from the continent crustal materials. They indicated that there was a large variation in the salinity of such fluids, from up to 15 mass%$_{NaCleq}$ to mostly solute-free for relatively high metamorphic grades (400–700 ºC). Gao and Klemd (2001) also reported that aqueous fluids released by the blueschist-eclogite transition reaction in Dabie Shan, China, have low salinities. Our data presented here also show scarce correlation between salinity, halogen content of minerals (Tables 2.2-4), and metamorphic grades/entrapment timing, however, the P-type veins seem to have relatively high-saline fluid inclusions.

In this study, a correlation between quartz fabric types in the veins and hydrochemical characteristics is observed, i.e. P-type quartz veins tends to contain Na-Cl type fluid, and DI- and DD-type quartz veins tend to have X-HCO_3 type fluids. This correlation suggests that Na-Cl type fluids are more likely to be produced at deeper parts of subduction zones, and X-HCO_3 type fluids are likely to be produced at depths

shallower than 15 km, which are defined by the peak *P-T* conditions (300 ºC/ 0.5 GPa) of the chlorite zone. However, the controlling factors of salinities in fluid inclusions still remain unclear in this study.

2.7.3. Volatile component of fluid inclusions

Aqueous fluid inclusions investigated in this study are commonly accompanied with N_2 and/or CH_4 (ten samples out of eleven). Chemical compositions of crush-leached fluids also suggest X-HCO_3 and intermediate type samples contain significant amount of HCO_3^-. We further observed type 4 anhydrous fluid inclusion groups with (SD09a, SSB04c, IR04b) or without (IR28a, SSB03b) CO_2 component. Although there is a possibility that type 4 fluid inclusions contain a small amount of water undetectable by ordinary Raman microscopy at room temperature, the amount of water should be less than a few mol% (e.g., Berkesi et al., 2009) and can be negligible for most discussion.

The origin of N_2 in metamorphic rocks is considered to be the oxidation reaction of NH_4-bearing mica and/or feldspar (e.g., Anderson et al., 1993), while that of CH_4 is considered to be the reductive reaction of CO_2 or thermal cracking of organic materials (e.g., Mazurek, 1999; Herms et al., 2012). Fluid inclusions with CO_2 are commonly reported from high grade metamorphic rocks in the world (e.g., Kobayashi et al., 2011) and also from mantle rocks (e.g., Yamamoto et al., 2007). H_2O-NaCl-CH_4 fluids are reported as the peak metamorphic stage fluid of the chlorite zone of the Sanbagawa belt (Nishimura et al., 2008) and as the prograde stage fluid of the sample IR04 (Yoshida and Hirajima, 2012), although Yoshida and Hirajima (2012) did not constrain the *P-T* condition of the entrapment of H_2O-NaCl-CH_4 fluid (IR04a). Thus, at the low to

medium grade part of the Sanbagawa metamorphic belt, the existence of H_2O-NaCl-CH_4 fluid is expected. Volatile-free aqueous fluid of WS04 could be similar to the exhumation stage fluid of the chlorite zone reported by Okamoto et al. (2008), which is possibly trapped at early stage of the exhumation. Since WS02 from the garnet zone sample and higher grade samples commonly contain N_2-bearing fluid, N_2 is a ubiquitous species at the depth greater than ca. 15 km. In the higher metamorphic grade samples, all CH_4-bearing aqueous fluids are free from CO_2. At high oxidation state, the oxidation reaction of CH_4 and H_2O can generate CO_2. Dissolved HCO_3 in X-HCO_3 type fluid (Fig. 2.7: SD09, IR28) with CH_4 are possibly originated from the partial oxidation of CH_4. Nevertheless, existence of CO_2-free, HCO_3-poor and CH_4-bearing aqueous fluid suggests that the maximum oxidation states of the high grade samples were not so high as to consume all of CH_4.

Sample SD09 from the albite-biotite zone and SSB04 and IR04 from the eclogite facies rock contain anhydrous CO_2-CH_4-bearing fluids. Carbon-rich anhydrous fluids are possibly originated from decarbonation of the carbonate minerals. Above-mentioned prograde CH_4-bearing fluids are also available for the carbon source. All type 4 fluids are obtained from the higher grade samples than the albite-biotite zone, suggesting such anhydrous fluids are expected at deeper part. Nevertheless, detailed discussion on the evolutional changes of carbon and other volatile species is beyond the purpose of this paper.

2.7.4. Relative B-Li-Cl compositions

The crush-leached fluids of this study are characterized by high B and Li contents, corresponding to very high (B+Li)/Cl ratios, though microthermometry results suggest that some of them have higher Cl content than the modern seawater. Among the studied samples, WS02 and 07113002, whose crush-leached fluids have intermediate type hydrochemical characteristics, show slightly lower (B+Li)/Cl compositions. For comparison, relative B-Li-Cl compositions of hydrothermal and metamorphic fluids in the literatures are compiled in Figures 2.8c and d (Scambelluri et al., 2004; Ohsawa et al., 2010; Kazahaya et al., 2014). The modern seawater and pore water squeezed out from marine sediments (Ohsawa et al., 2010) show low (B+Li)/Cl compositions (Fig. 2.8d). If such fluid infiltrated into the Sanbagawa metamorphic terrain and was trapped in quartz veins during the exhumation stage, the compositions of crush-leached fluids can be modified towards the Cl-corner of the diagram. However, this effect is scarce or limited for all the studied samples (Figs. 2.8a, b).

Crush-leached fluids are enriched in lithium and boron compared to modern seawater, but have a large variation in their Li/B ratio, ranging from 0.02 (WS04) to 1.99 (IR04). Dehydration fluids from serpentinites trapped in metamorphic olivine grains (400–700 ºC, 1.5–2.5 GPa: Scambelluri et al., 2004) have very high Li/B ratios (>2) and show large variation in their Li/Cl ratio (Fig. 2.8c). Scambelluri et al. (2004) estimated the partition coefficients between serpentinite and fluids at eclogite facies conditions based on their geochemical measurement and mass balance calculations, resulting in $D^{\text{rock/fluid}}_{\text{Cl}}$ =0.01–0.02 and $D^{\text{rock/fluid}}_{\text{B}}$ =0.02–0.04 as a first approximation. Based on their mass balance calculation, the B/Cl ratio of the dehydrated fluid from

serpentinite will be 0.04–0.16 (dashed-lined area in Fig. 2.8c), overlapping the range of our data (Figs. 2.8a, b).

Ohsawa et al. (2010) reported high B/Cl and low Li/B ratio fluids from the hot spring waters in the Miyazaki plain located in the fore-arc region of Kyushu Island, SW Japan (Fig. 2.8d). Based on the geochemical data combined with geochemical thermometry, they indicated that high B/Cl and low Li/B fluids are derived from dehydration of smectite interlayers. Ohsawa et al. (2010) and Amita et al. (2014) also reported relative B-Li-Cl compositions of hot spring waters obtained from deep wells in the fore-arc region of southwest Japan (S1, S2, O1, O2, and W in Fig. 2.8d). They proposed that diagenetic/metamorphic fluids show an evolutionary trend of increasing B/Cl ratio along the Cl-B axis and subsequent increase of the Li/B ratio with progressive diagenetic/metamorphic processes.

Recently, Kazahaya et al. (2014) investigated the isotopic and chemical compositions of hot spring waters in SW Japan and proposed that Arima-type hydrothermal fluids (e.g., Matsubaya et al., 1973) have Li/Cl ratios higher than 0.001 (shown in Fig. 2.8d) and high salinities (Cl >200 mg/L). These types of fluids show a δ^{18}O-shift and thus are supposed to be originated neither from meteoric water nor from seawater, but are supposed to have come up directly from lower crust or slab surface.

All of these studies suggest that fluids from the deep part of the subduction zone (e.g., at least 50-60 km depths) are characterized by high (B+Li)/Cl ratios.

Enrichment of Li and B can be partly explained by the partition coefficient data between solid phases and aqueous fluids (Brenan et al., 1998; Tenthorey & Hermann, 2004; Marschall et al., 2006). We calculated the bulk partition coefficient for our

samples from the mineral abundances and partition coefficients of Marschall et al. (2006) (Fig. 2.9), showing that most partition coefficient pairs are much lower than 1.

Published partition coefficient data of B and Li between whole rock and aqueous fluids are also shown in Figure 2.9. The data of Kessel et al. (2005) has been obtained experimentally for K-free MORB compositions, including a *T* range of 700–900ºC at 4GPa. Marschall et al. (2007) estimated the partition coefficients of altered oceanic crust subducting along the *P*-*T* path of relatively cold slab (~ 3.8 MPa/ºC). Yoshida et al. (2011) also calculated partition coefficients for the bulk composition of a specific pelitic schist along the metamorphic field gradient of the Sanbagawa belt (1.6 MPa/ºC, Enami et al., 1994), following the method of Marschall et al. (2007). Figure 2.9 shows that, in most cases, $D_{Li}^{rock/fluid}$ and $D_{B}^{rock/fluid}$ show the value less than 1, suggesting these elements would be released from the rock during water-rock interaction (e.g., Marschall et al., 2006). Since we have not measured the whole rock concentration of Li and B, let us assume that Li and B concentration of the high-pressure type metasedimentary rocks are 50-100 μg/g and 20-150 μg/g, respectively (e.g., Bebout et al., 2013; Nakano and Nakamura, 2001). If these rocks are equilibrated with the crush-leached fluid (e.g., IR27: 348 μg/g for Li and 256 μg/g for B), partition coefficients would be $D_{Li}^{rock/fluid}$ = 0.2-0.3 and $D_{B}^{rock/fluid}$ = 0.08-0.6. $D_{Li}^{rock/fluid}$ gave higher value than previously estimated, but $D_{B}^{rock/fluid}$ falls mostly similar range (Fig. 2.9).

Figure 2.10a summarizes the conclusion of the observed features of fluid composition and fabric of quartz veins. We can see that the Li- and B-enriched, high-salinity, and Na-Cl dominated fluid are stored in the P-type quartz veins, whereas B-enriched, low-salinity, and HCO_3 dominated fluid are stored in the deformed type (DI-

and DD-type) veins. P-type veins are the preserved fabric of the deep part of the subduction zone, and are thus, fluid characteristics observed in P-type veins are the representative of the deep-origin fluids. On the contrary, deformed type veins represent the later stage deformation, which are suffered by both high-grade and low-grade metamorphic rocks. Therefore the fluid characteristics observed in deformed type veins are attributed to the characteristics of the shallow depth fluids. These facts indicate that high-salinity aqueous fluids enriched with both boron and lithium are released at the deep part of the subduction zone, while dilute aqueous fluids enriched with boron are released at the shallower depths (Fig. 2.10b).

2.7.5. Implications for lithium and boron cycle in the subduction zone process

In this section, we are making a small discussion on the subduction cycle of lithium and boron, based on the above-mentioned data and the previous studies' contributions. Let us consider the input materials for the subduction zone system, at first. Subducting materials are, as a first order of approximation, assumed as layers of sedimentary rocks, igneous crust, and mantle (e.g., Hacker, 2008). Lithium and boron are generally regarded to be transported by sedimentary rocks and altered part of the igneous crust.

Input into the subduction zones

According to the extensive review of Nishio (2013), lithium abundance of the subducting pelagic sediments is up to 74 μg/g and altered igneous crust is up to 33 μg/g, while mantle contain only 1-2 μg/g. Boron content is briefly summarized by Bebout et

al. (1993), showing seafloor sediments and altered igneous crust both contain up to 300 μg/g. Kawakami (2001) reported boron content of the sedimentary-origin rock of the Mino-Tanba belt in the SW Japan, which suffered a diagenetic process, as 112 μg/g. This value can be regarded as a very early stage of the subduction. These data suggest that subducting materials contain boron and lithium at the order of hundreds μg/g.

Water-rock interactions within the subduction zones

Nature of the water-rock interactions are investigated mainly by geochemical study on the metamorphic and metasomatic rocks. As a first order of approximation, we can assume the equilibrium between rock and fluid. Boron and lithium are known as fluid-compatible elements, and there are a number of studies determining the partition coefficients of these elements between aqueous fluid and solid phase. Figure 2.11 and Table 2.7 shows the compile of published partition coefficients between aqueous fluid and solid phases ($D^{solid/fluid}$ = concentration in solid / concentration in aqueous fluid), including individual minerals and bulk rock (Berger et al., 1988; Hemming et al., 1995; Brenan et al., 1998; Johnson and Plank, 1999; Tenthorey and Hermann, 2004; Scambelluri et al., 2004; Kessel et al., 2005; Marschall et al., 2006; Caciagli et al., 2011; Martin et al., 2011; Decarreau et al., 2012). Calculated bulk partition coefficients (some data shown in Fig. 2.10: Marschall et al., 2007; Yoshida et al., 2011) are ignored. Although these values are determined for various *P-T* conditions, most partition coefficient data indicate that boron and lithium prefer aqueous fluid during water-rock interactions, except for some specific minerals. As shown in Figure 2.11, some carbonate minerals and white mica can retain considerable amount of boron and clay minerals are compatible for lithium. Under the existence of these minerals, release of

boron and lithium to the aqueous fluids would be strongly restricted (e.g., Domanik et al., 1993; Marschall et al., 2006; 2007; Ohsawa et al., 2010).

Based on the partition coefficient of representative metamorphic minerals, we can estimate the change of bulk partition coefficient along *P-T* changes. Marschall et al. (2007) performed thermodynamic calculation and estimated the phase mass fraction of a specific bulk composition along a *P-T* trajectory of high-*P/T* (3.8 MPa/ºC), using the mafic rocks of Syros, Greek. Yoshida et al. (2011) also performed the similar calculation using a pelitic rock of the Sanbagawa metamorphic belt (1.6 MPa/ºC). Both indicate that bulk partition coefficient ($D^{rock/fluid}$ = concentration in solid / concentration in aqueous fluid) of boron and lithium is very low under their calculation *P-T* ranges. However, these calculations indicate that evolutional phase changes along a specific *P-T* path do not affect the partition coefficient of boron and lithium in the case of high-*P/T* type metamorphic rocks, unless tourmaline do not precipitate. This is because the modal amount of phengite, which is the most powerful mineral affecting bulk partition coefficients of boron and lithium except for tourmaline, is mainly controlled only by the whole rock potassium content and does not change until its dehydration melting condition.

Some researcher pointed out that the element transport in the subduction zone is controlled by the redistribution of fluid-mobile elements in above-mentioned specific minerals during water-rock interaction. Nakano and Nakamura (2001) investigated the bulk composition of the metapelitic rocks in a series of metamorphic rocks in the Sanbagawa metamorphic belt, the formation conditions of which cover the *P-T* range of 300-600 ºC and 0.5-1.0 GPa. They indicate that boron content of the rock is mostly constant irrespective of the metamorphic grade of the rock. They also measured the

boron concentration of the representative boron-budget minerals, showing that boron concentration of white mica and chlorite decreases with the metamorphic grade, resulting in increase of the modal amount of tourmaline. This means that boron is progressively released from initial budget such as white mica and chlorite, and it is *in situ* consumed by the growth of tourmaline. Bebout et al. (2013) investigated change of the boron and lithium concentration compared with the metamorphic grade using metapelitic rocks of the Schistes Lustrés in the Cottian Alps and UHP Lago di Cignana locality (both in Italy), covering the *P*-*T* range of 350-550 ºC and 1.2-2.8 GPa. They also reached the same conclusion that whole rock lithium and boron had redistributed among the budget minerals, and had been thus uniform independently of the metamorphic grade.

On the other hand, Marschall et al. (2009) indicated that metamafic rocks suffered high-pressure type metamorphism show the decrease of boron and lithium with metamorphic grade. They use Be-normalized value and show that B/Be and Li/Be decrease from < 30 to ca. 2 and from < 45 to ca. 25, respectively. They also compare these values with those obtained from metasomatic rocks and concluded that lithium concentration is a good indicator for the retrograde metasomatic processes while boron abundance can be used to trace prograde dehydration.

Output from the subduction zones

In considering fluid extraction from the subduction zones, we have to be aware of the filtering process of the rocks within the subduction zone. Some researchers tried to establish the model of the geochemical cycle on several kinds of elements. Ikemoto and Iwamori (2014) performed a numerical modelling on the trace element transportation in

subduction zones. Based on their modelling, lead transportation to the magma source of the volcanic front would be very limited if the dehydrated fluid and mantle wedge materials have complete equilibration, despite the high lead content of arc volcanic rocks. Their calculation suggests that most of lead would be absorbed into the down-going hydrated mantle in spite of their high fluid mobility. Therefore, they indicated that most of the fluids, which is liberated at the deep part of the subduction zone, would not get equilibrium with the mantle rock just above and would arise without water-rock interactions to the melting region. By assuming such process, liberated fluid can deliver the key elements to the melting region and reproduce certain arc lava signatures.

Caciagli et al. (2011) modeled the effective transfer velocity of the solute in the aqueous liquid, assuming the mantle wedge as a chromatograph of 100 km in length (Navon and Stolper, 1987). The solute in the model aqueous liquid would move more slowly than the liquid itself due to water-rock interaction. Assuming the ascending velocity of the aqueous liquid as 1 to 10 m/year, their calculation indicates that lithium and boron transport velocities in the mantle are 12-120 and 92-920 cm/year, respectively. They suggest that boron transport is quick enough to follow the pervasive flow of aqueous liquid. However, the transport velocities of lithium are so low that they overlap, at the lower end, with plate convergence rates (0.4-12 cm/year: Jarrard, 1986), indicating that the zone of lithium enrichment would be removed from the locus of fluid influx.

Hot and mineral spring waters are also candidates for investigating the compositions of fluids coming out from subduction zones. The Arima-type brine is known as a candidate of deep-seated geofluid, with specific geochemical characteristics (e.g., Matsubaya et al., 1973; Ohsawa et al., 2010; Amita et al., 2014; Kazahaya et al.,

2014; Kusuda et al., 2014). On the basis of geochemical study on the hot springs of Arima-Takarazuka area, Kusuda et al. (2014) indicate that Arima-type hydrothermal fluids contain significant amount of lithium and chlorine. They indicate that spring water of Arima-Takarazuka area are originated from the subducting slab whose depth is approximately 60 km, on the basis of the isotope composition of hydrogen and oxygen of slab-fluid. Ohsawa et al. (2010) pointed out that ascending deep-seated geofluid has high B/Cl ratio, based on the investigation of the fore-arc hot spring water in the Miyazaki plain. Furthermore, Amita et al. (2014) indicated that this high-B/Cl compositions would change to lithium enriched compositions (i.e. high in Li/B ratio) with increasing of the depth of the subducting slab below the hot spring. Kazahaya et al. (2014) also pointed out that Arima-type brine coming up from slab surface would yield high Li/Cl ratio (>~ 0.01). These studies suggest that ascending fluid from the subducting slab is characterized by boron and lithium enriched compositions. On the other hand, Mottl et al. (2004) studied the drilling core of the Mariana fore-arc and determined the pore fluid composition stored there. They indicate that upwelling waters from the subducting slab are low chlorine content and are thus distinguished from the sea water, showing increase of their boron content with the distance from the trench.

Leaching of boron and lithium from the subducting slab

On the basis of above-mentioned information, simple calculation can be performed for the geochemical cycle of boron and lithium in the subduction zones. As shown in the previous sections, deep origin fluids recorded in the Sanbagawa metamorphic belt (ca. 30-60 km in depth) yield the composition with the following characteristics:

1) Na-Cl dominated

2) Salinity is higher than sea water (~ 10 mass%)

3) Lithium and boron enriched compositions

Let us assume a droplet of aqueous liquid coexisting with metamorphic rocks. We will consider the process that initially pure droplet would get equilibrium with the rock, and be removed from the system with its solute. We are going to consider the *P*-*T* ranges of the Sanbagawa metamorphic belt (up to 600 ºC and 2 GPa), and therefore, melting of the silicate phases can be ignored. We also ignored the dissolved silicate content into aqueous liquids, as for it is considered to be scarce for the given *P*-*T* range (e.g., Hermann et al., 2006).

Based on the relative B-Li-Cl compositions and representative fluid salinity, we can estimate the released content of boron and lithium during the water-rock interaction taken place at the deep part of the subduction zones. Sample IR27 is the available typical sample for the pelitic-rock-hosted vein. Fluid inclusions contained in IR27 are divided into two groups: IR27a and IR27b. Since occurrence of IR27b is restricted in the quartz grains near the wall of the vein and their amount is very limited while IR27a is abundant in the vein, crush-leached fluid of IR27 are thought to reflect the composition of IR27a. On the other hand, SSB3 is available typical sample for the estimation of the composition of fluid coexisting with mafic rocks. SSB3 contains three fluid inclusion groups: SSB3a, SSB3b, and SSB3c. Among them, Sample SSB3c is very rare, while SSB3b is of anhydrous fluid. Therefore, these two groups are considered to have scarce contribution to the composition of crush-leached fluid, and the crush-leached fluid would reflect the composition of SSB3a. For IR27a and SSB3a, we can calculate the concentration of lithium and boron as shown in Table 2.8. Based on these

data, aqueous fluids coexisting with metamorphic rocks at deep subduction zones have boron and lithium concentration of approximately 300 μg/g, except for the boron of the fluid coexisting with mafic rocks yielding ca. 800 μg/g (SSB3a).

The amount of the released fluid would be estimated by the thermodynamic calculation. Some recent studies indicate that water content of the subducting slabs would not change during the progressive subduction or even increase, when they undergo extremely high-*P/T* trajectory (e.g., Hacker, 2008; Kuwatani et al., 2011; Ao and Bhowmik, 2014). Nevertheless, dehydration of the subducting slab is the common phenomenon for many subduction zones which are composed of ordinary thermal gradient (e.g., Hacker et al., 2003; Hacker, 2008). Based on the thermodynamic calculation along a specific *P*-*T* path, dehydration timing, its amount, and water-rock interaction taken place can be modelled (e.g., Marschall et al., 2007; Konrad-Schmolke et al., 2011; Konrad-Schmolke and Halama, 2014). Here we would like to model rough estimation of the released amount of boron and lithium during intermediate high-*P/T* subduction process, such as the Sanbagawa metamorphism (~1.6 ºC/MPa). Given the temperature range up to 700 ºC, corresponding to the highest metamorphic grade of the Sanbagawa metamorphic belt, the expected total dehydration amount from both metamafic and metapelitic rocks are up to 3-5 mass% of the whole rock (e.g., Hacker et al., 2008). Therefore, we can assume a droplet of 3 mass% as the maximum single dehydration event.

If a droplet of 3 mass% with 300 μg/g solute is removed from the rock, the element loss of the rock would be 9 μg/g. This element loss accounts for 3 to 10 % of those initially stored in the subducting rocks (100-300 μg/g). In the case of the boron

loss due to the droplet with 1000 μg/g, it corresponds to 30 μg/g as the whole rock system, accounting for the similar order of the element loss (10 to 30 % of the whole rock elements). This rough calculation suggests that during the dehydration process taken place at the deep part (~30-60 km) of the subduction zone, the subducting rock would lose approximately 10 % of their boron and lithium. Let us consider the impact of this element loss.

Marschall et al. (2007) performed a thermodynamic calculation on the MORB composition and modelled the squeezing of boron and lithium from the rock subducting along a specific *P-T* trajectory. They calculated the evolutional change of the partition coefficients based on the change of phase fraction, and also estimated the dehydration amount. Using the calculated partition coefficients and dehydration amount at each *P-T* stage, they calculated the removal of the element from the rock during progressive dehydration. Their model indicates that during the subduction of slab with pressure range of 1.5 to 2.5 GPa, 60% and 40% of boron and lithium would be removed from the rock, respectively. It should be noted that their calculation are based on the low initial concentration of boron and lithium (B = 26 μg/g and Li = 14 μg/g). On the other hand, natural rock observation of Nakano and Nakamura (2001) and Bebout et al. (2013), using a series of metapelitic rocks, indicate that whole rock content of boron and lithium are almost independent from the metamorphic grade. Actually, the whole rock boron content reported in Nakano and Nakamura (2001) seems to show slight decrease with the metamorphic grade. The reported compositions of Bebout et al. (2013) also indicate the slight decrease of boron and lithium during the progressive dehydration of the subducting slab. This is partly depending of the whole rock composition. Marschall et al. (2007) uses altered MORB composition for the calculation while Nakano and

Nakamura (2001) and Bebout et al. (2013) investigated pelitic rocks, therefore, calculation of Marschall et al. (2007) ignores the precipitation of tourmaline.

Our simple calculation suggests that the degree of element loss from the subducting slab is not so large, even though the removed fluid has high concentration of lithium and boron. This is because the removed amount of the aqueous fluid is small. Therefore, if we consider the precipitation of boron and lithium as minerals such as tourmaline and lepidolite, boron and lithium are retained more strongly in the solid phase. Precipitation of tourmaline is common phenomena in the pelitic rock system and therefore releasing of boron from pelitic rocks is expected to be limited. This is consistent with the natural sample observation of Nakano and Nakamura (2001) and Bebout et al. (2013).

Ascending of the fluid from the slab surface

As mentioned-above, Ikemoto and Iwamori (2014) indicated the disequilibrium fluid transport from the slab surface to the melting region below the arc volcano. Based on the model calculation of Caciagli et al. (2011), however, lithium transport from the subducting slab surface to the top of the mantle wedge is very limited due to the downgoing mantle flow.

The similarity in the chemical compositions between deep fluids stored in the subduction-related metamorphic rocks and the Arima-type hydrothermal fluids attested the possibility that Arima-type hydrothermal fluids are originated from the dehydrated fluid from the subducting slab. These facts suggest that the transport of the key element, i.e. lithium, is possibly accomplished by disequilibrium process. As the simplest case, disequilibrium fluid transport is expected for the channelized fluid flow, which would

reduce the contacting surface between fluid and solid phase. Although ascending rate, degree of the reaction, and other detailed process connecting deep-origin B- and Li-enriched fluid and Arima-type hydrothermal fluid are still unraveled, present geochemical data indicate that disequilibrium fluid transport is one of the major processes taking place in the subduction zone.

Most of the previous studies have estimated “deep fluid composition” by either: 1) qualitatively by some key signature observed in the associated solid phases; or 2) assuming chemical equilibration using partition coefficients. Such method is, of course, powerful and useful for investigating the geochemical characteristic of the fluid activity in the subduction zone. However, such approaches have difficulty to treat the disequilibrium process quantitatively. In this thesis, we have attested the approach investigating fluid composition directly by using deep-origin fluid inclusions preserved in the metamorphic quartz. The obtained data have provided a picture of deep fluid activity qualitatively similar to those previously drown, and attested the idea of disequilibrium fluid ascent in the subduction zone. Although trace element analyses of individual fluid inclusions still have difficulty, the crush-leach method combined with conventional petrographical observations provides fruitful information on the chemical characteristics of the deep fluid in the subduction zone. Future work should focus on the chemical compositions of individual fluid inclusion related to the crystal growth of the metamorphic minerals, which would open up the high-resolution knowledge of *pressure-temperature-time-fluid* evolution in the plate convergent margins.

References

Amita, K., Ohsawa, S., Nishimura, K., Yamada, M., Mishima, T., Kazahaya, K., Morikawa, N. and Hirajima, T. (2014) Origin of saline waters distributed along the Median Tectonic Line in southwest Japan: Hydrogeochemical investigation on possibility of derivation of metamorphic dehydrated fluid from subducting oceanic plate. *Journal of Japanese Association of Hydrological Sciences*, **44**, 17–38.

Anderson, T., Austrheim, H., Burke, E. A. J. and Elvevold, S. (1993) N_2 and CO_2 in deep crustal fluids: evidence from the Caledonides of Norway. *Chemical Geology*, **108**, 113-132.

Ao, A. and Bhowmik, S. K. (2014) Cold subduction of the Neotethys: the metamorphic record from finely banded lawsonite and epidote blueschists and associated metabasalts of the Nagaland Ophiolite Complex, India. Journal of Metamorphic Geology 32, 829–860.Aoya, M., 2001. P–T–D path of eclogite from the Sambagawa belt deduced from combination of petrological and microstructural analyses. *Journal of Petrology*, **42**, 1225–1248.

Aoya, M., Endo, S., Mizukami, T. and Wallis, S. R. (2013) Paleo-mantle wedge preserved in the Sambagawa high-pressure metamorphic belt and the thickness of forearc continental crust. *Geology*, **41**, 451–454.

Aoya, M., Noda, A., Mizuno, K., Mizukami, T., Miyachi, Y., Matsuura, H., Endo, S., Toshimitsu, S. and Aoki, M. (2013) Geology of the Niihama District. Quadrangle Series, 1 :50,000, Geological Survery of Japan, AIST.

Aoya, M. and Wallis, S. R. (1999) Structural and microstructural constraints on the mechanism of eclogite formation in the Sambagawa belt, SW Japan. *Journal of Structural Geology*, **21**, 1561-1573.

Bakker, R. J. and Mamtani, M. A. (2000) Fluid inclusions as metamorphic process indicators in the Southern Aravalli Mountain Belt (India). *Contributions to Mineralogy and Petrology*, **139**, 163–179.

Banks, D. A. and Yardley, B. W. D. (1992) Crush-leach analysis of fluid inclusions in small natural and synthetic samples. *Geochimica et Cosmochimica Acta*, **56**, 245–248.

Bebout, G. E., Agard, P., Kobayashi, K., Moriguti, T. and Nakamura, E. (2013) Devolatilization history and trace element mobility in deeply subducted sedimentary rocks: Evidence from Western Alps HP/UHP suites. Chemical Geology 342, 1–20.Bebout, G. E., 2007. Metamorphic chemical geodynamics of subduction zones. *Earth and Planetary Science Letters*, **260**, 373–393.

Bebout, G. E., Ryan, J. G. and Leeman, W. P. (1993) B-Be systematics in subduction-related metamorphic rocks: Characterization of the subducted component. *Geochimica et Cosmochimica Acta*, **57**, 2227–2237.

Bebout, G. E., Ryan, J. G., Leeman, W. P. and Bebout, A. E. (1999) Fractionation of trace elements by subduction - zone metamorphism - effect of convergent-margin thermal evolution. *Earth and Planetary Science Letters*, **171**, 63–81.

Bebout, G. E., Agard, P., Kobayashi, K., Moriguti, T. and Nakamura, E. (2013) Devolatilization history and trace element mobility in deeply subducted sedimentary rocks: Evidence from Western Alps HP/UHP suites. *Chemical Geology*, **342**, 1-20.

Berger, G., Schott, J. and Guy, C. (1988) Behavior of Li, Rb and Cs during basalt glass and olivine dissolution and chlorite, smectite and zeolite precipitation from seawater: Experimental investigations and modelization between 50° and 300°C. *Chemical Geology*, **71**, 297–312.

Berkesi, M., Hidas, K., Guzmics, T., Dubessy, J., Bodnar, R. J., Szabo, C., Vajna, B. and Tsunogae, T. (2009) Detection of small amounts of H2O in CO2‐rich fluid inclusions using Raman spectroscopy. *Journal of Raman Spectroscopy*, **40**, 1461-1463.

Bodnar, R. J. (1993) Revised equation and table for determining the freezing point depression of H2O-NaCl solutions. *Geochimica et Cosmochimica Acta*, **57**, 683–684.

Bons, P.D. (2000) The formation of veins and their microstructures. *Journal of the Virtual Explorer*, **2**.

Bottrell, S. H., Yardley, B. W. D. and Buckley, F. (1988) A modified crush-leach method for the analysis of fluid inclusion electrolytes. *Bulletin de minéralogie*, **111**, 279–290.

Boullier, A.-M. (1999) Fluid inclusions: tectonic indicators. *Journal of Structural Geology*, **21**, 1229–1235.

Brenan, J. M., Ryerson, F. J. and Shaw, H. F. (1998) The role of aqueous fluids in the slab-to-mantle transfer of boron, beryllium, and lithium during subduction: experiments and models. *Geochimica et Cosmochimica Acta*, **62**, 3337–3347.

Bucher, K. and Stober, I. (2010) Fluids in the upper continental crust. *Geofluids*, **10**, 241–253.

Caciagli, N., Brenan, J. M., McDonough, W. and Phinney, D. (2011) Mineral–fluid partitioning of lithium and implications for slab–mantle interaction. *Chemical Geology*, **280**, 384–398.

Decarreau, A., Vigier, N., Pálková, H., Petit, S., Vieillard, P. and Fontaine, C. (2012) Partitioning of lithium between smectite and solution: An experimental approach. *Geochimica et Cosmochimica Acta*, **85**, 314–325.

Domanik, K. J., Hervig, R. L. and Peacock, S. M. (1993) Beryllium and boron in subduction zone minerals: An ion microprobe study. *Geochimica et Cosmochimica Acta*, **57**, 4997–5010.

Donnelly, T. W., Thompson, G. and Salisbury, M. H. (1980) The chemistry of altered basalts at site 417, Deep Sea Drilling Project Leg 75. Institute Report of DSPS, 51-53, 1319–1330.

Enami, M. (1982) Oligoclase-biotite zone of the Sanbagawa metamorphic terrain in the Bessi district, central Shikoku, Japan. *Journal of Geological Society of Japan*, **88**, 887–900.

Enami, M. (1994) Sanbagawa metamorphism: Implication for evolution of a subduction zone. *Japanese Magazine of Mineralogical and Petrological Sciences*, **89**, 409–422.

Endo, S. (2010) Pressure-temperature history of titanite-bearing eclogite from the Western Iratsu body, Sanbagawa Metamorphic Belt, Japan. *Island Arc*, **19**, 313–335.

Endo, S., Wallis, S. R., Tsuboi, M., Torres De León, R. and Solari, L. A. (2012) Metamorphic evolution of lawsonite eclogites from the southern Motagua fault zone, Guatemala: insights from phase equilibria and Raman spectroscopy. *Journal of Metamorphic Geology*, **30**, 143–164.

Gao, J. and Klemd, R. (2001) Primary fluids entrapped at blueschist to eclogite transition: evidence from the Tianshan meta-subduction complex in northwestern China. *Contributions to Mineralogy and Petrology*, **142**, 1–14.

Hacker, B. R. (2008) H_2O subduction beyond arcs. *Geochemistry Geophysics Geosystems*, **9**, Q03001, doi:10.1029/2007GC001707.

Hacker, B. R., Abers, G. A. and Peacock, S. M. (2003) Subduction factory 1. Theoretical mineralogy, densities, seismic wave speeds, and H 2 O contents. *Journal of Geophysical Research*, **108**, 1–26.

Hemming, N. G., Reeder, R. J. and Hanson, G. N. (1995) Mineral-fluid partitioning and isotopic fractionation of boron in synthetic calcium carbonate. *Geochimica et cosmochimica acta* **59**, 371–379.

Hermann, J., Spandler, C., Hack, A. and Korsakov, A. (2006) Aqueous fluids and hydrous melts in high-pressure and ultra-high pressure rocks: Implications for element transfer in subduction zones. *Lithos*, **92**, 399–417.

Higashino, F., Kawakami, T., Satish-Kumar, M., Ishikawa, M., Maki, K., Tsuchiya, N., Grantham, G. H. and Hirata, T. (2013) Chlorine-rich fluid or melt activity during granulite facies metamorphism in the Late Proterozoic to Cambrian continental collision zone—An example from the Sør Rondane Mountains, East Antarctica. *Precambrian Research*, **234**, 229–246.

Higashino, T. (1990) The higher grade metamorphic zonation of the Sambagawa metamorphic belt in central Shikoku, Japan. *Journal of Metamorphic Geology*, **8**, 413–423.

Ikemoto, A. and Iwamori, H. (2014) Numerical modeling of trace element transportation in subduction zones: implications for geofluid processes. *Earth, Planets and Space*, **66**, 26.

Jarrard, R. D. (2003) Subduction fluxes of water, carbon dioxide, chlorine, and potassium. *Geochemistry Geophysics Geosystems*, **4**.

Johnson, M. C. and Plank, T. (1999) Dehydration and melting experiments constrain the fate of subducted sediments. *Geochemistry Geophysics Geosystems*, **1**, 1007–26.

Kawakami, T. (2001) Boron Depletion Controlled By the Breakdown of Tourmaline in the Migmatite Zone of the Aoyama Area, Ryoke Metamorphic Belt, Southwestern Japan. *The Canadian Mineralogist*, **39**, 1529–1546.

Kazahaya, K., Takahashi, M., Yasuhara, M., Nishio, Y., Inamura, A., Morikawa, N., Sato, T., Takahashi, H. a., Kitaoka, K., Ohsawa, S., Oyama, Y., Ohwada, M., Tsukamoto, H., Horiguchi, K., Tosaki, Y., Kirita, T. (2014) Spatial distribution and feature of slab-related deep-seated fluid in SW Japan. *Journal of Japanese Association of Hydrological Sciences*, **44**, 3–16.

Van den Kerkhof, A. (2001) Fluid inclusion petrography. *Lithos*, **55**, 27–47.

Kessel, R., Schmidt, M. W., Ulmer, P. and Pettke, T. (2005) Trace element signature of subduction-zone fluids, melts and supercritical liquids at 120-180 km depth. *Nature*, **437**, 724–7.

Kobayashi, T., Hirajima, T., Kawakami, T., Svojtka, M. (2011) Metamorphic history of garnet-rich gneiss at Ktiš in the Lhenice shear zone, Moldanubian Zone of the southern Bohemian Massif, inferred from inclusions and compositional zoning of garnet. *Lithos*, **124**, 46-65.

Kogiso, T., Tatsumi, Y. and Nakano, S. (1997) Trace element transport during dehydration processes in the subducted oceanic crust: 1. Experiments and implications for the origin of ocean island basalts. *Earth and Planetary Science Letters*, **148**, 193–205.

Konrad-Schmolke, M. and Halama, R. (2014) Combined thermodynamic–geochemical modeling in metamorphic geology: Boron as tracer of fluid–rock interaction. *Lithos*, **208-209**, 393–414.

Konrad-Schmolke, M., O'Brien, P. J. and Zack, T. (2011) Fluid Migration above a Subducted Slab--Constraints on Amount, Pathways and Major Element Mobility from Partially Overprinted Eclogite-facies Rocks (Sesia Zone, Western Alps). *Journal of Petrology*, **52**, 457–486.

Kouketsu, Y., Enami, M. and Mizukami, T. (2010) Omphacite-bearing metapelite from the Besshi region, Sambagawa metamorphic belt, Japan: Prograde eclogite facies metamorphism recorded in metasediment. *Journal of Mineralogical and Petrological Sciences*, **105**, 9–19.

Kouketsu, Y., Enami, M., Mouri, T., Okamura, M., & Sakurai, T. (2014) Composite metamorphic history recorded in garnet porphyroblasts of Sambagawa metasediments in the Besshi region, central Shikoku, Southwest Japan. *Island Arc*, **23**, 263-280.

Krenn, K. (2010) Fluid inclusions in quartz related to subsequent stages of foliation development during a single metamorphic cycle (Schneeberg Fault Zone, Eastern Alps, Austria). *Lithos*, **118**, 255–268.

Krenn, K., Bauer, C., Proyer, A., Mposkos, E. and Hoinkes, G. (2008) Fluid entrapment and reequilibration during subduction and exhumation: A case study from the high-grade Nestos shear zone, Central Rhodope, Greece. *Lithos*, **104**, 33–53.

Kunugiza, K., Takasu, A. and Banno, S. (1986) The origin and metamorphic history of the ultramafic and metagabbro bodies in the Sanbagawa belt. *Geological Society of America Memoir*, **164**, 375–385.

Kurata, H. and Banno, S. (1974) Low-grade progressive metamorphism of pelitic schists of the Sazare area, Sanbagawa metamorphic terrain in central Sikoku, Japan. *Journal of Petrology*, **15**, 361–382.

Kusuda, C., Iwamori, H., Nakamura, H., Kazahaya, K. and Morikawa, N. (2014) Arima hot spring waters as a deep-seated brine from subducting slab. *Earth, Planets and Space*, **66**, 119.

Küster, M. and Stöckhert, B. (1997) Density changes of fluid inclusions in high-pressure low-temperature metamorphic rocks from Crete: A thermobarometric approach based on the creep strength of the host minerals. *Lithos*, **41**, 151–167.

Leeman, W. P. and Sisson, V. B. (1996) Geochemistry of boron and its implications for crustal and mantle processes. *Reviews in Mineralogy and Geochemistry*, **33**, 645–707.

Makimoto, H., Miyata, T., Mizuno, K. and Sangawa, A., 2004. Geology of the Kokawa District. Quadrangle Series, 1 :50,000, Geological Survery of Japan, AIST.

Marschall, H. R., Altherr, R., Gméling, K. and Kasztovszky, Z. (2009) Lithium, boron and chlorine as tracers for metasomatism in high-pressure metamorphic rocks: a case study from Syros (Greece). *Mineralogy and Petrology*, **95**, 291–302.

Marschall, H. R., Altherr, R., Ludwig, T., Kalt, A., Gméling, K. and Kasztovszky, Z. (2006) Partitioning and budget of Li, Be and B in high-pressure metamorphic rocks. *Geochimica et Cosmochimica Acta*, **70**, 4750–4769.

Marschall, H. R., Altherr, R. and Rüpke, L. (2007) Squeezing out the slab–modelling the release of Li, Be and B during progressive high-pressure metamorphism. *Chemical Geology*, **239**, 323–335.

Marschall, H. R., Korsakov, a. V., Luvizotto, G. L., Nasdala, L. and Ludwig, T. (2009) On the occurrence and boron isotopic composition of tourmaline in (ultra)high-pressure metamorphic rocks. *Journal of the Geological Society*, **166**, 811–823.

Martin, L. a. J., Wood, B. J., Turner, S. and Rushmer, T. (2011) Experimental Measurements of Trace Element Partitioning Between Lawsonite, Zoisite and Fluid and their Implication for the Composition of Arc Magmas. *Journal of Petrology*, **52**, 1049–1075.

Matsubaya, O., Sakai, H., Kusachi, I. and Satake, H. (1973) Hydrogen and oxygen isotopic ratios and major element chemistry of Japanese thermal water systems. *Geochemical Journal*, **7**, 123–151.

Matsumoto, K. and Hirajima, T. (2006) Modal analysis using scanning electron probe microanalyzer. *Japanese Magazine of Mineralogical and Petrological Sciences*, **35**, 97–108.

Mazurek, M. (1999) Evolution of gas and aqueous fluid in low-permeability argillaceous rocks during uplift and exhumation of the central Swiss Alps. *Applied Geochemistry*, **15**, 211-234.

Mori, H. and Wallis, S. (2010) Large-scale folding in the Asemi-gawa region of the Sanbagawa Belt, southwest Japan. *Island Arc*, **19**, 357–370.

Mottl, M. J., Wheat, C. G., Fryer, P., Gharib, J. and Martin, J. B. (2004) Chemistry of springs across the Mariana forearc shows progressive devolatilization of the subducting plate. *Geochimica et Cosmochimica Acta*, **68**, 4915–4933.

Nakano, T. and Nakamura, E. (2001) Boron isotope geochemistry of metasedimentary rocks and tourmalines in a subduction zone metamorphic suite. *Physics of The Earth and Planetary Interiors*, **127**, 233–252.

Navon, O. and Stolper, E. (1987) Geochemical consequences of melt percolation: the upper mantle as a chromatographic column. *The Journal of Geology*, **95**, 285–307.

Newton, R. C. and Manning, C. E. (2010) Role of saline fluids in deep-crustal and upper-mantle metasomatism: insights from experimental studies. *Geofluids*, **10**, 58–72.

Nishimura, K., Amita, K., Ohsawa, S., Kobayashi, T. and Hirajima, T. (2008) Chemical characteristics and trapping P-T conditions of fluid inclusions in quartz veins from the Sanbagawa metamorphic belt, SW Japan. *Journal of Mineralogical and Petrological Sciences*, **103**, 94–99.

Nishio, Y. (2013) Geofluid research using lithium isotopic tool advances understanding of whole crustal activity. Journal of Japanese *Association of Hydrological Sciences*, **43**, 119–135.

Ohsawa, S. (2004) Geochemical characteristics of carbonated brines along Median Tectonic Line, South-west Japan: implication for upward migration of dehydrated-fluid from subducting Philippine Sea plate. In *The 2nd KAGI21 International Symposium Beppu, 2004 Proceeding*. B-Con Plaza, Beppu city, Oita, Japan, pp. 45–46.

Ohsawa, S., Amita, K., Yamada, M., Mishima, T. and Kazahaya, K. (2010) Geochemical features and genetic process of hot-spring waters discharged from deep hot-spring wells in the Miyazaki Plain, Kyushu Island, Japan: Diagenetic dehydrated fluid as a source fluid of hot-spring water. *Journal of Hot Spring Science*, **59**, 295–319.

Ota, T., Terabayashi, M. and Katayama, I. (2004) Thermobaric structure and metamorphic evolution of the Iratsu eclogite body in the Sanbagawa belt, central Shikoku, Japan. *Lithos*, **73**, 95–126.

Passchier, C. W. and Trouw, R. A. J. (2005) Microtectonics 2nd Ed., Heidelberg, Berlin: Springer-Verlag.

Peacock, S. M. (1990) Fluid processes in subduction zones. *Science*, **248**, 329–337.

Piper, A. M. (1944) A graphic procedure in geochemical interpretation of water analyses. *Transactions, American Geophysics Union*, **25**, 914–928.

Scambelluri, M., Müntener, O., Ottolini, L., Pettke, T. T. and Vannucci, R. (2004) The fate of B, Cl and Li in the subducted oceanic mantle and in the antigorite breakdown fluids. *Earth and Planetary Science Letters*, **222**, 217–234.

Seyfried Jr., W. E., Janecky, D. and Mottl, M. (1984) Alteration of the oceanic crust: Implications for geochemical cycles of lithium and boron. *Geochimica et Cosmochimica Acta*, **48**, 557–569.

Shaw, D. M., Vatin-Perignon, N. and Muysson, J. R. (1977) Lithium in spilites. *Geochimica et Cosmochimica Acta*, **41**, 1601–1607.

Stöckhert, B., Massonne, H.-J. and Ursula Nowlan, E. (1997) Low differential stress during high-pressure metamorphism: The microstructural record of a metapelite from the Eclogite Zone, Tauern Window, Eastern Alps. *Lithos*, **41**, 103–118.

Sumino, H., Burgess, R., Mizukami, T., Wallis, S. R., Holland, G. and Ballentine, C. J. (2010) Seawater-derived noble gases and halogens preserved in exhumed mantle wedge peridotite. *Earth and Planetary Science Letters*, **294**, 163–172.

Takasu, A. (1984) Prograde and retrograde eclogites in the Sambagawa metamorphic belt, Besshi district, Japan. *Journal of Petrology*, **25**, 619–643.

Tatsumi, Y. (1989) Migration of fluid phases and genesis of basalt magmas in subduction zones. *Journal of Geophysical Research*, **94**, 4697–4707.

Tenthorey, E. and Hermann, J. (2004) Composition of fluids during serpentinite breakdown in subduction zones: Evidence for limited boron mobility. *Geology*, **32**, 865.

Touret, J. L. (2001) Fluids in metamorphic rocks. *Lithos*, **55**, 1–25.

Wallis, S. R. and Aoya, M. (2000) A re-evaluation of eclogite facies metamorphism in SW Japan: proposal for an eclogite nappe. *Journal of Metamorphic Geology*, **18**, 653–664.

Whitney, D. L. and Evans, B. W. (2010) Abbreviations for names of rock-forming minerals. *American Mineralogist*, **95**, 185–187.

Yamamoto, J., Kagi, H., Kawakamo, Y., Hirano, N. and Nakamura, M. (2007) Paleo-Moho depth determined from the pressure of CO_2 fluid inclusions: Raman spectroscopic barometry of mantle-and crust-derived rocks. *Earth and Planetary Science Letters*, **253**, 369-377.

Yardley, B. W. D. and Graham, J. T. (2002) The origins of salinity in metamorphic fluids. *Geofluids*, **2**, 249–256.

Yoshida, K. and Hirajima, T. (2012) Annular fluid inclusions from a quartz vein intercalated with metapelites from the Besshi area of the Sanbagawa belt, SW Japan. *Journal of Mineralogical and Petrological Sciences*, **107**, 50–55.

Yoshida, K., Sengen, Y., Tsuchiya, S., Minagawa, K., Kobayashi, T., Mishima, T., Ohsawa, S. and Hirajima, T. (2011) Fluid inclusions with high Li/B ratio in a quartz vein from the Besshi area of the Sambagawa metamorphic belt: implications for deep geofluid evolution. *Journal of Mineralogical and Petrological Sciences*, **106**, 164–168.

You, C. F., Castillo, P. R., Gieskes, J. M., Chan, L. H. and Spivack, A. J. (1996) Trace element behavior in hydrothermal experiments : Implications for fluid processes at shallow depths in subduction zones. *Earth and Planetary Science Letters*, **140**, 41–52.

Zaw, W. K., Enami, M. and Aoya, M. (2005) Chloritoid and barroisite-bearing pelitic schists from the eclogite unit in the Besshi district, Sanbagawa metamorphic belt. *Lithos*, **81**, 79–100.

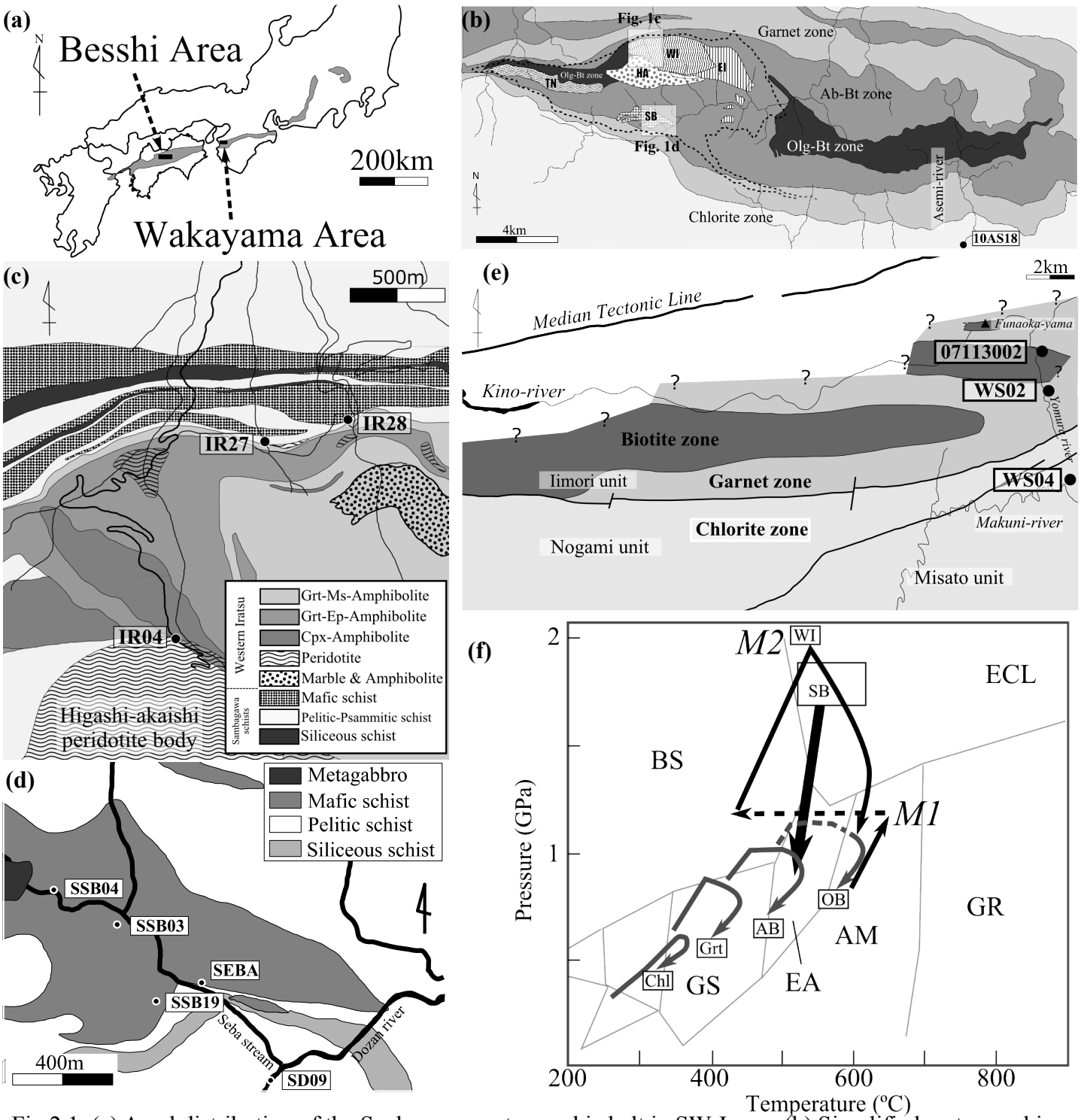

Fig.2.1. (a) Areal distribution of the Sanbagawa metamorphic belt in SW Japan. (b) Simplified metamorphic zonal map of central Shikoku with the sample locality of the later stage quartz vein collected in the Asemigawa area (10AS18). The dashed line shows the newly proposed boundary of eclogite-nappe in the Besshi area (Aoya et al., 2013). Abbreviations of eclogite units are: Tonaru, TN; Seba, SB; Higashi-Akaishi, HA; Western Iratsu, WI; Eastern Iratsu, EI. (c) Lithological map of the study area of the Western Iratsu body (Kugimiya and Takasu, 2002) and sample localities. (d) Lithological map of the study area of the Seba body (Aoya, 2001) and sample localities. (e) Simplified metamorphic zonal map of the Wakayama area after Makimoto et al. (2004) and sampling localities. (f) *P-T* estimation of the Western Iratsu body, Seba body and non eclogitic part of the Sanbagawa metamorphic belt (Enami et al., 1994; Aoya, 2001; Zaw et al., 2005; Endo, 2010).

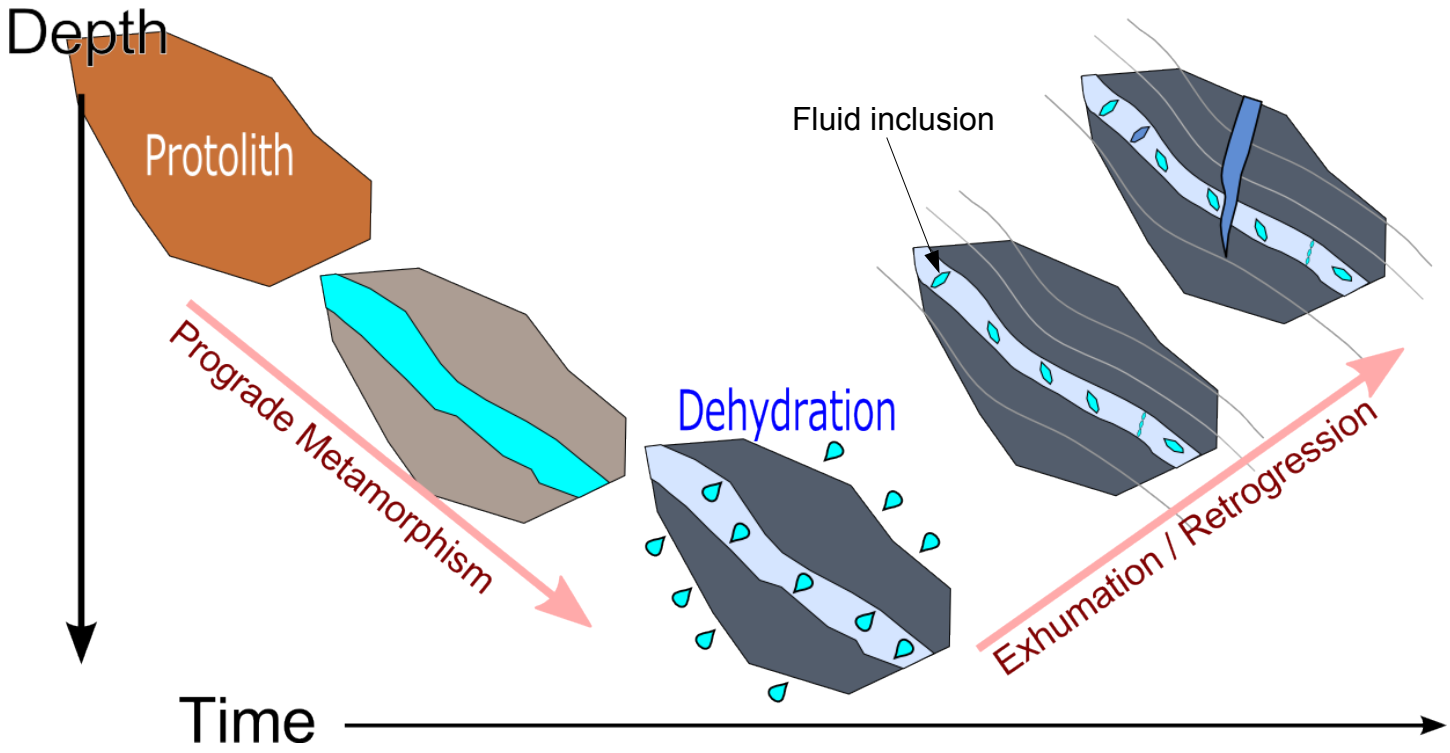

Fig.2.2. Schematic image of vein formation and fluid activities suffered by the metamorphic rock.

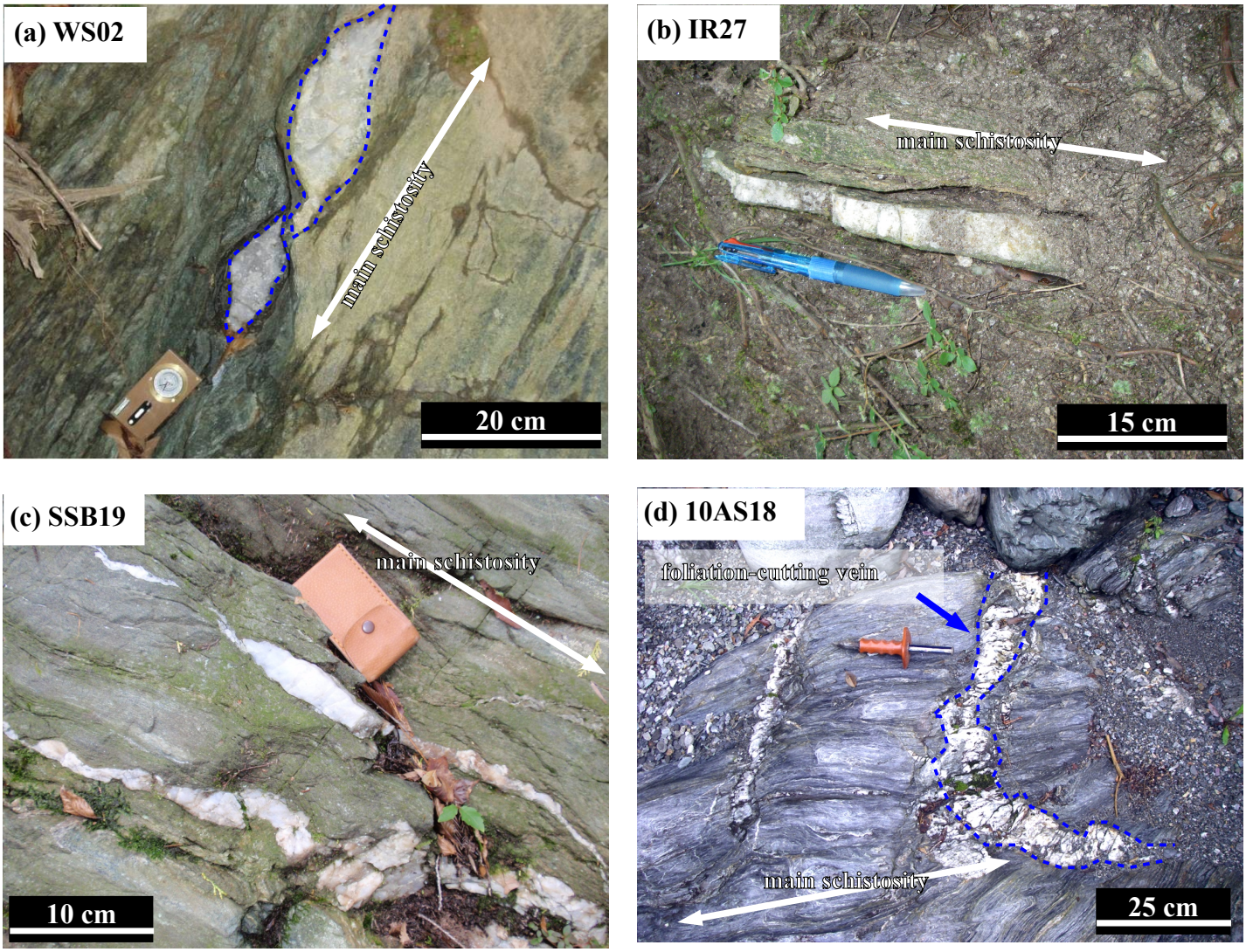

Fig.2.3. Typical outcrop photos of (a-c) foliation parallel quartz veins from the Wakayama and Besshi areas; (d) foliation-cutting vein in the Asemigawa area (10AS18).

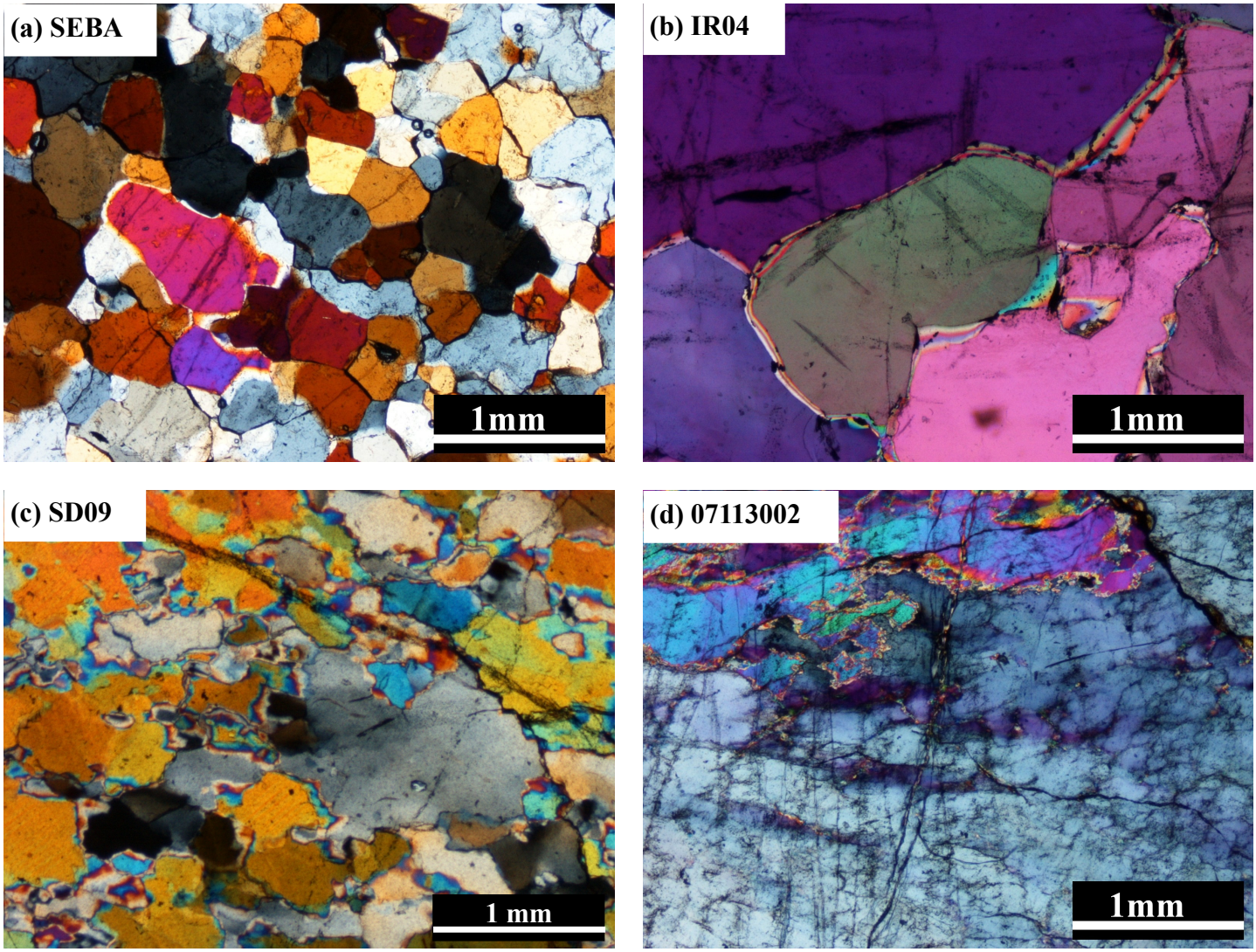

Fig.2.4. Typical quartz fabrics of (a-b) coarse grained P-type veins; (c) DI-type vein; (d) DD-type vein.

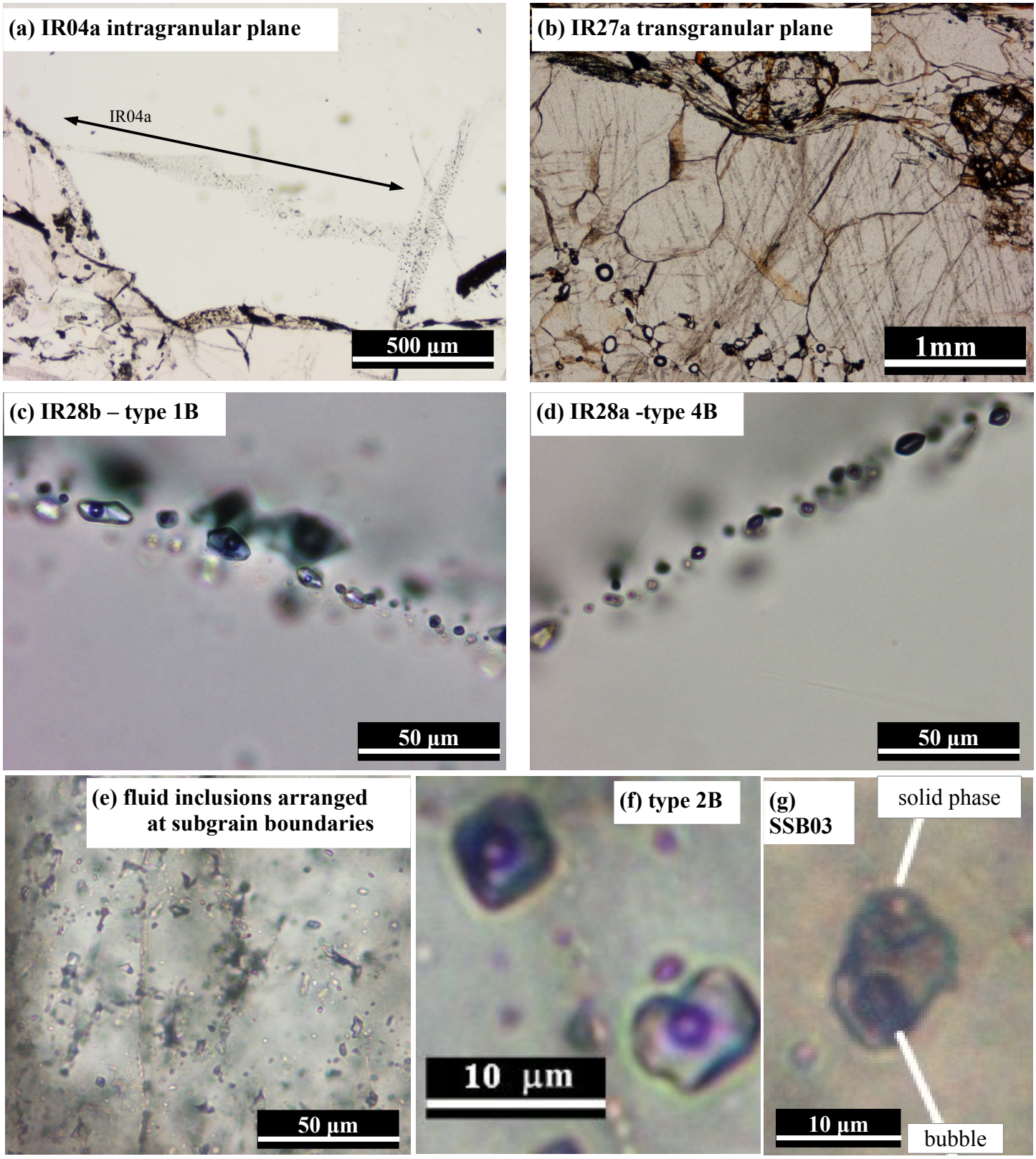

Fig.2.5. Typical occurrences of fluid inclusions. (a) Fluid inclusions arranged along intragranular planes (IR04a). (b) Type 2B fluid inclusions which are characterized by high-saline aqueous fluid, and are generally arranged along transgranular planes (IR27a). (c) Typical fluid inclusions of type 1B which are characterized by diluted aqueous fluid and are generally arranged at transgranular planes. (d) Dark colored type 4B fluid inclusions which are characterize by anhydrous composition and are generally arranged at transgranular planes. (e) Fluid inclusions arranged at subgrain boundaries observed in 10AS18. (f) Close-up photo of inclusions of IR27a composed of aqueous fluid and CH_4-N_2 gas. (g) A type 3 inclusion of SSB03 containing solid, bubble and liquid phases.

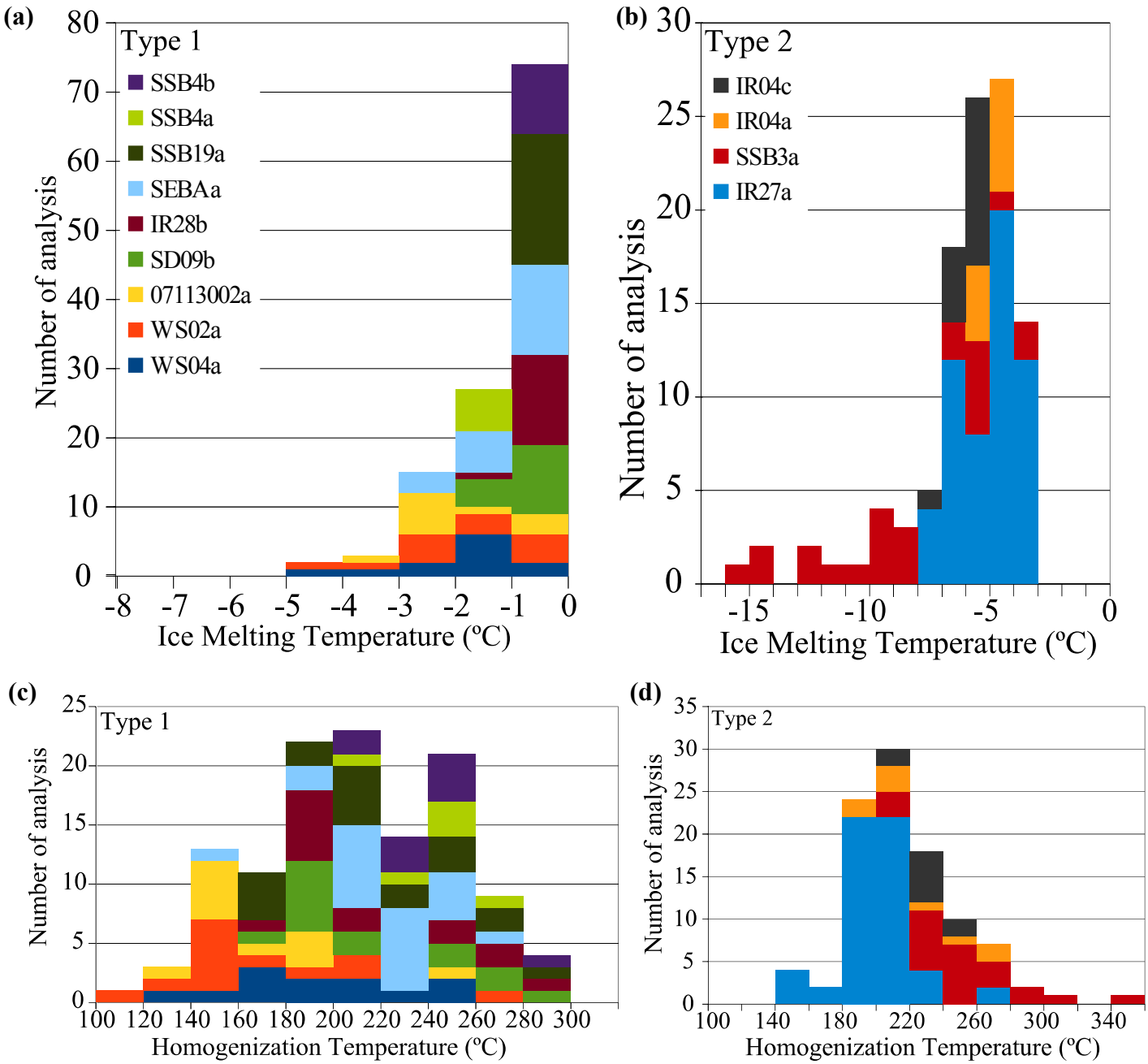

Fig.2.6. Histograms of the results of microthermometry. (a) and (b) are ice melting temperature of type 1 and 2, respectively. (c) and (d) are homogenization temperature of type 1 and 2, respectively.

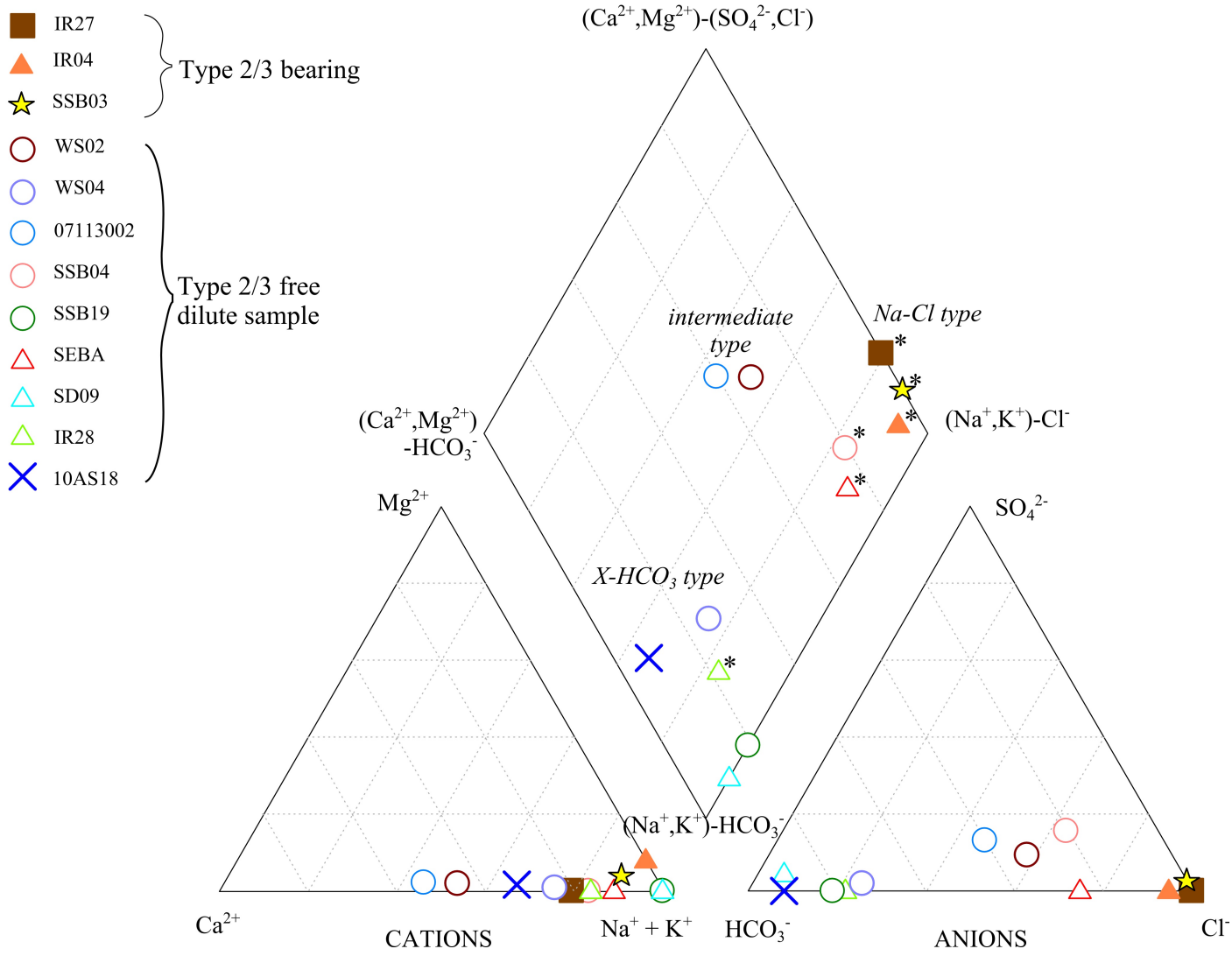

Fig.2.7. Hydrochemical characteristics of the crush-leached fluids plotted in a Piper's diagram. Ternary diagrams in the left-bottom and right-bottom show relative compositions of cations [Mg^{2+}-Ca^{2+}-(Na, K)$^{+}$] and anions [SO_4^{2-}-HCO_3^{-}-Cl^{-}], respectively. Asterisks (*) indicate data obtained from P-type quartz veins. The rhomboid-cation-anion plot shows that Na and Cl are primary components in P-type quartz veins.

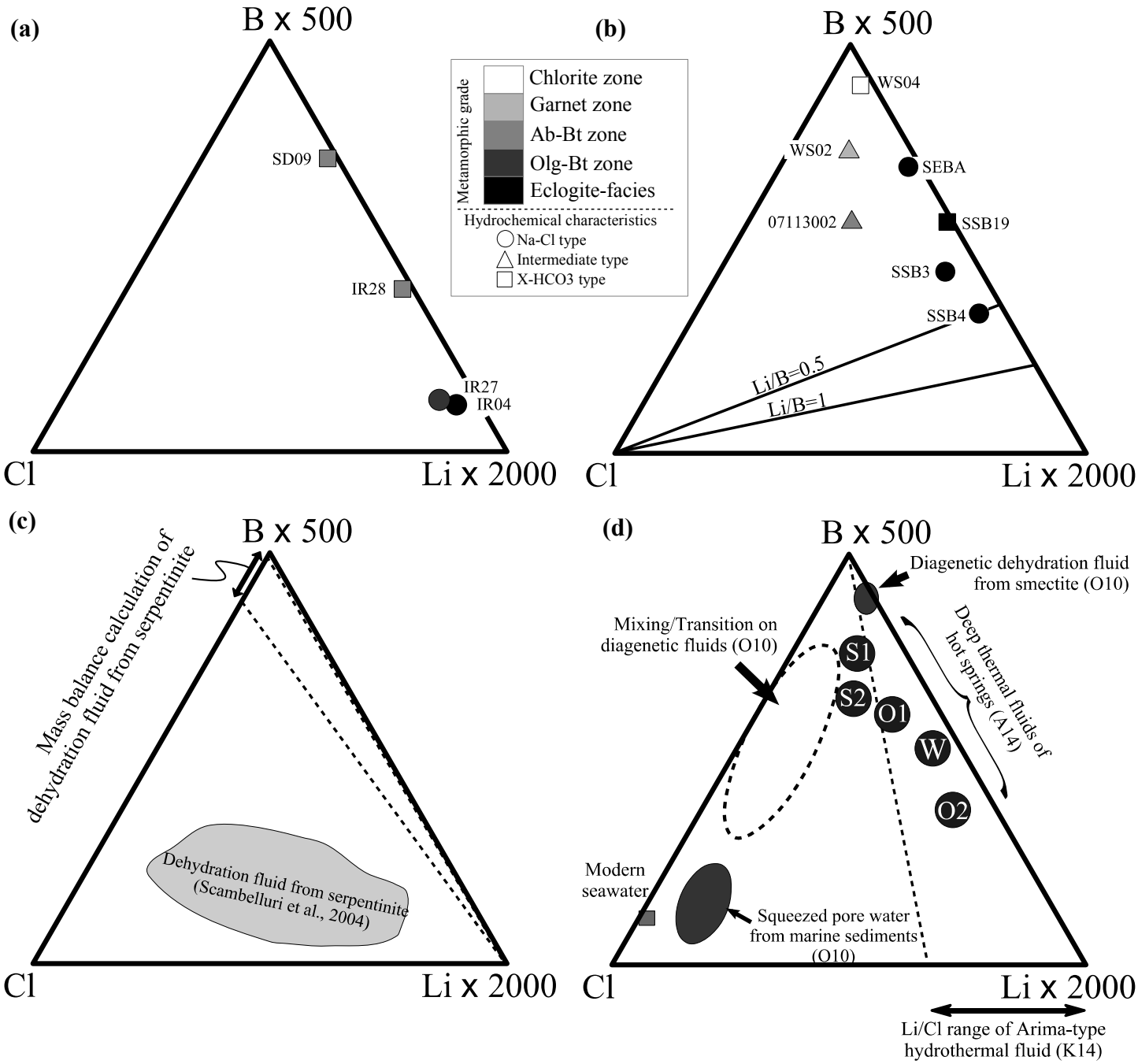

Fig.2.8. B-Li-Cl ternary diagram plotted after Ohsawa et al. (2010). (a-b) Compositions of crush-leached fluid concerning the lithotype of host rock, for (a) metasediment and (b) meta-mafic rock hosted veins, respectively. Shape of marks and filled colors show hydrochemical characteristics of major components and metamorphic grade of host rocks, respectively. (c) B-Li-Cl compositions of fluid inclusions contained in olivine and calculated B/Cl ratio of the dehydrated fluid and mass balance calculation results obtained from serpentinite dehydration (Scambelluri et al., 2004). (d) Compositions of hydrothermal fluids obtained from hot springs in the fore-arc region in SW Japan (Ohsawa et al., 2010; Amita et al., 2014) and Li/Cl range of Arima-type hydrothermal fluids (K14: Kazahaya et al., 2014). O10 and A14 represent Ohsawa et al. (2010) and Amita et al. (2014) respectively. Among the data points of Amita et al. (2014), S1 and S2 are obtained from the Shikoku area, W is from the Wakayama area, and O1 and O2 are from the Oita area.

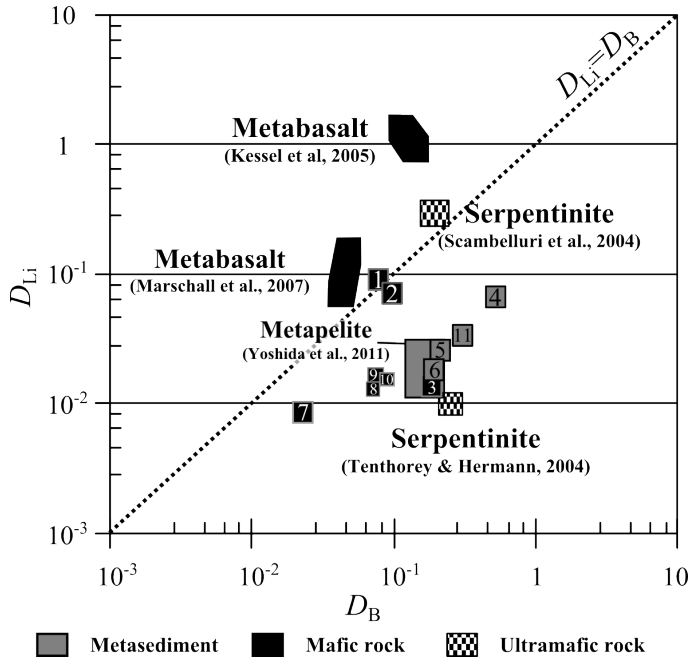

	rock type	method
Scambelluri et al. (2004)	serpentinite	mass balance calculation based on the mineral abundance of natural samples
Tenthorey and Hermann (2004)	serpentinite	high-pressure experiment
Kessel et al. (2005)	K_2O-free MORB	high-pressure experiment
Marschall et al. (2007)	K_2O-added MORB	calculation based on pseudosection modeling of the subducting MORB
Yoshida et al. (2011)	pelite	calculation based on pseudosection modeling of the subducting pelite
this study	mafic and sedimentary rocks	calculation based on the measured mineral abundances of the sample

Fig.2.9. Partition coefficient data of B and Li between whole rock and aqueous fluid (concentration in rock/ concentration in aqueous fluid). Methods used in previous studies are also summarized in the right column. Numbered boxes are samples used in this study. Numbers refer: (1) WS04; (2) WS02; (3) 07113002; (4) SD09; (5) IR28; (6) IR27; (7) SSB03; (8) SSB04; (9) SEBA; (10) SSB19; (11) IR04.

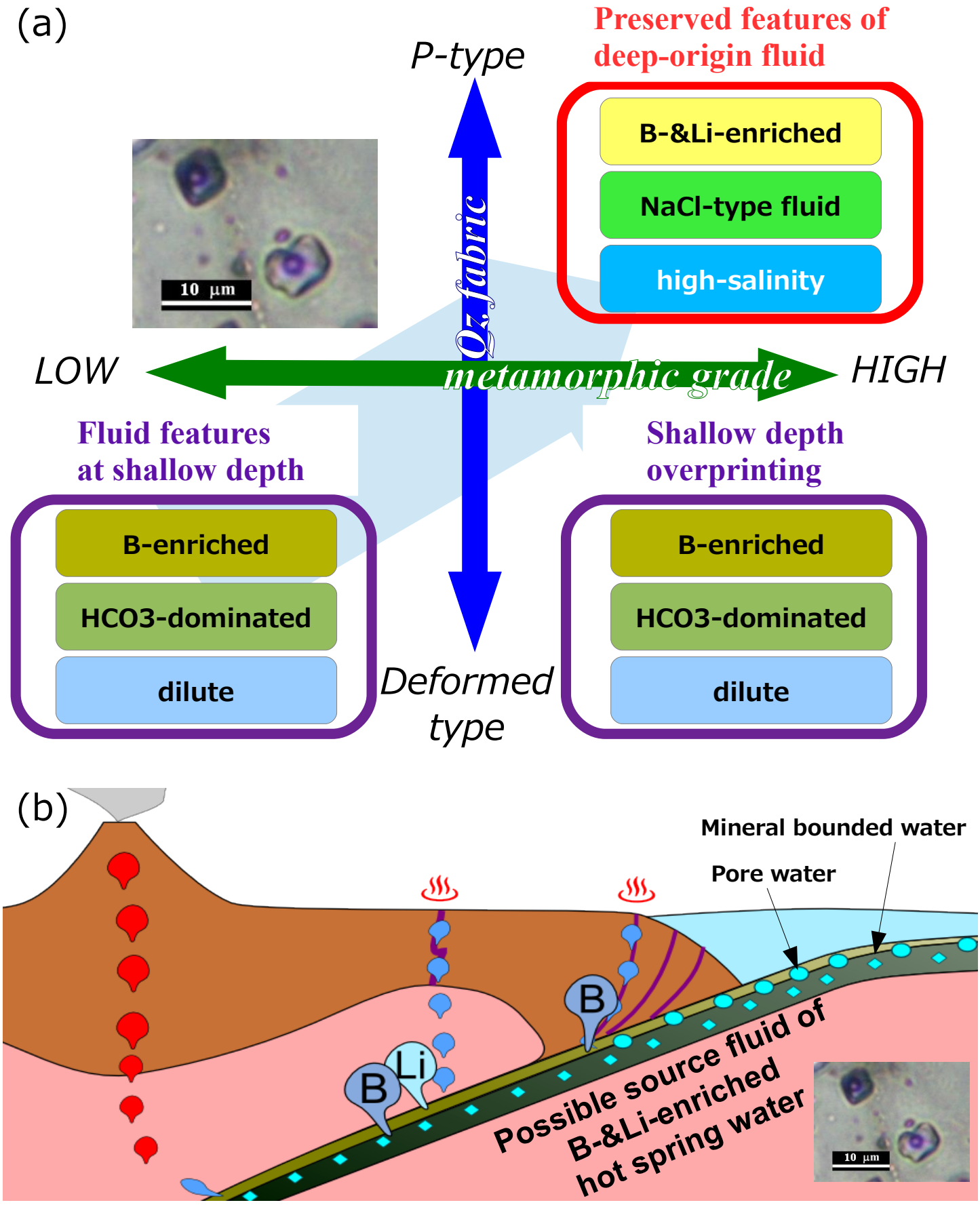

Fig.2.10. (a) Summary of the relationship between fluid composition and fabrics of quatz veins. P-type veins are considered to preserve the deep-origin features, whereas deformed type veins are considered to be overprineted at shallower depths. (b) Schematic image of the fluid occurrence in the subduction zone.

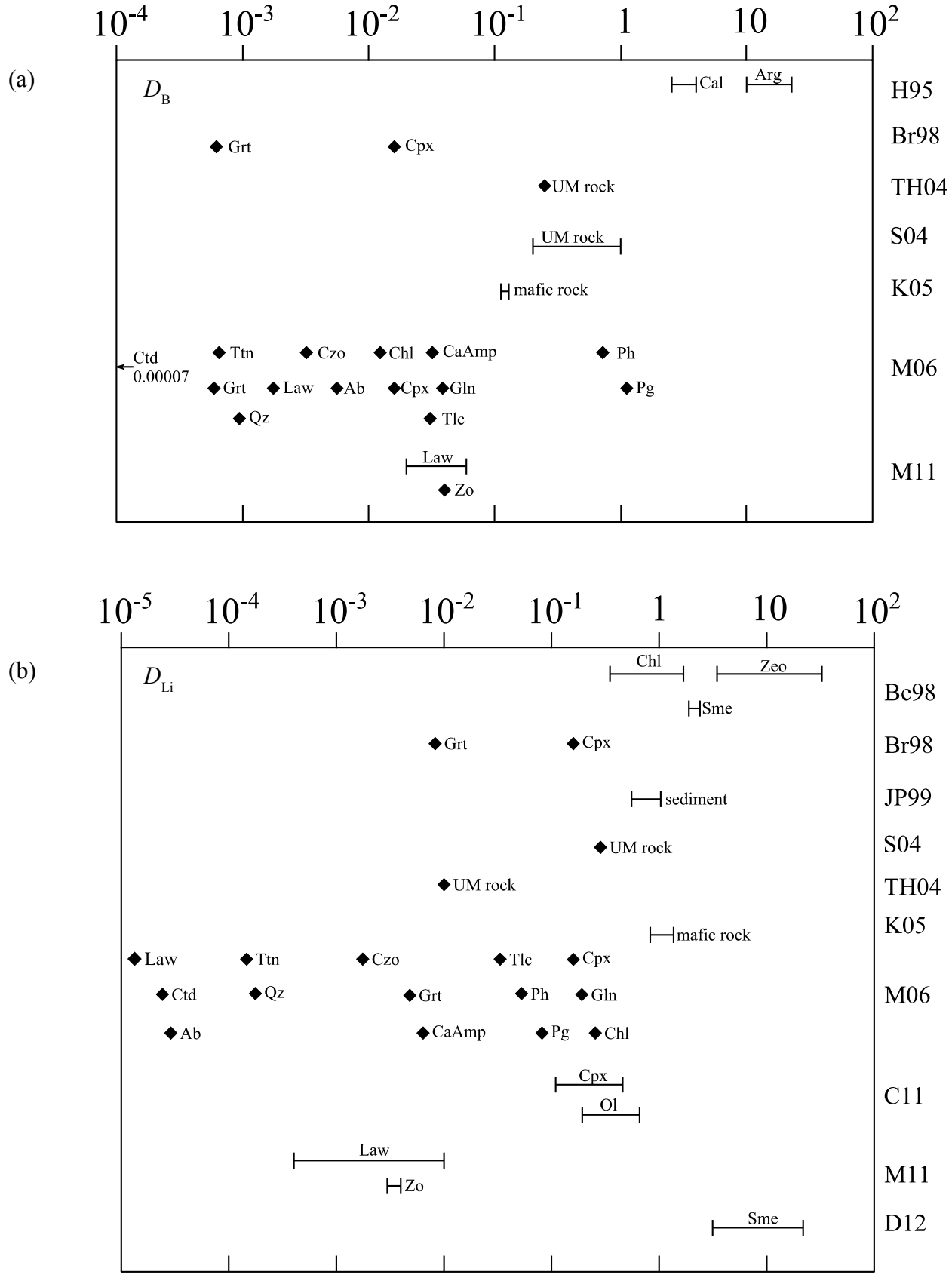

Fig. 2.11. Compile of the previously studied partition coefficient between aqueous fluid and solid phases for (a) boron and (b) lithium. Abbreviations for the references are as follows: H95, Hemming et al. (1995); Br98, Brenan et al. (1998); TH04, Tenthorey and Hermann (2004); S04, Scambelluri et al. (2004); K05, Kessel et al. (2005); M06, Marschall et al. (2006); C11, Caciagli et al. (2011); M11, Martin et al. (2011); D12, Decarreau et al. (2012).

Table 2.1. Estimated mineral abundances in the host metamorphic rock of the studied quartz veins.

Sample	grade	Rock type	Ttn	Rt	Grt	Ep	Cpx	Amp	Chl	Bt	Ph	Pg	Pl	Qz	Other minerals	Method
WS04	Chl	mafic	12.2			25.0		17.4	29.5		8.8		6.8	0.1	Cal, Ccp	**
WS02	Grt	mafic	2.3			24.1		21.2	18.8		9.6		14.6†	0.1	Cal, Ap	**
07113002	Ab-Bt	mafic	5.9			13.3		11.7			22.1		40.4	2.5	Cal, Ap, Ccp	**
SD09	Ab-Bt	pelitic	2nd	1.0	1.6				9.8		66.4		7†	13	Cal, Ap	**
IR28	Ab-Bt	pelitic	2nd		2.3			13.7	3.6		28.1		0.4	52.0		**
IR27	Olig-Bt	pelitic	0.7	<0.1	0.9	3.2		6.8	1.5		24.3	0.1	20.6	40.4	Hem	*
SSB03	ECL	mafic	2nd			32.6		49.3	1.8		0.7		13.6		Cal	***
SSB04	ECL	mafic		1.9	22	12.4		51.8	2		8.6		0.5†	0.4	Hem	**
SEBA	ECL	mafic	2.0		10.9	4.5	1.6	10.5	1.6	6.0	7.4		21.6	15.2	abundant Cal, Hem	**
SSB19	ECL	mafic	2nd	0.7	7.8	10.4	1.7	50.7	1.4		10.8		10.6	3.8	Cal, Hem	**
IR04	ECL	sedimentary	2nd	1.0	7.7			41.8	3.8		43.0		2.7		Apt	**

Estimation methods are *: semi-quantitative analysis of EDS; **: X-ray chemical mapping; ***: optical microscopy. † occurring as large porphyroblasts and are conisidered to be retrograde origin. 2nd: Titanite observed at the rim of rutile, and observed scarce amount.

Table 2.2. Representative chemical composition of amphiboles

Sample	WS04	WS02	07113002	SD09	IR28	IR27	SSB03	SSB04	SEBA	SSB19	IR04
Mineral	Amp	Amp	Amp	-	Amp	Amp	Amp	Amp	Amp	Amp	Amp
SiO_2	55.37	53.14	54.21	-	45.49	44.56	48.36	48.62	42.43	47.59	45.85
TiO_2	0.00	0.21	0.14	-	0.40	0.34	0.45	0.47	0.32	0.53	0.48
Al_2O_3	1.26	4.16	1.70	-	14.52	15.25	10.52	10.30	14.96	12.21	14.51
Cr_2O_3	0.00	0.09	0.00	-	0.06	0.00	0.02	0.02	0.00	0.00	0.01
FeO*	14.65	10.62	13.59	-	12.62	13.52	13.76	14.76	19.13	13.94	13.65
MnO	0.32	0.20	0.40	-	0.08	0.07	0.22	0.08	0.10	0.06	0.17
MgO	14.42	16.01	15.22	-	11.69	10.37	11.61	12.10	7.48	11.40	11.17
CaO	11.76	10.13	10.19	-	9.63	10.23	8.11	7.42	10.14	8.57	10.32
Na_2O	0.78	2.15	1.67	-	2.62	2.53	3.85	3.67	3.06	3.92	2.24
K_2O	0.10	0.12	0.09	-	0.44	0.46	0.45	0.35	0.78	0.52	0.37
BaO	0.02	0.00	0.06	-	0.03	0.04	0.00	0.14	0.00	0.01	0.02
F	0.00	0.00	0.00	-	0.00	0.00	0.00	0.00	0.00	0.00	0.00
-O=F	0.00	0.00	0.00	-	0.00	0.00	0.00	0.00	0.00	0.00	0.00
Cl	0.01	0.00	0.00	-	0.00	0.01	0.00	0.00	0.00	0.00	0.00
-O=Cl	0.00	0.00	0.00	-	0.00	0.00	0.00	0.00	0.00	0.00	0.00
total	98.64	96.82	97.20	-	97.55	97.33	97.35	97.75	98.40	98.72	98.78
Number of ions on the basis of 23 O				-							
Si	7.92	7.58	7.77	-	6.50	6.46	6.98	6.91	6.30	6.79	6.51
Ti	0.00	0.02	0.01	-	0.04	0.04	0.05	0.05	0.04	0.06	0.05
Al	0.21	0.70	0.29	-	2.45	2.61	1.79	1.72	2.62	2.05	2.43
Cr	0.00	0.01	0.00	-	0.01	0.00	0.00	0.00	0.00	0.00	0.00
Fe^{3+}	0.11	0.38	0.53	-	0.71	0.41	0.49	1.03	0.46	-6.64	0.62
Fe^{2+}	1.65	0.88	1.10	-	0.80	1.23	1.17	0.73	1.92	7.86	1.00
Mn	0.04	0.02	0.05	-	0.01	0.01	0.03	0.01	0.01	0.01	0.02
Mg	3.07	3.40	3.25	-	2.49	2.24	2.50	2.56	1.66	2.43	2.37
Ca	1.80	1.55	1.57	-	1.47	1.59	1.25	1.13	1.61	1.31	1.57
Na	0.21	0.59	0.46	-	0.73	0.71	1.08	1.01	0.88	1.08	0.62
K	0.02	0.02	0.02	-	0.08	0.09	0.08	0.06	0.15	0.10	0.07
Ba	0.00	0.00	0.00	-	0.00	0.00	0.00	0.01	0.00	0.00	0.00
F	0.00	0.00	0.00	-	0.00	0.00	0.00	0.00	0.00	0.00	0.00
Cl	0.00	0.00	0.00	-	0.00	0.00	0.00	0.00	0.00	0.00	0.00

Table 2.3. Representative chemical composition of micas

Sample	WS04	WS02	07113002	SD09	IR28	IR27	SSB03	SSB04	SEBA		SSB19	IR04
Mineral	Ph	Ph	Ph	Ph	Ph	Ph	Ph	Ph	Ph	Bt	Ph	Ph
SiO_2	51.09	49.82	48.30	48.19	48.60	48.95	49.44	50.07	50.09	37.38	50.28	49.35
TiO_2	0.07	0.27	0.22	0.21	0.51	0.55	0.47	0.60	0.34	1.29	0.43	0.73
Al_2O_3	22.96	26.58	23.95	29.73	32.35	30.98	26.82	26.35	27.61	16.05	27.75	32.11
Cr_2O_3	0.09	0.07	0.00	0.03	0.01	0.03	0.20	0.03	0.00	0.03	0.00	0.05
FeO*	5.08	3.44	7.22	3.02	1.39	1.66	4.00	3.70	2.46	18.96	2.93	1.76
MnO	0.03	0.00	0.10	0.00	0.02	0.00	0.00	0.00	0.00	0.08	0.00	0.09
MgO	4.31	3.42	3.01	2.47	1.84	2.10	2.91	3.00	3.03	10.60	2.97	2.12
CaO	0.09	0.01	0.01	0.00	0.00	0.02	0.00	0.00	0.00	0.00	0.04	0.03
Na_2O	0.07	0.52	0.12	0.65	1.27	1.47	0.74	0.63	0.71	0.12	0.66	0.89
K_2O	10.70	10.62	10.92	9.88	9.01	8.92	10.13	10.06	10.24	9.45	10.12	8.87
BaO	0.04	0.14	0.19	0.03	0.39	0.28	0.21	0.05	0.12	0.08	0.10	0.25
F	0.00	0.02	0.00	0.04	0.02	0.00	0.00	0.00	0.01	0.00	0.00	0.00
-O=F	0.00	0.01	0.00	0.02	0.01	0.00	0.00	0.00	0.00	0.00	0.00	0.00
Cl	0.00	0.00	0.01	0.00	0.01	0.00	0.00	0.00	0.00	0.01	0.00	0.00
-O=Cl	0.00	0.00	0.00	0.00	0.00	0.00	0.00	0.00	0.00	0.00	0.00	0.00
Total	94.49	94.75	93.85	94.17	94.97	94.70	94.72	94.43	94.47	93.95	95.18	96.00
Number of the ions on the basis of 11 O												
Si	3.50	3.38	3.44	3.26	3.22	3.26	3.36	3.39	3.37	2.88	3.37	3.23
Ti	0.00	0.01	0.01	0.01	0.03	0.03	0.02	0.03	0.02	0.07	0.02	0.04
Al	1.85	2.12	2.01	2.37	2.53	2.43	2.15	2.11	2.19	1.46	2.19	2.48
Cr	0.01	0.00	0.00	0.00	0.00	0.00	0.01	0.00	0.00	0.00	0.00	0.00
Fe^{3+}	0.15	0.13	0.11	0.10	0.03	0.05	0.14	0.10	0.06	0.00	0.08	0.05
Fe^{2+}	0.14	0.07	0.69	0.07	0.04	0.04	0.09	0.11	0.08	1.22	0.09	0.05
Mn	0.00	0.00	0.01	0.00	0.00	0.00	0.00	0.00	0.00	0.01	0.00	0.01
Mg	0.44	0.34	0.32	0.25	0.18	0.21	0.29	0.30	0.30	1.22	0.30	0.21
Ca	0.01	0.00	0.00	0.00	0.00	0.00	0.00	0.00	0.00	0.00	0.00	0.00
Na	0.01	0.07	0.02	0.08	0.16	0.19	0.10	0.08	0.09	0.02	0.09	0.11
K	0.93	0.92	0.99	0.85	0.76	0.76	0.88	0.87	0.88	0.93	0.86	0.74
Ba	0.00	0.00	0.01	0.00	0.01	0.01	0.01	0.00	0.00	0.00	0.00	0.01
F	0.00	0.00	0.00	0.01	0.00	0.00	0.00	0.00	0.00	0.00	0.00	0.00
Cl	0.00	0.00	0.00	0.00	0.00	0.00	0.00	0.00	0.00	0.00	0.00	0.00
Total	7.05	7.05	7.60	7.02	6.97	6.98	7.04	7.00	7.00	7.80	6.99	6.92

Table 2.4. Representative chemical composition of apatites

Sample	WS02	07113002	SD09	IR04
Mineral	Ap	Ap	Ap	Ap
SiO_2	0.04	0.02	0.05	0.00
TiO_2	0.09	0.03	0.24	0.00
Al_2O_3	0.00	0.00	0.00	0.01
Cr_2O_3	0.02	0.04	0.03	0.00
FeO*	0.08	0.13	0.05	0.15
MnO	0.05	0.04	0.00	0.02
MgO	0.01	0.03	0.00	0.05
CaO	55.16	55.28	55.29	54.62
Na_2O	0.00	0.00	0.00	0.00
K_2O	0.00	0.01	0.01	0.00
P_2O_5	45.33	44.08	45.93	42.65
BaO	0.00	0.00	0.00	0.00
F	2.95	2.89	3.72	2.39
-O=F	1.24	1.22	1.57	1.00
Cl	0.00	0.00	0.00	0.02
-O=Cl	0.00	0.00	0.00	0.00
total	102.49	101.33	103.75	98.88
Number of cations on the basis of 26 (O, OH, F, Cl)				
Si	0.01	0.00	0.01	0.00
Ti	0.01	0.00	0.03	0.00
Al	0.00	0.00	0.00	0.00
Cr	0.00	0.01	0.00	0.00
Fe^{2+}	0.01	0.02	0.01	0.02
Mn	0.01	0.01	0.00	0.00
Mg	0.00	0.01	0.00	0.01
Ca	9.33	9.51	9.13	9.72
Na	0.00	0.00	0.00	0.00
K	0.00	0.00	0.00	0.00
P	6.06	5.99	5.99	6.00
Ba	0.00	0.00	0.00	0.00
F	1.47	1.47	1.81	1.25
Cl	0.00	0.00	0.00	0.01

Table 2.5. Summary of textural and chemical characteristics of fluid inclusions observed in the studied samples. Quartz fabric characteristics are also included.

Sample	Mineral zone	Host rock type	Qz-Fabric	FI-group	FI-type	Textural appearance	Size (μm)	Abundance	*n*/ phases	T_m(ice) (ºC)	T_m Average	T_h(total) (ºC)	T_h Average	Total salinity (mass%$_{NaCleq}$)	Chemical species
WS04	Chl	mafic	DD	WS04a	1C	Subgrain boundary	<5	+++	2/L-V	-0.1 to -3.3	-1.8	120 to 255	194	0.2 to 5.4	Aq
WS02	Grt	mafic	DD	WS02a	1B	Transgr. FIP	5 to 10	+++	2/L-V	-0.1 to -4.1	-1.6	160 to 280	176	0.2 to 9.2	Aq-N_2
07113002	Ab-Bt	mafic	DD	07113002a	1B	Transgr. FIP	<5	++	2/L-V	-0.4 to -3.6	-2.0	140 to 245	170	0.7 to 5.9	Aq
SD09	Ab-Bt	pelitic	DI	SD09a	4A	Intragr. FIP	~5	+	1/V	——		——		-	CO_2-N_2-CH_4
				SD09b	1B	Transgr. FIP	3 to 15	++	2/L-V	-0.2 to -1.6	-0.7	170 to 275	220	0.4 to 2.7	Aq-CH_4-N_2
IR28	Ab-Bt	pelitic	P	IR28a	4B	Transgr. FIP	5 to 40	++	1/V	——		——		-	N_2-CH_4
				IR28b	1B	Transgr. FIP	1 to 20	++	2/L-V	-0.5 to -1.3	-0.7	198 to 241	213	0.9 to 2.2	Aq-N_2-CH_4
IR27	Olg-Bt	pelitic	P	IR27a	2B	Transgr. FIP	1 to 15	+++	2/L-V	-3.4 to -7.1	-5.1	154 to 276	202	5.7 to 10.5	Aq-N_2-CH_4
				IR27b	-	Intragr. FIP	<3	+	2/L-V	*		*		*	unidentified
SSB03	ECL	mafic	P	SSB03a	2B	Transgr. FIP	~20	+++	2/L-V	-3.0 to -18.0	-8.6	210 to 350	249	1.7 to 21.0	Aq-N_2-CH_4
				SSB03b	4B	Transgr. FIP	5 to 10	+	1/V	——		——		-	N_2
				SSB03c	3	Isolated	~10	+	3/L-V-S	above halite saturation		312		above halite saturation	Aq
SSB04	ECL	mafic	P	SSB04a	1B	Transgr. FIP	5 to 15	++	2/L-V	-1.1 to -1.3	-1.2	207 to 275	241	1.9 to 2.2	Aq-N_2-CH_4
				SSB04b	1B	Transgr. FIP	5 to 15	+++	2/L-V	-0.1 to -0.3	-0.2	215 to 259	241	0.2 to 0.5	Aq-N_2
				SSB04c	4A	Intragr. FIP	5 to 15	+	1/V	——		——		-	CO_2-N_2-CH_4
SEBA	ECL	mafic	P	SEBAa	1B	Transgr. FIP	5 to 20	++	2/L-V	-0.4 to -2.1	-1.2	150 to 270	226	0.7 to 3.6	Aq-N_2-CH_4
SSB19	ECL	mafic	DI	SSB19a	1B	Transgr. FIP	5 to 15	+++	2/L-V	0.0 to -0.3	-0.2	166 to 257	219	0.0 to 0.5	Aq-N_2
IR04	ECL	sedimentary	P	IR04a	2A	Intragr. FIP	1 to 15†	+	2/L-V	-4.4 to -5.6	-4.9	190 to 269	228	7.0 to 8.7	Aq-CH_4
				IR04b	4A	Intragr. FIP	5 to 20	++	2/L-V	——		——		-	CO_2-N_2-CH_4-H_2
				IR04c	2B	Transgr. FIP	1 to 10	+++	2/L-V	-5.7 to -6.2	-6.0	218 to 255	230	8.7 to 9.5	Aq-N_2-CH_4
10AS18	LS vein /Chl	pelitic	DD	10AS18a	1C	Subgrain boundary	<20	+++	2/L-V	-0.6 to -1.4	-1.0	99 to 210	137	1.1 to 2.4	Aq

Abundance of fluid inclusions are; +++: abundant; ++: common; +: rare. Aq: aqueous fluid; *: not determined due to its small size; LS means later stage (for details, see text); †except for annular shaped ones (~30 μm). FIP means “fluid inclusion plane.”

Table 2.6. Chemical compositions of extracted fluids obtained by the crush-leach method.

Sample	Mineral zone	Host rock type	Qz fabric	Hydrochemical characteristics	Na (mg/L)	NH_4 (mg/L)	K (mg/L)	Mg (mg/L)	Ca (mg/L)	F (mg/L)	Cl (mg/L)	SO_4 (mg/L)	HCO_3 (mg/L)	Li (µg/L)	B (µg/L)	Li/B	(B+Li)/Cl ($\times 10^{-3}$)
SSB04	ECL	mafic	P	Na-Cl	***0.8***	**0.3**	0.2	0	0.1	0.1	***1.7***	-0.04	**0.99**	8.59	19.5	0.44	16.5
SEBA	ECL	mafic	P	Na-Cl	***0.9***	0.4	**0.4**	0	0.2	0	***0.9***	0.3	**0.5**	4.3	44	0.10	53.7
SSB3	ECL	mafic	P	Na-Cl	***3.7***	0.3	**0.6**	0.1	0.3	0	***5.3***	**0.2**	0	16	59	0.27	14.2
IR04	ECL	sedimentary	P	Na-Cl	***2.1***	0.1	**0.2**	0.1	0	0	***4.3***	-0.05	**0.44**	36.89	18.5	1.99	12.9
IR27	Olg-Bt	pelitic	P	Na-Cl	***4.3***	0.1	**0.9**	0	1.1	0	***12.2***	0	0	63.89	37.5	1.70	8.3
IR28	Ab-Bt	pelitic	P	K-HCO3	**0.3**	0	***0.5***	0	0.1	0	**0.4**	0	***2.44***	5.29	14.5	0.36	49.5
SSB19	ECL	mafic	DI	K-HCO3	**0.2**	0	***0.7***	0.0	0.0	0	**0.2**	-0.01	***1.47***	2.89	15.5	0.19	92.0
SD9	Ab-Bt	pelitic	DI	K-HCO3	**0.2**	0.2	***0.3***	0	0	0	0.1	0.1	***2.6***	0.7	8.2	0.09	89.0
07113002	Ab-Bt	mafic	DD	intermediate	**4.43**	0.54	0.49	0.12	***4.83***	0.12	**7.94**	3.03	***11.73***	4	42	0.10	5.8
WS02	Grt	mafic	DD	intermediate	***4.45***	0.47	0.51	0.09	**3.53**	0.11	***8.46***	1.85	**8.13**	4	94	0.04	11.6
WS04	Chl	mafic	DD	Na-HCO3	***6.34***	0.33	0.03	0.04	**1.79**	0.13	**3.34**	0.37	***16.96***	4	200	0.02	61.1
10AS18	p-C	pelitic	DD	Na-HCO3	***5.78***	0.34	0.37	0.08	**2.53**	0	**0.89**	0	***17.69***	-	-	-	-

Host rock type: b/p/s are basic/pelitic/sedimentary, respectively and Chl/Grt/Ab-Bt/Olg-Bt/ECL are chlorite/garnet/albite-biotite/oligoclase-biotite zones and eclogite, respectively. ***Bold and italic*** and **bold** lettering show the highest and second highest values, respectively, among cations and anions.

Table 2.7. Experiments and natural sample observation for the boron and lithium vs. fluid partitioning.

Reference	Applicable rocks/minerals	Studied elements	*P-T* conditions
vs. aqueous fluid			
Berger et al. (1988)	Chl, Sme, Zeo	Li, Rb, Cs	vapor pressure, 50-260ºC
Hemming et al. (1995)	Ca-/Mg-carbonate	B	100KPa, 20ºC
Kogiso et al. (1997)	mafic rock (amphibolite)	Li, Be, LILE, REE	5.5 GPa, 900ºC
Brenan et al. (1998)	Cpx, Grt	Li, B, Be, Nb	2.0 GPa, 900ºC
Johnson and Plank (1999)	sediment	Li, Be, LILE, REE	2-4 GPa, 650-900ºC
Scambelluri et al. (2004)	ultramafic rock	Li, B	2-2.5 GPa, 550-800ºC^{N}
Tenthorey and Hermann (2004)	ultramafic rock	Li, B, Be, LILE	3.0 GPa, 750ºC
Kessel et al. (2005)	mafic rock (altered MORB)	Li, B, Be, LILE, REE, HFSE	4 GPa, 700-900ºC
Marschall et al. (2006)	mafic, felsic	Li, B, Be	0.6-2.0 GPa, 400-500ºC^{N}
Caciagli et al. (2011)	Cpx, Ol, Pl	Li	1.0 GPa, 800-1100ºC
Martin et al. (2011)	Law, Zo	Li, B, Be, LILE, REE, HFSE	3.0-3.5 GPa, 650-850ºC
Decarreau et al. (2012)	Sme	Li	equilibrium water pressure, 75-150ºC

^{N} indicates the data obtained from the natural samples.

Table 2.8 Calculated fluid composition.

	salinity (mass%)	concentration in extracted fluid (ng/g)		estimated original concentration (µg/g)	
		Li	B	Li	B
IR27a	7.7	64	38	347	203
SSB3a	12.4	16	59	219	808